Impacts of Climate Change on Power Systems

A thesis submitted to the The University of Manchester for the degree of

Doctor of Philosophy

In the Faculty of Engineering and Physical Sciences

2015

Mr Xiaolong Hu, BEng

Table of Contents

List of Figures

List of Tables

Acronyms

ACAR	Aluminium Conductor Alloy Reinforced
ACCR	Aluminium Conductor Composite Reinforced
ACSR	Aluminium Conductor Steel Reinforced
ACSR	Aluminium Conductor Steel Reinforced
AGCM	Atmospheric General Circulation Model
AOGCM	Atmosphere Ocean General Circulation Model
BADC	British Atmospheric Data Centre
CDF	Cumulative Distribution Function
EDLC	Expected Duration of Load Curtailments
EENS	Expected Energy Not Supplied
ENA	Energy Networks Association
ENLC	Expected Number of Load Curtailment
GCM	General Circulation Model
GHG	Greenhouse Gas
HadCM3	Hadley Centre Coupled Climate Model
HLI	Hierarchal Level I
HLII	Hierarchal Level II
HLIII	Hierarchal level III
IPCC	Intergovernmental Panel on Climate Change
LOEE	Loss of Energy Expectation
LOLD	Loss of Load Duration
LOLE	Loss of Load Expectation
MTTF	Mean Time To Failure
MTTR	Mean Time To Repair
NERC	North American Electric Reliability Corporation
NERC	North American Electric Reliability Corporation
OD	Oil-Directed
OF	Oil-Forced
OGCM	Ocean General Circulation Model
OHL	Overhead Line
ONAF	Oil-Nature-Air-Force

OPF	Optimal Power Flow
PLC	Probability of Load Curtailments
PPE	Perturbed Physics Ensemble
RCM	Regional Climate Model
RTS	Reliability Test System
SMCS	Sequential Monte Carlo Simulation
SRES	Special Report on Emission Scenarios
TTF	Time of a component To Failure
TTR	Time To Repair the failure component
UKCP	UK Climate Projections
UKCP09	UK Climate Projections 2009
WG	Weather Generator
WS	Weather Series

Abstract

Impacts of Climate Change on Power Systems

Mr Xiaolong Hu, The University of Manchester, September 2015

The global mean surface temperature rise was observed in the past century and proved the warming of the earth climate system. Global warming is believed to continue into the next decades due to unprecedented increases in greenhouse gas emissions. As a consequence of global warming, extreme weather scenarios are also expected to occur more frequently. In such a context, it is of vital importance to assess the impacts of climate change on the operational performance of power systems.

This thesis investigates the impacts of climate change on the operational performance of power systems. The future climate is simulated based on emission scenarios and is then used as an input to the thermal models of power system components to assess their ratings and ageing, and further the reliability of the system.

This research contributes to a number of areas in power system research. In the literature review, the risks that climate change may cause to power systems are identified. The models used for the simulation of future climate are firstly introduced. The weather variables that can be simulated from the models include air temperature, solar radiation, wind speed and direction, soil moisture and soil temperature. Among the models, the one for soil temperature is originally developed in this thesis. Following this, the component thermal models of overhead line, cable and transformer, from different standards are compared and selected. After that, the sensitivity of component ratings to individual weather variables is investigated, as a preliminary study for the later research in this thesis. Then, the impacts of climate change on component ratings (including both static and dynamic rating) are comprehensively and probabilistically assessed. The assessment results indicate the reduction of component ratings due to climate change. The impacts of climate change on system reliability is further examined on the IEEE Reliability Test System. Results demonstrate and quantify the reduction of both component ratings and system reliability, and prove that the dynamic rating can be used to mitigate the reduction. Finally, the preliminary exploration of transformer ageing is carried out and shows an increased ageing rate due to air temperature rises.

Declaration

No portion of the work referred to in this thesis has been submitted in support of an application for another degree or qualification of this or any other university or institute of learning.

Copyright Statement

[1] See http://www.campus.manchester.ac.uk/medialibrary/policies/intellectual-property.pdf

[2] See http://www.manchester.ac.uk/library/aboutus/regulations

Acknowlegements

First and foremost, I would like to express my sincere gratitude to my supervisor, Prof. Ian Cotton, for his continuous guidance and support throughout this research. I really appreciate his helpful comments and discussions which have contributed a lot to this achievement.

A special acknowledgement goes to the Engineering and Physical Sciences Research Council (EPSRC) who has sponsored this project. I would particularly like to thank all the members in the Resilient Electricity Networks for Great Britain (RESNET) project.

I would also like to thank all my friends and colleagues in the Electrical Energy and Power Systems (EEPS) research department at the University of Manchester. Their good companionship and the excellent opportunities they provided to me to develop ideas and exchange knowledge have made this journey very enjoyable.

I am wholly indebted to my parents, for their encouragement and unwavering belief in me during this research. They brought me up with unconditional love and taught me to be who I am.

Finally, I would like to express my gratitude to Miss Tingyan Guo for being always next to me and unconditionally supporting me throughout all these years we have been together.

To my parents,

Chapter 1 Introduction

The global mean surface temperature rise was observed in the past century and proved the warming of the earth climate system. Caused by the unprecedented rate of increase of greenhouse gas (GHG) emissions, global warming is believed to continue in the next decades. As indicated in the latest IPCC (Intergovernmental Panel on Climate Change) Fifth Assessment Report (AR5) issued in 2014 [1], an average surface temperature rise from 0.3 ℃ to 4.8 ℃ is expected to take place by the end of this century, supported by the evidence from climate modelling experiments. As a consequence of global warming, extreme weather scenarios, such as floods, storms and heat waves are expected to occur more frequently and be more severe than those nowadays.

In such a context, the electricity power system is being challenged on three fronts. Firstly, the existing supply mix will be altered as required by the policies that are aimed at reducing GHG emissions through the widespread use of renewable energy generation. Secondly, demand is expected to increase and load profile patterns are expected to change as the result of electrification of energy systems towards a decarbonised future. Finally, the climate change will affect the operational and infrastructural performance of electric power systems in terms of long-term climatic conditions and short-term adverse weather events. Facing these challenges, it is urgent to assess the performance of

existing power systems in future climate scenarios and to investigate the adaptation measures to mitigate the impacts of climate change.

This chapter will firstly give a general introduction to climate change concepts, will identify climatic-related risks, and will give a background knowledge of power system components and reliability. An overview of the past work in the area researched in this thesis is then provided. At the end, the aims and contributions of this research and an overview of the thesis are provided.

1.1 Climate Change

1.1.1 Terms and Definitions

The term *weather* is defined in the Oxford English Dictionary [2] as follows:

"The state of the atmosphere at a particular place and time as regards heat, cloudiness, dryness, sunshine, wind, rain, etc."

The definition of the term *climate* in IPCC glossary [3] is given as:

"Climate in a narrow sense is usually defined as the "average weather," or more rigorously, as the statistical description in terms of the mean and variability of relevant quantities over a period ranging from months to thousands or millions of years. The classical period is 30 years, as defined by the World Meteorological Organization (WMO). These quantities are most often surface variables such as temperature, precipitation, and wind. Climate in a wider sense is the state, including a statistical description, of the climate system."

IPCC [3] also describes the term *climate change* as follows:

"Climate change refers to a statistically significant variation in either the mean state of the climate or in its variability, persisting for an extended period (typically decades or longer). Climate change may be due to natural internal processes or external forcings, or to persistent anthropogenic changes in the composition of the atmosphere or in land use."

According to the above definitions, it can be summarized that weather describes the short-term conditions of the variables, such as temperature, humidity, wind, precipitation, atmospheric pressure and etc, in a given region at a time. Climate is used to present a pattern of weather over a long period of time, typically 30 years. This pattern can be described statistically by the average and variation of the weather. Climate change refers to changes in future weather patterns.

1.1.2 Causes

The climate system on earth is a complex combination of many elements including atmosphere, soil earth, hydrosphere and biosphere. It takes the incoming energy from the sun as short wave solar radiation penetrating the earth's atmosphere with little transit loss. Meanwhile, it emits energy from heated surfaces into space in the form of long wave radiation which mostly gets absorbed by the atmosphere. In this process, the heat can be trapped by water vapour and Greenhouse Gas (GHG) [4].

When the incoming and outgoing energy are balanced, the earth's climate is under a stable condition. However, the plenary balance can be broken by forcings, also known as climate forcings, imposed on the climate system. Consequently, this imbalance leads to a change in global temperature and a series of other climate changes.

The climate forcings fall into two catalogues: external forcings and internal forcings. External forcings are the variations of agents outside the earth's climate system, for example solar activity and Milankovitch variations [4]. On the other hand, internal forcings are the variations of the elements in the climate system and can be classified as nature changes and human-introduced changes. Volcanic eruptions and ocean circulation changes are two main factors of nature changes. The former injects aerosol containing stratospheric H_2SO_4 droplets which have an influence on the absorption of the solar radiation. The latter plays an important role in absorbing the heat from the ocean surface and in circulating this energy [4]. The human-introduced forcings include emissions of GHG in land-use and the depletion of stratospheric ozone. Among these internal forcings, increasing emissions of GHG as a result of burning fossil fuels are of major concern and are believed to be the cause of global warming. The classification of

climate forcings is summarized by Fig. 1-1. By taking these climate forcings as the input of the climate models, the future climate can be simulated according to various assumptions.

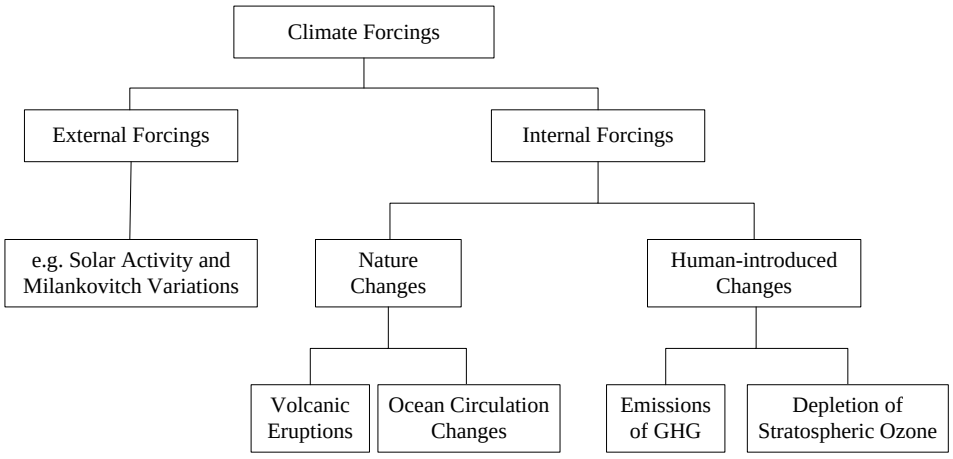

Fig. 1-1: Classification of Climate Forcings[4]

1.1.3 Emission Scenarios

The future climate projections are produced based on the emission levels of Green House Gas (GHG) which is considered as the main driver of the potential climate change in the future. The pathway of future GHG emissions is driven by multiple forces, such as changes in demographic development, social and economic development, and in the rate and direction of technological change. Because the future of these forces is highly uncertain, the emission scenarios have to be developed by imaging alternative combinations of the changes and assessing their influence on emission outcomes according to each combination. A number of emissions scenarios leading to different levels of climate change are therefore gained.

The Special Report on Emission Scenarios (SRES) [5] published by the IPCC in 2000 is currently the most authoritative report on future emission scenarios' assumptions and is widely used by climate change researchers and modellers for driving the global circulation models to develop climate projections. SRES was firstly developed to replace the IS92 emission scenarios for the IPCC Second Assessment Report [6] and

was then used for the following IPCC 3rd, 4th and the latest 5th; the assessment reports were published in 2001, 2007 and 2013 respectively [1, 7, 8].

In the SRES report, forty emission scenarios are developed based on the assumptions covering a wide range of main demographic, economic and technological driving forces of GHG emissions. These forty scenarios are divided into four families which are A1, A2, B1 and B2. Each of them describes a consistent storyline of relationship between the emission driving forces and their evolution in a different context. Furthermore, six scenario groups are drawn from these four families to give more narrative catalogues: one group in each of A2, B1, B2, and three groups in A1 including A1T (predominantly non-fossil fuel), A1FI (fossil fuel intensive), and A1B (Balanced).

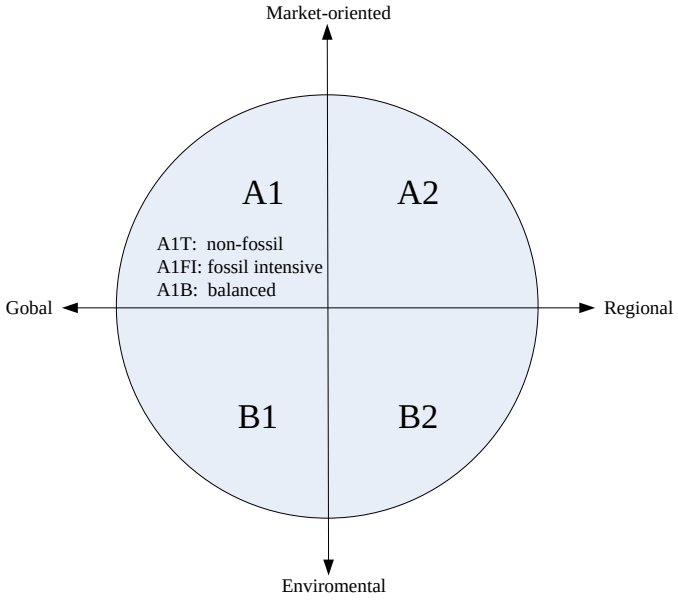

Fig. 1-2: The SRES storylines/emissions families

The GHG emissions are expected to be the greatest in A1 scenarios and the least in B2. A2 scenarios are assumed to produce fewer GHG emissions than A1 and more than B1. Theoretically, a higher emission scenario leads to a greater change in climate. Thus, a greater level of climate change is assumed to take place within A1 scenarios than the other ones.

Fig. 1-2 is an illustration of the SRES scenario families. More details will be briefly introduced in the following sections. It should be noted that no single most likely or "best-guess" scenario exists because of the high uncertainty of the future.

a) A1 Scenario Family

The A1 family of scenarios describes a convergent future world:

- Very rapid economic growth
- Global population that will reach a peak in 2050 and then will decline gradually thereafter
- The quick introduction of new and more efficient technologies
- Convergence among regions and increased social and cultural interactions
- A substantial reduction in regional differences in per capita income

Three groups of scenarios are developed within A1 family. Each of them emphasizes an alternative direction of technological change in energy systems: non-fossil energy sources (A1T), fossil intensive (A1FI), and a balance of sources assuming that similar improvement rates are applied to all energy supplies and end use technologies (A1B).

b) A2 Scenario Family

The future world described in A2 scenario family is very heterogeneous. It is characterized by:

- A world being independently operated in a way of self-reliance and preservation of local identities
- Continuous increase in the global population
- Primarily regional oriented economic development
- More fragmented and slower technological changes and per capita economic growth than the storylines of other scenario families

c) B1 Scenario Family

The B1 scenario family is a world which is convergent and more ecologically friendly. This world is described as:

- The same global population that peaks in mid-century and declines thereafter as in A1 storyline
- Rapid economic growth as that in A1, but with rapid changes in economic structures towards a service and information economy
- The introduction of clean and resource-efficient technologies and reductions in material intensity
- Global solutions to economic, social, and environmental sustainability, including improved equity, but without additional climate initiatives

d) B2 Scenario Family

B2 scenario family describes a divided and more ecologically friendly world which is characterized by:

- Continuous increase in the global population at a slower rate than that in A2 family
- Intermediate levels of economic development
- Less rapid and more fragmented technological changes than those in A1 and B1 storylines.
- Local solutions to economic, social and environmental sustainability which are orientated toward environmental protection and social equity

1.2 Identifying the Risks due to Climate Change

1.2.1 Climate Change Characteristics

To address the risks that may be caused by future climate change, nine specific climate change characteristics are identified in total by UK Climate Projections 2009 (UKCP09), Met Office and electricity system operators [9-11]. The climate change characteristics identified by UKCP09 were obtained from its published work on climate projections simulated from the climate models and have a high probability of occurring in the future. The characteristics identified by the Met Office were taken from its work on "Risk Assessment on Future Network Resilience", but not supported by UKCP09 data (i.e.,

lack of evidence). Furthermore, another two additional characteristics (i.e., costal and river erosion, and subsidence) were added by the electricity system operators for a comprehensive identification of the possible risks. However, it is not known whether these two characteristics are likely to occur or not.

The nine characteristics are given below:

UKCP09 Characteristics:

- ***Summer mean temperature rise*** - The mean summer temperature rise of 8.1℃ by 2080.
- ***Increased heavy rainfall*** - Days of heavy rainfall (>25mm/day) are likely to increase.
- ***Sea level rises*** - Sea levels may rise by 43.3cm by 2080.

Met Office Characteristics:

- ***Increased lightning*** - Increased intensity, frequency of cloud to ground lightning strikes.
- ***Increased wind and gale*** - Increased wind and gusts expected, including potential changes in direction.
- ***Increased snow, sleet, blizzard, ice and freezing fog***
- ***Increased flooding*** - Increased frequency of flooding is expected due to increased rainfall intensity.

Other Characteristics:

- ***Increased coastal and river erosion*** - Increased erosion of coastal defences and river banks due to increased rainfall and storms.
- ***Increased subsidence*** - Possible subsidence issues due to increased rainfall and greater anticipated season swings.

1.2.2 Identifying the Risks

1.2.2.1 Risks Identified by ENA Report

Against the climate change characteristics described in the previous section, the risks that power systems may face are comprehensively identified in the adaptation report published by Energy Networks Association (ENA) [12]. A total of 12 risks are concluded and are labelled as "AR" and numbered from 1 to 12. The details of them are given as follows:

- AR1: Overhead line conductors affected by temperature rise, reducing rating and ground clearance.
- AR2: Overhead line structures affected by summer droughts and consequent ground movement.
- AR3: Overhead lines affected by interference from vegetation due to prolonged growing seasons.
- AR4: Underground cable systems affected by increases in ground temperature, reducing ratings.
- AR5: Underground cable systems affected by summer droughts and consequent ground movement, leading to mechanical damage.
- AR6: Substation and network earthing systems adversely affected by summer drought conditions, reducing the effectiveness of the earthing systems.
- AR7: Transformers affected by temperature rises, reducing ratings.
- AR8: Transformers affected by urban heat islands and coincident air conditioning demands leading to overloading in summer months.
- AR9: Switchgear affected by temperature rises, reducing ratings.
- AR10: Substations affected by river flooding due to increased winter rainfall.
- AR11 Substations affected by flash flooding due to increased winter rainfall.
- AR12 Substations affected by sea flooding due to increased sea levels and/or tidal surges

Furthermore, a risk matrix is used to illustrate the impacts and likelihood of the risks as shown in Fig. 1-3 [12]. It should be noted that there is no adaptation measure assumed

to be taken in this matrix. The risks in the matrix are assessed in the context of climate provided by the UKCP09 climate projections by 2080 according to SRES A1FI emissions scenario. Five impacts levels are used in the matrix, including extreme, significant, moderate, minor and limited, which are defined below [12]:

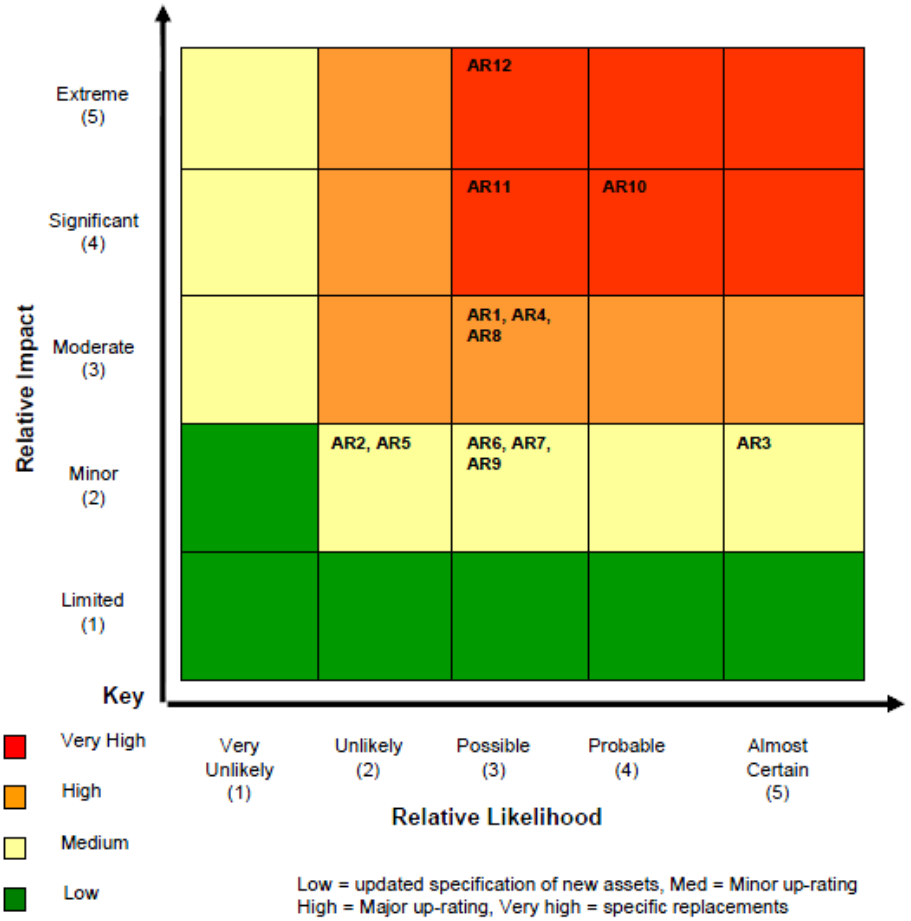

Fig. 1-3: Risk Matrix for Power Network against Future Climate Change [12]

- Extreme: Regional areas affected. People without supply for a month or more OR asset de-rating exceeds ability to reinforce network leading to rota disconnections on peak demand.
- Significant: County or city areas affected. People without supply for a week or more OR asset de-rating requires a significant re-prioritisation of network reinforcement and deferment of new connection activities.
- Moderate: Large town or conurbations without supply for up to a week OR significant increase in cost of network strengthening.

- Minor: Small towns without supply for a 24 hour period OR significant increase in cost of network maintenance requirements.
- Limited: Limited impact that can be managed within "business as usual" processes.

Combining the impacts level (y-axis) with the relative occurrence likelihood (x-axis), the risks are calculated as the product of impact and likelihood and can be classified into four levels from low to very high. The highest risk is identified as the one with the most serious impacts and highest possibility of occurrence. Therefore, the risks on the top right corner of the matrix are the highest risks, highlighted in red. The ones on the bottom left corner are the lowest risks, presented in green. The other two levels in between are presented in orange and yellow. Furthermore, the risks can be measured as the cost as described in [13, 14].

This thesis only concentrates on the impacts of climate change on the operational performance of the transmission network. Hence, the risks that will be investigated are AR1, AR4 and AR7. All of these three risks are de-ratings of power system components as a result of temperature rise and have a relatively high likelihood of occurring. The impact level of the rating reduction of overhead line and cable (AR1 and AR4) are defined as moderate, whilst that of the transformers de-rating is defined as minor.

1.2.2.2 Other Risks

Apart from the risks identified in the ENA adaptation report, two other risks are identified in this thesis, which have impacts on component ageing and power system reliability.

a) Component Ageing

The thermal ageing of cable and transformer insulation is always a major concern in component operations. The ageing rate of a component usually depends on its operating temperature which is affected by both the load and the ambient weather conditions. As a

result of climate change, the temperature rise may elevate the operating temperature and increase the ageing rate.

Component ageing assessment is extremely complicated and requires massive computation time and effort [15, 16]. The ageing assessment of transformers is relatively simple since it only considers the air temperature as the influencing weather condition. In this thesis, only the impacts of climate change on transformer ageing is investigated as a preliminary study.

b) Power System Reliability

The power system reliability can be affected by weather/climate directly and indirectly from three perspectives.

Firstly, the climate change is expected to further increase the frequency, intensity and duration of extreme weather events, for example storms and flooding, which can cause more outages of the components within the system. This impact was reviewed in [17, 18]. A framework was proposed to assess the system reliability against the high-impact low-probability weather event in the climate change context in [19, 20].

Secondly, the climate change will affect the demand and supply scenarios. The link between climate change and electricity demand has been widely investigated in past research [21-23]. Furthermore, the power system supply is also influenced by climate change as the renewable generation plants, such as wind power, solar PV, hydro power plants, are weather dependent [24-28]. The combination of the above changes in demand and supply scenario will change the power flow pattern of the system and affect the system reliability.

Finally, the reduction in the power system component ratings as a result of temperature rise can thermally constrain the power delivery capacity of the transmission lines. This can potentially influence the power system reliability.

As described in Section 1.2.2.1, the de-ratings of power system components as a result of temperature rise are identified as the main risks to be investigated in this thesis. Therefore, this thesis only looks at the final perspective regarding the reliability of power systems.

1.3 Power System Components

The power system is an assembly of electrical components to supply, deliver and use electrical power. These components include generators, loads, overhead lines, cables, transformers, protection and communication devices, etc. Since this thesis focuses on the transmission network of the system, the components being investigated are overhead lines (OHL), cables and transformers. Their operational characteristics which can be affected by the climate system, such as rating and ageing, are introduced in this section.

1.3.1 Overhead Lines

Fig. 1-1: Example of overhead line mounted on metal pylon (left) and wood pole (right)

Overhead lines (OHLs) are the power transmission lines suspended between towers or poles. Since they are insulated by the air, they can save a large amount of cost on the insulation material. Moreover, the exposed overhead lines need less time and cost for

maintenance. Because of such advantages, they are extensively used to deliver electric energy.

The OHL conductors are generally made up by combinations of aluminium for conductivity and steel for strength. Copper conductors are sometimes used on low voltage networks. In transmission systems operated at voltages of 66 kV and above, the OHLs are suspended between metal pylons. In distribution systems operated at voltages between 11 kV and 66 kV, the wood pole are used with OHL conductor fixed to the porcelain insulators onto metallic cross-arms. An example of overhead line mounted on metal pylon (left) and wood pole (right) is shown in Fig. 1-1.

1.3.2 Cables

Cables, or underground cables, are alternatives to overhead lines and transmit electrical power. It is used not only for the purposes of aesthetics due to growing public pressure to preserve the amenities of both town and countryside, but also for making the lines less susceptible to extreme weather events, such as high wind, heavy snow or storms. The insulation of a cable conductor is provided by the surrounding insulation layers and is protected by the sheath and armor. Cables are commonly buried directly or installed in ducts or pipes depending on the installation environment and requirements. Fig. 1-2 shows an example of single-core (left) and three-core (right) cable.

Fig. 1-2: Example of single-core (left) and three-core (right) cable

1.3.3 Transformers

Transformers are utilized to transfer the electric energy from one circuit to another through electromagnetic induction. They can either increase or decrease the voltage of an alternating current when they make a transfer. Transformers can be classified into distribution transformers and power transformers, depending on their rating. Transformers are usually insulated by mineral oil and cellulose paper, whilst some of distribution transformers use cast-resin as the main insulation material and are known as dry-type transformers. Moreover, transformers can also be classified by the cooling methods as ONAN (Oil Nature Air Nature), ONAF (Oil Nature Air Force), OF (Oil Flowed), OD (Oil Directed) and so on. An example of a HV oil-immersed transformer (left) and an dry type transformer (right) is given in Fig. 1-3.

Fig. 1-3: Example of a HV oil-immersed transformer (left) and an dry type transformer (right)

1.3.4 Component Ratings

Ratings, also known as current ratings or ampacity, are defined as the maximum amount of electrical current which can be carried by a component. They are limited by the maximum operating hot-spot temperature influenced by the load current and the ambient weather conditions.

OHL conductors operated over the allowed temperature will cause significant mid-span sag due to thermal expansion. This will reduce the distance between the conductor and ground and violate the minimum clearance requirement. The OHL conductor temperature is affected by weather conditions including the air temperature, solar radiation and wind speed.

Cable conductors exceeding the allowed temperature will damage their insulation layers and hasten insulation ageing. The ambient conditions, which can affect an underground cable, are soil temperature and soil moisture content.

Transformer windings, as hot-spots, operated over the rated temperature can increase the insulation ageing speed. If the winding temperature ever exceeds a critical temperature (typically 140℃) [29], the gas bubble may develop and damage the dielectric properties of the insulation. The air temperature is a major weather condition which can influence a transformer's rating.

1.3.4.1 Static and Dynamic Ratings

For the implementation purpose, there are two component rating methods: static rating and dynamic rating. The former has historically been widely used by system operators whilst the latter is being implemented only on some of the systems.

The static rating is fixed and conservative rating determined by historical weather observations to ensure that the component does not exceed the rated temperature for most of the time. The static rating can be used in two situations, i.e., pre-fault and post-fault. The pre-fault static rating, also known as continuous rating, is used to implement a component under normal operation conditions. On the other hand, the post-fault static rating, also known as emergency rating, is used when a component has to be overloaded due to the outage of some elements of the system to keep continuity of the load for economical or reliability reasons. A component can be operated at post-fault rating only within a predetermined period.

Different from a static rating, a dynamic rating varies depending on real-time weather conditions. It can maximize a component's current carrying ability by benefiting from a favourable weather condition. However, the implementation of a dynamic rating largely relies on the support of monitoring and communication systems.

1.3.5 Transformer Ageing

Transformer ageing is caused by the electric load loss which leads to thermal stress and decomposition of both liquid and solid insulation material, i.e., oil and celluloses. The life span of a transformer is determined by the solid insulation system's mechanical resistance to withstand the high radial and compressive forces caused by short circuit currents. As a result of ageing, its mechanical strength is reduced and may not sustain the force and so the transformer fails. The ageing rate of transformer insulation can be affected by four factors including temperature, moisture content, oxygen content and acid content [12, 30, 31].

1.4 Power System Reliability

As discussed in Section 1.2, the de-rating of components is one of the risks due to climate change. This will constrain the power delivery ability of a power system and affect system reliability. In this section, a brief overview is given on the power system reliability, its hierarchal levels, reliability indices and evaluation methods.

1.4.1 Reliability Definition and Attributes

The definition of power system reliability given by North American Electric Reliability Corporation (NERC) is:

"*Reliability is the ability to meet the electricity needs of end-use customers, even when unexpected equipment failures or other factors reduce the amount of available electricity*." [32]

To "*meet the electricity needs of end-use customers*", the system should maintain the ability of electricity supply under both steady state and transition. Therefore, the system reliability has two attributes: adequacy and security. The system adequacy concerns the system's supplying ability in steady state cases based on the existence of generation, transmission and distribution facilities. The system security focuses on transition between steady states and studies the ability of the system to recover after disturbance involving system dynamics and transients [33]. Compared to the system adequacy, the system security is not well researched because of its complexity. In fact, system reliability studies are mostly carried out to assess the system adequacy.

The outputs of reliability evaluation are known as reliability indices which are used to measure the "*ability*" mentioned in the definition. These indices are not deterministic, but statistical since the "*unexpected equipment failures or other factors*" are stochastic.

1.4.2 Hierarchal Levels of System Reliability Evaluation

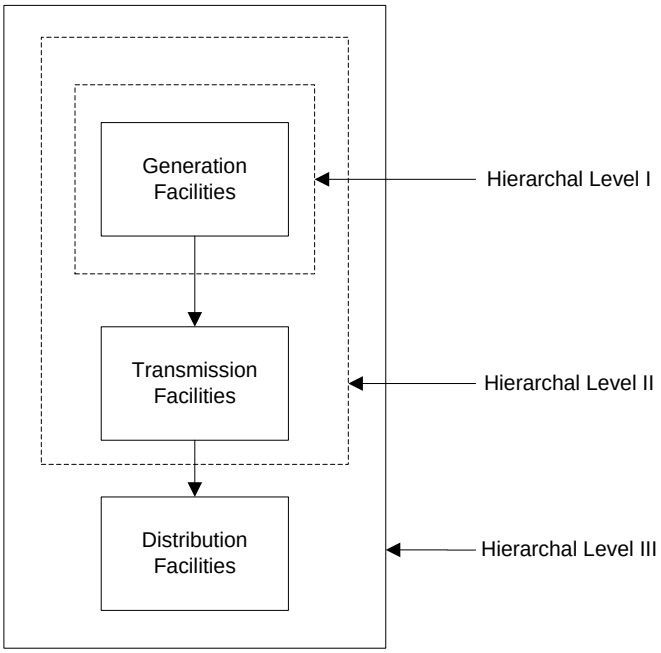

Fig. 1-4: Hierarchal levels of system reliability evaluation

The system reliability evaluation is generally performed considering three elements of the power system, which are generation, transmission and distribution. Depending on

the relationship of these three elements, three hierarchal levels are applied in the reliability evolution as illustrated in Fig. 1-4 [33-36]. Hierarchal Level I (HLI) concerns the reliability of generation only to assess how generation matches the demand, especially during peak demand. Hierarchal Level II (HLII) evaluates the ability of both generation and transmission to meet the electricity demand at grid supply points. The transmission operational constraints, such as thermal limits and voltage limits, are considered in HLII. Hierarchal level III (HLIII) is the most complex level of system reliability evolution considering all three system elements to assess the ability of generation, transmission and distribution as a whole to meet end-use customers' demand. In this thesis, the power system reliability is assessed at Hierarchal Level II.

1.4.3 Reliability Indices

As introduced before, reliability indices are the output of power system reliability evaluation and are used to measure the system reliability. These indices are not deterministic but are the expected value of a random variable based on the long-run average of the studied phenomenon [36]. Different indices are used in different evaluation techniques and hierarchal levels. At HLI, four basic indices are used to evaluate generation system reliability, including the loss of load expectation (LOLE), loss of energy expectation (LOEE), loss of load frequency (LOLF) and loss of load duration (LOLD). The indices are usually used at HLII and include Probability of Load Curtailments (PLC), Expected Duration of Load Curtailments (EDLC), Expected Number of Load Curtailment (ENLC) and Expected Energy Not Supplied (EENS). The definitions and calculation of these indices are described in [35].

1.4.4 Reliability Evaluation Methods

Two power system reliability evaluation methods are developed, including deterministic approach and probabilistic approach [33].

With the deterministic approach, cases are set that one or more components are out of service due to incidents [33]. The evaluation is then performed to assess the reliability

based on these cases. N-1 transmission system planning criteria and percentage reserve in generation planning are two examples of the application of this approach. It assumes that all the incidents have the same likelihood of occurrence. So neither the probabilistic nature of the equipment failure nor the operational uncertainties are reflected in this approach.

The probabilistic approach, also known as the risk assessment of the power system, considers the probability of occurrence of incidents and operating cases [33]. It evaluates system reliability according to two principles. One is the characterisation of system states, including components' outages and operating cases. This characterisation is determined by probabilistic models which are built based on historical operation and failures data. The other is the quantification of individual system states consequences.

The probabilistic approach is the most commonly used approach. In fact, the reliability assessment generally refers to the probabilistic reliability evaluation in current power system reliability studies. The probabilistic approach is used to evaluate the system reliability in this thesis.

1.5 Overview of Past Research

Although climate change is one of the most important and most active research topics nowadays and its impacts are investigated on various disciplines such as environment, health and economy, the literature of its impacts on power system operation is actually not extensive. In fact, not many past publications can be found and none of them provides a systematic and comprehensive assessment.

As addressed in Section 1.2, five risks caused by climate change to the power system are mainly identified according to the knowledge of power system engineering, including:

- Overhead line rating reduction
- Cable rating reduction
- Transformer rating reduction
- Transformer ageing acceleration

- Power system reliability reduction

The past research on the above risks will be reviewed in this section, respectively. All the references cited in this section present initial investigations and preliminary results.

1.5.1 Overhead Line Ratings

The impacts of climate change on OHL ratings are preliminarily explored in [2, 37, 38]. In all of these references, the rating reduction of OHL is calculated as a linear function of temperature rise, i.e., a fixed number of de-rating is assumed to take place for every 1 ℃ the air temperature increases. For example, the rating reduction of Lynx, Zebra and Rubus conductors are taken as 1.6%/℃, 0.81%/℃ and 0.63%/℃ of the designed rating, respectively. Given the air temperature changes at different climate change levels, the percentage of de-ratings can be gained by multiplying the air temperature change in ℃ by the % rating reduction per ℃.

In the ENA climate adaptation report [37], the OHL rating reduction is calculated in the above approach against the change of maximum daily air temperature provided by UKCP09 data. Following ENA, the UK transmission and distribution operators, such as National Grid, Scottish power and etc, carried out the assessment on their own OHLs in the reports [9, 10, 39-42]. However, the method to calculate the de-rating is simple and quantitative. It neglects the effects of other weather variables, like wind and solar radiation. Taking all of the weather variables into consideration, the rating reduction is non-linear to the climate change, rather than linear. Furthermore, since ENA uses the daily maximum temperature to derive the rating reduction, the temperature variation and high temperature duration of the day, which are very important in the static rating determination, are not included in the assessment.

An assessment of impacts of climate change on OHL dynamic ratings was presented in [43]. The work introduced hourly time series weather data to calculate the dynamic rating of a Lynx OHL conductor, used as an example. The results concluded that the the mean OHL dynamic de-ratings caused by climate change are around 3%. However, the study is only based on an OHL conductor used in distribution networks under climate

conditions that assume a medium emission scenario by 2050. The impacts on transmission OHLs within other emission scenarios and time frames are unknown.

1.5.2 Cable Ratings

The past research of climate change on cable ratings is also presented in ENA report [37]. The report adopts the suggestions from Met Office Energy Phase 2 project that the soil temperature at depth of 0.45 – 1.2m can be expected to increase by 0.75℃ for every 1℃ rise in air temperature, and reduced precipitation will only impact the ground resistivity values and have a small effect on them at 1.2 m depth and below. Based on the above assumptions, the change in soil temperature is derived from the maximum daily air temperature change provided by UKCP09. The cable rating reduction is then calculated as a linear function of the daily maximum soil temperature change, similar to the approach used for OHL rating reduction calculation described in the previous section. The UK case studies can also be found in [9, 10, 39-42].

However, the ENA approach ignores the non-linearity of the cable thermal model. The cable rating reduction is non-linear to the soil temperature change, especially at a high soil temperature. The use of maximum daily temperature again fails to show the temperature variation and high temperature duration during the day. More importantly, the soil temperature is actually a result of a complex weather process involving air temperature, solar radiation, wind, precipitation and etc. The soil temperature is determined only by air temperature in an experiential approach in the ENA report, which is not reliable for future soil temperature prediction. For the above reasons, the work in ENA can be only considered as initial research into the impact of climate change on cable ratings. Moreover, the assessment is based on the soil temperature at 1.2 m. However, the studies on the transmission cables which are mostly buried at 2 m depth are not included.

1.5.3 Transformer Ratings

The same straightforward approach, as that for OHL and cables, is also adopted in [9,

10, 37, 39-42] to investigate the impacts of climate change on transformer ratings. According to the work in [29], the rating reduction of distribution transformer and larger transformer over 33 kV are given as 1.0%/℃ and 0.7%/℃. Then the rating reduction is calculated linearly according to the projected air temperature change. However, the transformer thermal model is also non-linear. Furthermore, the transformer types are not considered in the studies. The same percentage de-ratings are applied to different types of transformers depending on the rated load only. But the influence of transformer types is not investigated.

1.5.4 Transformer Ageing

The air temperature rise is the major weather variable which has effect on transformer ageing. The influence of temperature rise on transformer ageing was investigated in [44-46]. In [44], a differential ageing calculation model is developed based on IEEE standard [47] to include ambient temperature dynamics and to improve the model's accuracy. A preliminary case study was given assuming that two transformers are located in different places with an average monthly air temperature difference of 11.1℃. The results showed that the selected type of transformer aged 2.53 times faster at the location with higher temperature. However, the research in [44] did not include the impacts of climate change.

The research presented in [45] provided a standardized method to estimate the life loss on the basis of a steady-state transformer thermal model and gave a case study on the life loss of a oil-immersed distribution transformer. The life loss in the case study was based on the simulated future air temperature time series pseudo randomly generated from the observed historical data but with varied mean and standard deviations to reflect the temperature rise as a result of climate change. According to the same method proposed in [45], a further study was carried out in [46] with air temperature series generated by Monte Carlo simulation. The future temperature projections used in [45, 46] were generated by a random approach without the knowledge of physical climate modeling. Moreover, the transformer model used in [45, 46] was a steady-state model which cannot capture the dynamic features of hot-spot temperature and ageing rate variation, and can misestimate transformer life loss.

1.5.5 Power System Reliability

As discussed in Section 1.2.2.2, this thesis will investigate the risks caused by climate change to power system reliability from the perspective of the reduction in the power system component ratings. Having reviewed the literature, however, no post publication has been found which looks at this issue.

1.6 Research Aims and Objectives

This thesis aims to address many of the issues which have been identified within the current body of research. The main aim of this research is to assess the impacts of climate change on the power system operational performance including component ratings, thermal ageing and system reliability. In order to achieve these aims, the following research objectives have been defined:

1. To review and select the climate models and tools for the purpose of future weather data simulation.
2. To develop the soil temperature model for the assessment of future soil temperature change and cable rating calculation.
3. To review, select and develop the thermal models for the calculation of component ratings and thermal ageing rate.
4. To apply the developed thermal models to establish the sensitivity of component ratings to different weather variables.
5. To assess the impacts of climate change on the component ratings using a probabilistic approach.
6. To assess the power system reliability in the context of climate change on suitable test network developed in MATLAB.
7. To investigate the performance of adaption measures, i.e. dynamic ratings, on mitigating the impacts of climate change.
8. To assess the impacts of air temperature rises on the ageing rate of transformers. It should be noted that the de-rating of transformer is not coupled in this investigation.

1.7 Main Contributions of this Research

The main contributions within this thesis can be summarized as follows:

- For the simulation of future climate, a physical soil temperature model (rather than experience based one as used in the past work) is adopted. The application of this model provides more reliable soil temperature data to assess the future cable ratings. This is the ***first*** original contribution of the thesis.

- Precise and non-liner thermal models (instead of the linear models used in the literature) of power system components, including OHL, cables and transformers, have been reviewed and selected from the published standards, and applied to the investigation of impacts on climate change.

- The sensitivity of the power system components ratings to each individual weather variables involved in their thermal models has been established.

- Comprehensive and probabilistic assessment of the impacts of climate change on power system component ratings have been carried out. This is the ***second*** original contribution of the thesis. For OHL, the benefits from novel technologies including high-temperature conductor and dynamic ratings to mitigate the impacts of climate change have been presented.

- The impacts of climate change on power system reliability have been investigated from the perspective of components de-rating. In this previously unexplored area, the reliability indices including LOLF, EENS and constraint cost have been evaluated. This is the ***third*** original contribution of this thesis.

- The impacts of climate change on transformer ageing have been studied. A dynamic thermal model and a increased future load profile have been considered. This is the ***fourth*** original contribution of this thesis.

A full list of publications resulting from this thesis is included Appendix D.

1.8 Thesis Overview

This thesis consists of eight chapters in total. The seven chapters which follow this introductory chapter are outlined below:

Chapter 2 – Climate Simulation

This chapter introduces the models and tools that are used throughout the thesis to simulation climate data. It first provides an overall description of the climate simulation methodology. The UKCP09 Climate Projections, UKCP09 Weather Generator, wind model, soil temperature model and soil moisture model are then explained in detail. The weather parameters that can be generated include air temperature, solar radiation, soil temperature, soil moisture, wind speed and wind direction.

Chapter 3 – Power System Component Modelling

The modelling of power system components used within this thesis is presented in this chapter. For overhead lines, cables and transformers, the thermal models provided in various power system standards (including IEEE, IEC and CIGRE) are reviewed and compared. The ones that are selected for the use of this research are outlined.

Chapter 4 – Sensitivity of Component Rating to Weather Variables

This chapter presents a sensitivity analysis of the component ratings to individual weather variables, as the preliminary study to the investigation of climate change in later chapters. Air temperature, solar radiation, wind speed and direction are first investigated for overhead line ratings. Soil temperature and soil thermal resistivity are then carried out for cable ratings. Finally, the sensitivity of transformer ratings are assessed against air temperature.

Chapter 5 – Impacts of Climate Change on Component Rating

In this chapter, a comprehensive and probabilistic investigation into the impacts of climate change on power system component ratings is carried out. First, the methodology to determine static rating is provided for all the three components (overhead lines, cables and transformers), and the methodology to determine dynamic

ratings is only given for overhead lines. After this, the probabilistic approaches to assess the impacts of climate change on both rating implementation methods are outlined. The assessment results are then presented.

Chapter 6 – Impacts of Climate Change on System Reliability

The methodology to investigate the impacts of climate change on power system reliability is firstly outlined in this chapter, and then applied to the IEEE Reliability Test System. The assessment is carried out under two different conditions: with and without component failure. The detailed assessment process is described for each of the conditions. Following this, case studies are carried out with different assumptions of rating and load scenarios.

Chapter 7 – Impacts of Climate Change on Transfer Ageing

An investigation into the impacts of climate change on transformer ageing is given. The calculation of transformer ageing and hot-spot temperature is introduced, together with the methodology to assess the impacts of climate change on them. Case studies are also provided in this chapter.

Chapter 8 – Conclusions and Future Work

In this chapter, the main conclusions of the thesis are presented and discussed. Suggestions are also given for the future improvement of the presented research.

Chapter 2 Climate Simulation

There are various well documented approaches available to scientists and engineers for the simulation of future climate projections. In this chapter, the models used for the climate simulation in this thesis, including UK Climate Projections 09 (UKCP09) projections, UKCP09 Weather Generator (WG), wind model and soil temperature model, are described along with the sources of constants for soil moisture and wind direction data. An overview of the climate simulation methodology used in this research is given first. Following this, detailed descriptions are provided for each of the above models. The simulation output of each model is also presented.

Among the climate models, the soil temperature model is originally developed based on physical laws and is modified for the future soil temperature projection. This represents the *first original contribution* of this thesis.

2.1 Overview of Methodology for Climate Simulation

Fig. 2-1 illustrates an overview of the climate simulation process. There are six weather parameters (as highlighted in the grey boxes), including air temperature, solar radiation, soil temperature, soil moisture, wind speed and wind direction, and it is necessary to

investigate their impacts on the power system components. The five sources of these weather parameters include UKCP09 projections, UKCP09 Weather Generator (WG), Wind Model, Constants and Soil temperature model (as shown in the white boxes).

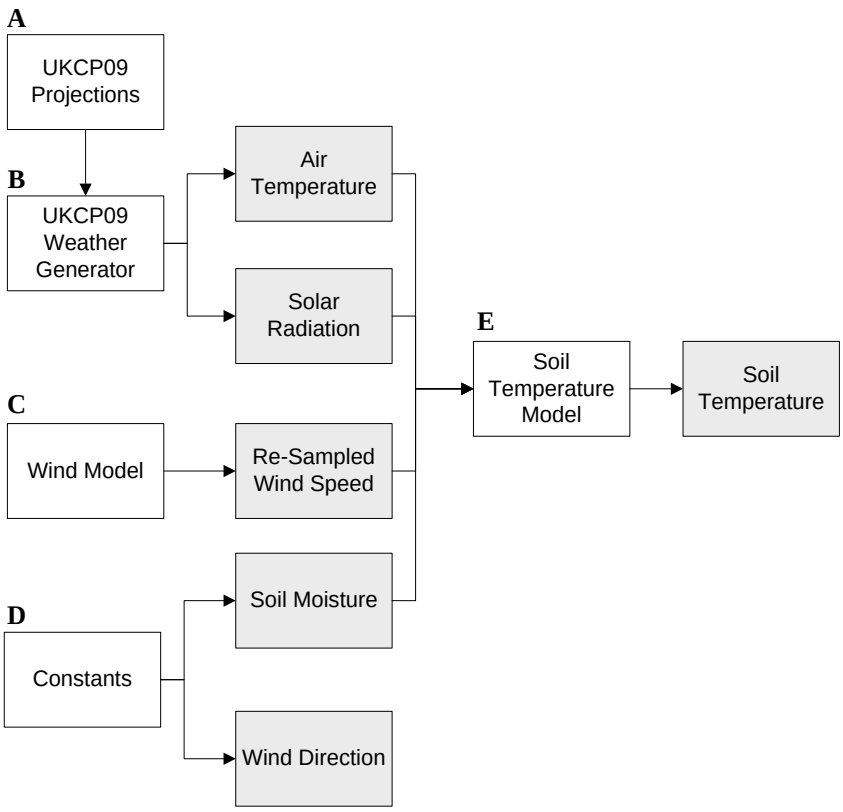

Fig. 2-1: Overview of the climate simulation process proposed in this thesis

In this research, the primary climate change information is given by the UKCP09 projections (box A). These climate projections are simulated from the Hadley Centre Coupled Climate Model (HadCM3), Global Climate Model (GCM) and Regional Climate Model (RCM runs), and are given in the form of probability distributions over a selected time period at a spatial resolution of 25 km.

The hourly weather data is required for the studies of impacts of climate change on power systems to reflect the weather variation during the day. It is to be used as the input of the soil temperature model which is operated on the basis of hourly time steps and is to be used for the determination of static ratings and dynamic ratings. This is not

provided by UKCP09 projections but can be gained from UKCP09 Weather Generator (WG) (box B) which is trained based on historical weather observations in the UK and provides time series of weather data with local features at a fine resolution of 5 km. However, the weather data that can be simulated through the WG only includes air temperature and solar radiation. As changes in wind are considered to be highly uncertain, UKCP09 WG does not include wind speeds and directions in its outputs.

The only information about future changes in wind speed is provided by the HadCM3 RCMs runs. It shows that the average surface wind speeds will lie within the variation range of +10% to -15% by the end of this century [48]. However, UKCP stated that the robustness of the above estimations cannot be guaranteed as the error of the model outputs could be greater than the estimations. The future wind speeds are therefore considered to remain the same as those today. Furthermore, the hourly wind speeds are required in this research rather than the averages since the power system components ratings are calculated on an hourly time scale. As a result, the historical observed that hourly wind speeds are re-sampled and fit into time series through the wind model (box C) for the following studies.

Wind direction and soil moisture are considered as constants (box D) in this research for two reasons. Firstly, they are extremely difficult to be simulated. Secondly, they could be affected to a large extent by local features, e.g., hills, vegetable types, etc. Constant values of both wind direction and soil moisture, which are suggested by industrial practice, technical guide notes and papers, are therefore used [49-51] [52]..

The soil temperature model (box E) takes the weather data, i.e., air temperature, wind speed, solar radiation and soil moisture, from all the above sources as the input and calculates the future changes in soil temperature.

The details of climate simulation processes will be given in the following sections in this chapter.

2.2 UKCP09 Climate Projections

UK Climate Projections (UKCP) is a climate analysis tool that provides the projections of climate change for the UK [53]. The first version of it, namely UKCP02, was published in 2002. The latest version, known as UKCP09, is used as the main information source of climate change in this thesis. Compared to previous UK climate scenarios, UKCP09 gives greater spatial and temporal detail, and more information on uncertainty.

Generally speaking, UKCP09 gives projections of changes for a number of climate variables, averaged over seven overlapping 30-yr time periods, at 25 km resolution and for administrative regions and river basins over land, and over marine regions around the UK [11]. It is the first set of projections that attach probabilities to different levels of future climate change. The probabilities given in UKCP09 represent the relative degree to which each climate outcome is supported by the evidence currently available, taking into account the understanding of climate science and observations, and using expert judgments. Using the methodology designed by Met Office Hadley Centre, probabilistic projections are provided for each of the three IPCC's Special Report on Emissions Scenarios (SRES) scenarios.

This section will firstly give a brief overview of the emission scenarios used in UKCP09. The methodology used to construct the probabilistic climate projections is then described. The examples of outputs and the key findings are also summarized at the end of this section.

2.2.1 UKCP09 Emission Scenarios

As introduced in Chapter 1, the climate change will be influenced by both external forcing, such as solar activity and volcanic eruptions, and internal forcing, such as human involved changes, i.e., emissions of Greenhouse Gases (GHG) (CO2, methane, nitrous oxide, etc.) and aerosol (or aerosol precursor emissions such as sulphur dioxide). UKCP09 assumes no future changes in natural external forcing, apart from a prescribed

repetition of the 11-year cycle of solar insulation based on past observations. The climate projections mainly depend on internal human activities.

The pathway of future emissions of Greenhouse Gases (GHG) and aerosols will depend upon the assumptions of many social and economic factors. As introduced in Section 1.1.3, IPCC published a Special Report on Emissions Scenarios (SRES), in which climate-relevant emissions were calculated based on a number of storylines, each describing a possible pathway of how the world might develop over the course of the 21st Century. In UKCP09, three of the IPCC SRES scenarios are adopted, including A1FI, A1B and B1. Both A1FI and A1B belong to the A1 scenario family which describes a high energy demand future world in a case of rapid economic development. The difference between them is that A1FI is assumed to be a fossil intensive scenario whilst A1B uses a balance of energy sources. B1 scenario is featured by a high level of environmental and social consciousness. It expects a more sustainable future than A1FI and A1B scenarios through the introduction of clean and resource efficient technologies.

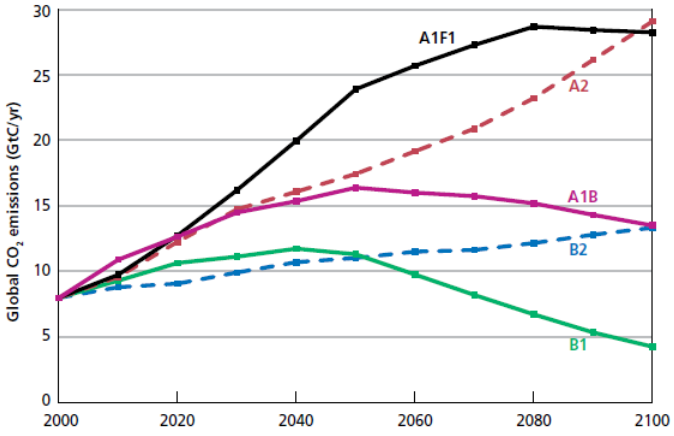

Fig. 2-2: Annual global CO2 emissions (expressed as gigatonnes of carbon) under the three IPCC SRES marker scenarios used in UKCP09: A1FI (black: High emissions), A1B (purple: Medium emissions) and B1 (green: Low emissions). Also shown dotted are two SRES emission scenarios in A2 and B1 family.

Fig. 2-2 shows the changes of the annual global CO_2 emission in the three emission scenarios, expressed as gigatonnes of carbon (i.e., GtC), from the year of 2000 to 2100

[2]. It can be seen from this figure that the amount of CO_2 emission in A1FI scenario is much larger than the other two scenarios. B1 scenario has the least CO_2 emission among the three and A1B scenario is in between. In B1 scenario, the CO_2 emission reaches its peak value around 12 GtC/yr in 2040, but drops to lower than 5 GtC/yr in 2100. In A1B scenario, it reaches the peak value about 16 GtC/yr in 2050 which is 10 years later than that in B1, and decreases to around 13 GtC/yr in 2100. However, the CO_2 emission in A1FI scenario keeps increasing until the 2080s to the value of 28 GtC/yr, approximately, and only decreases slightly afterwards.

Depending on the amount of CO_2 emission produced in each scenario, three levels of emission scenarios are named in UKCP09: high emission scenario (A1FI), medium emission scenario (A1B) and low emission scenario (B1). In the rest of the thesis, the high, medium and low emission scenarios refer to the above IPCC SRES scenarios, respectively. In theory, the higher the GHG emission scenario is, the greater climate change levels are expected to be. High emission scenario (A1FI) is therefore considered as the worst case in the study.

2.2.2 Methodology for Construction of Probabilistic Climate Projections

For each of the three given emission scenarios, UKCP09 constructs probabilistic climate projections which reflect major known uncertainties in relevant climate system processes. A high level introduction to the methodology for the construction is presented in this section. Detailed mathematical descriptions, however, are out of the scope of this thesis and can be found in the references in [11].

The methodology for the construction of probabilistic climate projections in UKCP09 consists of two stages, as illustrated in Fig. 2-3. The first stage produces the climate projections at a global level by running the Global Climate Model (GCM). In the second stage, the outputs from GCM are downscaled to regional level (i.e., Europe, which is the region of interest) by running the Regional Climate Models (RCM).

Due to the lack of sufficiently detailed observations or sufficiently precise theoretical understanding, some of the climate model parameters are uncertain. An approach named Perturbed Physics Ensemble (PPE) is used to sample the key uncertainties systematically. In this approach, the identification of these uncertain parameters and the specification of the distributions of them are firstly achieved by asking experts. A set of variants are then created to setup the climate models by altering the values of uncertain model parameters. Doing this ensures that all the key uncertainties are sampled in a way consistent with the present state of scientific understanding. As a result, the probabilistic climate projections are produced.

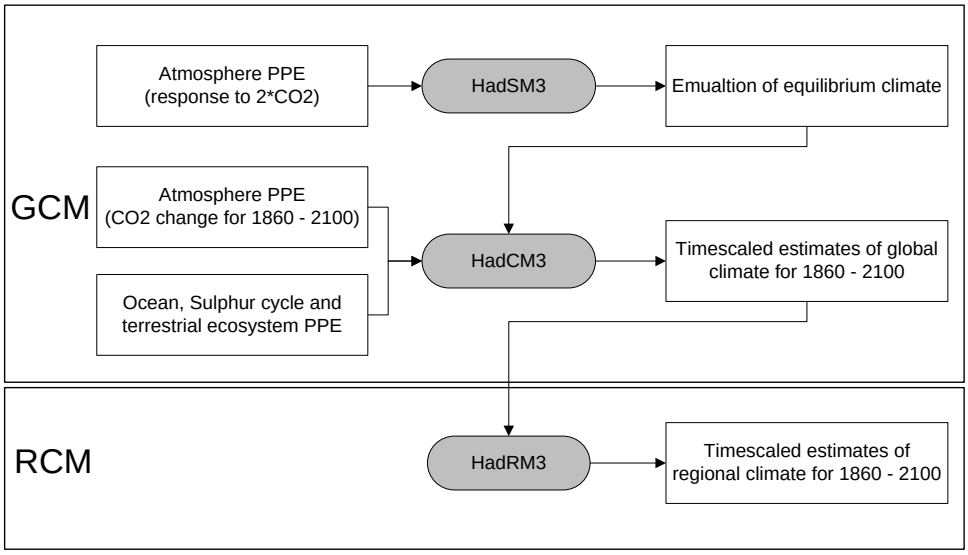

Fig. 2-3: Flow chart of the construction of climate projections in UKCP09

2.2.2.1 Running of Global Climate Models

The construction of the global climate projections involves the running of two GCMs: HadSM3 and HadCM3.

HadCM3 is short for Hadley Centre Coupled Model version 3 and is developed by Hadley Centre in the UK. It is a coupled Atmosphere and Ocean GCMs composed of atmosphere model, HadAM3, and ocean model, HadOM3 [54-56]. The HadAM3 has a resolution of 2.5° latitude × 3.75° longitude over land areas and divides the atmosphere

and the soil into 23 layers vertically. The ocean model has a finer resolution of 1.25° latitude × 1.25° longitude with 20 layers vertically. HadCM3 was used as one of major models in three IPCC Assessment Reports [1, 3, 8] and was also the configuration of UK Climate Projections [11].

Moreover, HadSM3 is a simplified version of HadCM3. It is a combination of the atmospheric component of HadCM3 and a slab ocean, and does not include ocean feedbacks. This makes HadSM3 a faster and less computationally intensive GCM than the fully coupled HadCM3.

a) HadSM3 Running

The modeling of the climate system is extremely complex as it models the climate feedbacks not only between the land surface and atmosphere, but also those of the ocean, carbon cycle and sulphur cycle. The land surface and atmospheric feedbacks are the most comprehensive ones which are parameterized by more than hundred parameters. The perturbations of all these parameters are not computationally feasible. The experiments are then firstly carried out on HadSM3 to find out the parameters which have dominated influence on the outputs of the climate model. The rest of the parameters are then set as the constant values suggested by experts.

The experiment is carried out by feeding the atmosphere PPE in response up to doubled CO_2 concentration into HadSM3 to emulate the equilibrium climate. The doubled CO_2 concentration is widely used to demonstrate the empirical estimation of climate change [57]. The use of HadSM3 ensures the computational efficiency of the emulation at this stage by simplifying the thermodynamics between the atmospheres and the near-surface ocean. As this experiment focuses on the parameters perturbations regarding the climate processes between the land surface and the atmosphere, such configurations applied in HadSM3 are widely accepted as a standard benchmark of climate change studies.

Each combination of values of the modeling parameters is regarded as a variant. An ensemble of 280 HadSM3 runs are implemented to sample the effects of perturbation of

these parameters valued by the published standard HadCM3 variants [54]. Each run consists of a control simulation of recent climate and a simulation of climate response to doubled CO_2 concentration. The difference between these two simulations is defined as climate change. A sufficient length of time is taken to allow the climate to reach equilibrium. The influence of each parameter on climate change is then evaluated by comparing the resulting climate response to the doubled CO_2 concentration to the controlled climate.

As a result, 31 key parameters are chosen for the perturbation in the next stages. It is assumed that the neglect of possible perturbations to the rest of the parameters does not significantly affect the spread of model behavior generated from the simulations.

b) HadCM3 Running

The next step of the climate projection construction is to obtain the time-dependent climate projections for the 21st century at global level. This is done by running the full three-dimensional HadCM3 to simulate the climate change transients with time series of historical and future forcing involved with ocean heat uptake, sulphur cycle and terrestrial ecosystem which are not included in the running of HadSM3. The simulation from the years 1860 to 2000 is driven by historical time series of concentrations of GHG, sulphur emission, solar activity, and volcanic aerosol. From 2000 to 2100, climate change is driven by future concentrations of GHG and sulphur emissions that are given in the SRES scenarios and described in Section 2.2.1. These emissions are used as input to the simulation.

The ranges of the values of the 31 key parameters selected through the HadSM3 experiments are determined by the perturbation based on relevant uncertainties [11]. 10,000 variants are finally produced containing 10,000 combinations of parameter values from the determined value ranges. Each variant is treated as a set of individual estimation of the parameters of equal likelihood. These variants are then used as the setup of the HadCM3 and result in the spread of climate projections.

2.2.2.2 Running of Regional Climate Models

The final step of the UKCP09 climate projection construction is to downscale the outputs from HadCM3 to the targeted locations. The downscaling is achieved by running a high resolution Regional Climate Model (RCM), i.e., HadRM3, at the specified areas. The HadRM3 is configured from HadCM3, and takes the regional features, such as mountains, coastlines and land surface properties, into consideration. In such a way, the climate projections from HadCm3 are downscaled from a resolution of 300 km horizontal resolution to a finer resolution of 25 km.

Five non-overlapping 30-year periods (1950-1979, 1980-2009, 2010-2039, 2040-2069, 2070-2099) are used as the timeframes. At the start of each HadRM3 run, the HadCM3 outputs from the previous time period are taken as the boundary conditions. The lateral boundary conditions include the atmospheric pressure, wind, temperature, humidity, etc. The surface boundary conditions are sea surface temperatures and the extent of sea ice.

In each HadRM3 run, the model parameters are set to be consistent with the values used in the relevant HadCM3 simulation. Therefore, 10,000 HadRM3 variants are derived from the 10,000 HadCM3 variants, accordingly. With these variants, 10,000 equiprobable climate projections are produced for UKCP09 target locations.

2.2.3 Outputs and Key Findings

The weather variables provided by UKCP09 include air temperature, precipitation, sea level pressure, total cloud, humidity, and surface longwave and shortwave fluxes. The most relevant variable to the study in this thesis is the projections of the change in air temperatures. The key findings of changes in air temperatures are therefore chosen to be presented in this section.

As introduced in the previous two sections, 10,000 equiprobable climate projections are produced based on different variant settings for each emission scenario. These projections presented the uncertainties of climate change and are also known as

probabilistic climate change projections. As a result, 10,000 values of air temperature are obtained from all the climate projections at each time point and are put into a Cumulative Distribution Function (CDF). Fig. 2-4 gives an example of the CDF of average annual air temperatures based on 10,000 UKCP09 climate projections in the London area of the 2050s under the assumption of high emission scenario.

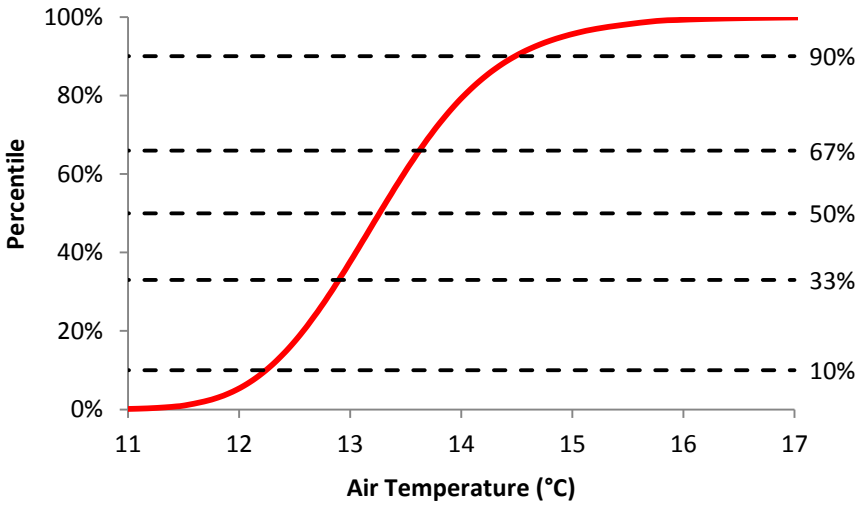

Fig. 2-4: CDF of average annual air temperatures based on 10,000 UKCP09 climate projections at London area of the 2050s under the assumption of high emission scenario.

At the same time, UKCP09 uses five probability levels to describe the strength of evidence associated with the values of weather variables. The percentiles used to interpret the likelihood of occurrence of the projected climate are 10, 33, 50, 67 and 90. The interpretation of each probability level is given in Table 2-1. Taking the CDF of temperature in Fig. 2-4 as an example, the annual average air temperature of 13.26°C is the central estimation in the London area in the 2050s for the UKCP09 high emission scenario. The air temperature at 90 percentile is 14.48°C. This indicates that there is a 90% likelihood that the annual average temperature will be less than 14.48°C. Conversely, there is a 10% likelihood that annual average temperatures will be greater than 14.48°C in this case.

Table 2-1: Interpretations of the probability levels used in UKCP09

Probability Level	Comment
0%	Never to be less than
10%	Very unlikely to be less than
33%	Unlikely to be less than
50%	Average: central estimate
67%	Unlikely to greater than
90%	Very unlikely to greater than
100%	Never to be greater than

In UKCP09 climate projections, climate change is relative to baseline climate recorded from 1961 to 1990. For all three emission scenarios, the changes of air temperature are expected to be different and those in the high emission scenario are expected to be the largest. A summary of the key findings on air temperature changes over UK under the assumption of high emission scenario is given below. Full details of the outputs from UKCP09 can be found in [58].

- Compared to the reference of 1961 to 1990, temperatures keep increasing from the 2020s to the 2050s, then to the 2080s over the whole UK. Moreover, the temperature rises are greater in summer than in winter.

- For central estimation (at the 50% probability level), the highest change of the mean temperatures will occur in the summers of the 2080s in southern England, which is up to 5°C. Furthermore, these changes are very unlikely to be less than 2.6°C (at the 10% probability level) and very unlikely to be greater than 8.1°C (at 90% probability levels).

- By the 2080s, the changes in summer mean temperatures are the least in northern Scotland which range between 1.9°C and 6°C for 10% probability level and 90% probability level, respectively. Central estimation is up to 3.7°C at 50% probability level.

2.3 UKCP09 Weather Generator

The assessment of power system components ratings requires the hourly weather data which cannot be provided by UKCP09 climate projections. The UKCP09 Weather Generator (WG) is therefore utilized to produce the synthetic hourly time series of future weather variables based on the UKCP climate projection outputs.

In this section, a general description of the mechanism of a WG and the UKCP09 WG is firstly given in section 2.3.1. The implementation of UKCP09 WG in this thesis is described in section 2.3.2. The examples of outputs are also provided at the end of this section.

2.3.1 General Description

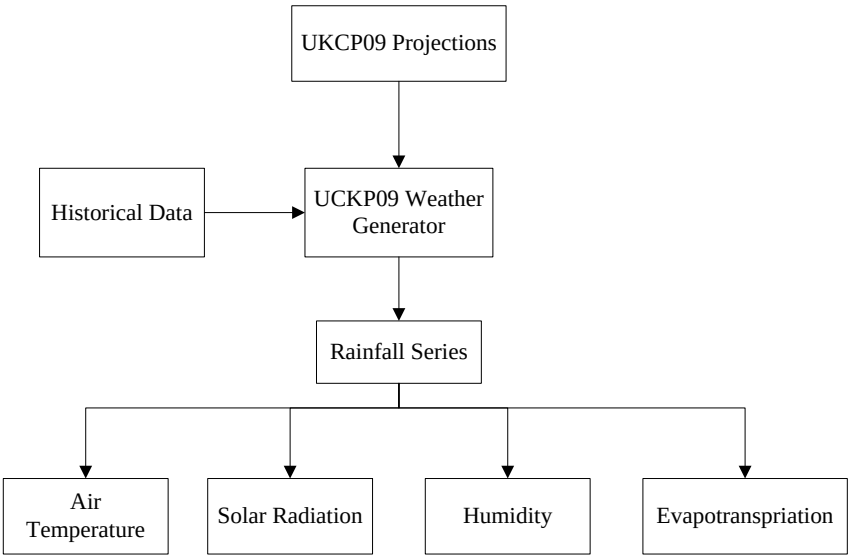

Fig. 2-5: The approach of the data simulation used in UKCP09 weather generator.

A Weather Generator (WG) uses a statistical method to produce synthetic time series of weather variables on a daily or hourly basis. These variables are temperature, rainfall, humidity and sunshine amount whilst information on other aspects of weather such as wind, thunder/lightning and atmospheric pressure is not provided. A WG is generally trained based on the observed historical local weather data and the simulations of

weather processes at hourly steps. The WG's configurations can be modified according to future climate projections then the WG can be used to produce the future weather series which fit the climate projections statistically.

Most WGs are based on an approach known as "Richardson-type" [59]. Within this approach, rainfall is taken as the primary variable and so the first step in a run of WG is to simulate a future rainfall series with a stochastic model. The rainfall series are fitted to the historical weather record statistically to present the local features. Other weather variables, such as air temperature, sunshine, vapour pressure, are then determined by the mathematical/statistical relationships between these variables and rainfall. The weather is consistent in sequence, i.e., the simulation result of the weather in day 2 is based on the weather in day 1. In such a way, a weather generator can mimic the real weather process.

- The WG provided by UKCP09, i.e., UKCP09 WG, follows the "Richardson-type" described above and produces the future weather series according to the UKCP09 climate projections. The general approach used in the UKCP09 WG is illustrated in Fig. 2-5 and can be described as follows: the observed local historical daily rainfall data between 1961 and 1990 and values of other weather variables data between 1990 and 1995 are used to calibrate the WG. These historical data are regarded as the baseline data presenting the existing climate.

- The climate change factors [11], which describe the changes of the climate in the specified future compared to the baseline climate, are taken from the UKCP09 probabilistic projections at the monthly time scale. These Change Factors are then used to configure the UKCP09 WG variables to give the range of possible climate change futures.

- Daily rainfall series is generated from the stochastic rainfall model using perturbed future rainfall statistics configured by the Change Factors.

- Other weather variables, including air temperature, solar radiation, humidity, and evapotranspriation, are then derived from rainfall series using the observed relationships among these variables.

2.3.2 Implementation

The UKCP09 WG can be implemented with various settings for different purposes. In this section, the setting for the implementation of UKCP09 WG for the study in this thesis is described.

2.3.2.1 Emission Scenarios

UKCP09 WG provides the simulation of weather series in three CO_2 emission scenarios. These three scenarios are the same as those used in UKCP09 projections (as introduced in detail in Section 2.2.1), namely high emission scenario (A1FI), medium emission scenario (A1B) and low emission scenario (B1) [60].

2.3.2.2 Time Frames

Apart from the baseline period, another three time frames are adopted in this study, including 2020s (2010-2039), 2050s (2040-2069) and 2080s (2070-2099). These three time frames divide the years from 2010 to 2100 into three non-overlapping periods of 30 years.

2.3.2.3 Locations

The levels of climate change are different over the UK. Generally, temperature rises in southern UK are expected to be greater than those in the northern UK. Three locations, Slough, Manchester, and Edinburgh, are selected to investigate the impacts of different levels of climate change on power systems. Slough is in the southeast UK and is expected to have the greatest temperature rise. Edinburgh, however, is located in the north of UK and has the least temperature rise among the three selected locations. Manchester is in the middle of UK, between Edinburgh and Slough. The temperature rise at Manchester is expected to be less than Slough and greater than Edinburgh. In the UKCP09 WG, the spatial grid at the above three locations are numbered as 3200665, 3950405 and 5050185, respectively.

2.3.2.4 Variants

A run of WG is configured by setting the values of the variables used in the weather model. The WG output with standard configuration is taken as the baseline weather. To produce various weather series, the change factors (obtained from UKCP09 projections), which measures the difference between future climate and baseline climate, are applied to change the WG configuration. Such a run of WG is called a variant and generates a weather series (containing 30-year of hourly variables) at a specified level of climate change. Given various change factors, the UKCP09 WG variants can output weather series at a range of climate change levels.

Within the variables used in the weather model, a part of them is determined by the assumptions of emission scenarios. In the UKCP09 WG, three variants, whose emission scenario relevant variables are set at three levels (i.e., high, medium, and low), respectively, and other variables remains the same, are assigned to the same variant ID number. For a specific variant ID, the simulated weather series remain consistent in both time frames and between emission scenarios, i.e., the climate change is greater in high emission scenarios than that in lower emission scenarios; meanwhile, the climate change in later time frames, e.g. the 2080s, is greater than that in earlier time frames, e.g. the 2020s. However, the weather simulated in different variant IDs is inconsistent. For example, the climate change in a low emission scenario in one variant ID can be greater than that in a high emission scenario in another.

As an example, Fig. 2-6 shows the average air temperature generated from the WG. The bars on the left side of the figure result from the same variant ID (i.e., Variant ID: 61). Consistency is shown since the average air temperature decreases from high to low emission scenarios. In contrast, the bars on the right side of the figure are generated from different variant IDs. It can be seen that the temperature rise in low emission scenarios generated in variant ID: 9971 is even higher than that in high emission scenarios generated in variant ID: 286.

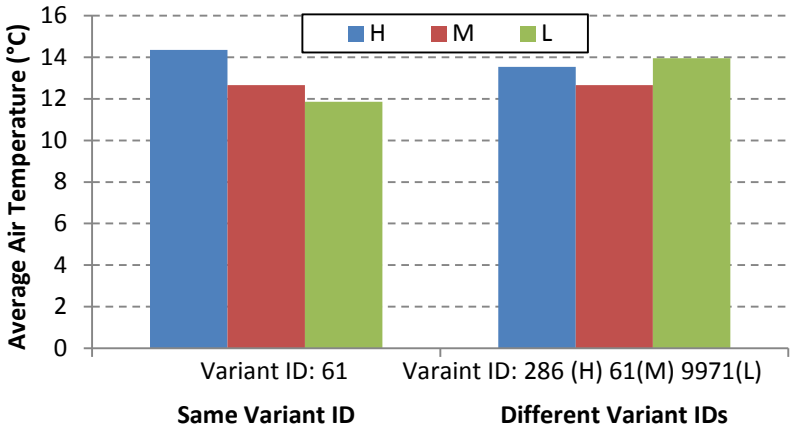

Fig. 2-6: Average air temperatures for three emission scenarios within the same WG variant ID and different WG variant IDs (H: high emission scenario, M: medium emission scenario, L: low emission scenario)

Because of the properties of variants described above, the simulated weather data from UKCP09 WG should be used in line with the two rules: 1) a sufficient number of variants should be used to give a comprehensive assessment of climate change covering a reasonable wide range of possible projections; 2) Each variant should be treated as an independent climate projection. The evaluation of climate change as the result of each variant and its impacts should be taken individually.

a) Determination of the Number of Weather Generator Variants

In UKCP09 WG, a total of 10,000 combinations of WG configurations are used to produce 10,000 variants. The parameterization of these configurations follows those in the UKCP09 projections. In each variant, the weather series generated is consistent with the climate change level provided in UKCP09 projections. Although a sufficient number of the WG variants should be used, it is impossible to use all the 10,000 in this study because of the computational limitation. Therefore, it is crucial to determine the least number of variants to guarantee that the simulated weather data covers a reasonably wide range of possible climate projections.

The simulated weather variable in each variant can be presented in a form of a probability distribution which reflects its statistical properties. The most important three are mean, variance and extreme values. To find out the number of variant to be used, the weather data from all variants are combined into one probability distribution. The changes of these three properties are monitored when weather data from an increasing number of variants joins the distribution gradually. The number of variant is considered to cover enough versions of climate projections when the values of these properties stabilize around certain values.

The simulated air temperature in the variants from 1,500 WG runs in the 2080s in Slough are used to demonstrate the changes of mean, variance and extreme values as a function of the number of WG variants. These 1,500 variants are selected from 10,000 UKCP09 WG variants randomly.

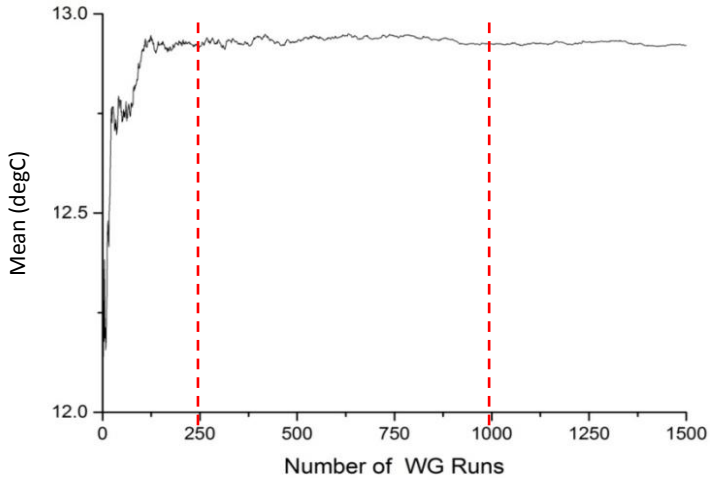

Fig. 2-7: The change of mean of air temperature as a function of number of weather generator runs

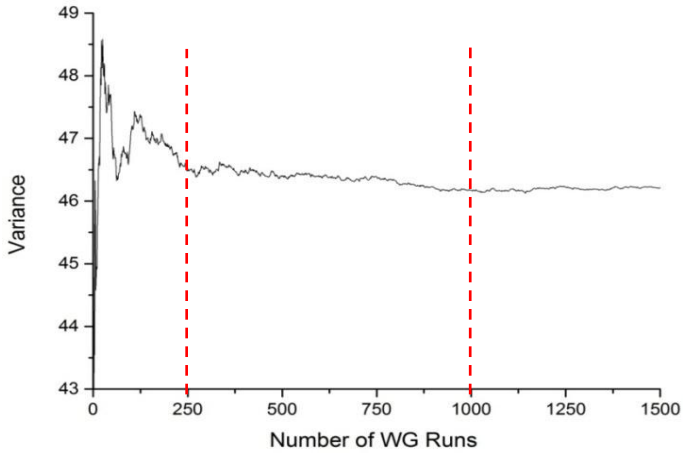

Fig. 2-8: The change of Variance of air temperature as a function of number of weather generator runs

It can be seen from Fig. 2-7 and Fig. 2-8 that the mean and variance change dramatically when the number of variants increases from 0 to 250, as the new joined weather variants are providing diversities in climate projections. After 250 runs, the fluctuations are observed to decrease as the number of runs increases, and eventually converge after 1,000 runs, in which the change caused by the new joined variants remain within 1% of the average value.

Regarding the extreme values, the extreme weather is theoretically expected to have a higher probability of occurrence in a higher emission scenario. Fig. 2-9 shows the cumulative probability distribution formed by the summer hourly temperatures in Slough in the 2080s simulated from different numbers of the variants. The air temperature over 30 ℃ (right to the dashed line in Fig. 2-9) is considered to be extremely high temperatures. It can be seen in Fig. 2-9(a) that the extremely high temperatures have almost the same probability of occurrence in medium and low scenarios simulated with only 100 variants. By increasing the number of variants, the curves start to separate from each other. In Fig. 2-9(d), when the number of the variants is increased to 1000, the consistency among the three emission scenarios can be clearly observed.

From the above studies on the influence of the number of WG variants on the mean, variance and extreme values of simulated weather data, at least 1,000 should be used.

The ID numbers of UKCP09 WG variants used for the following studies are provided in Appendix A.

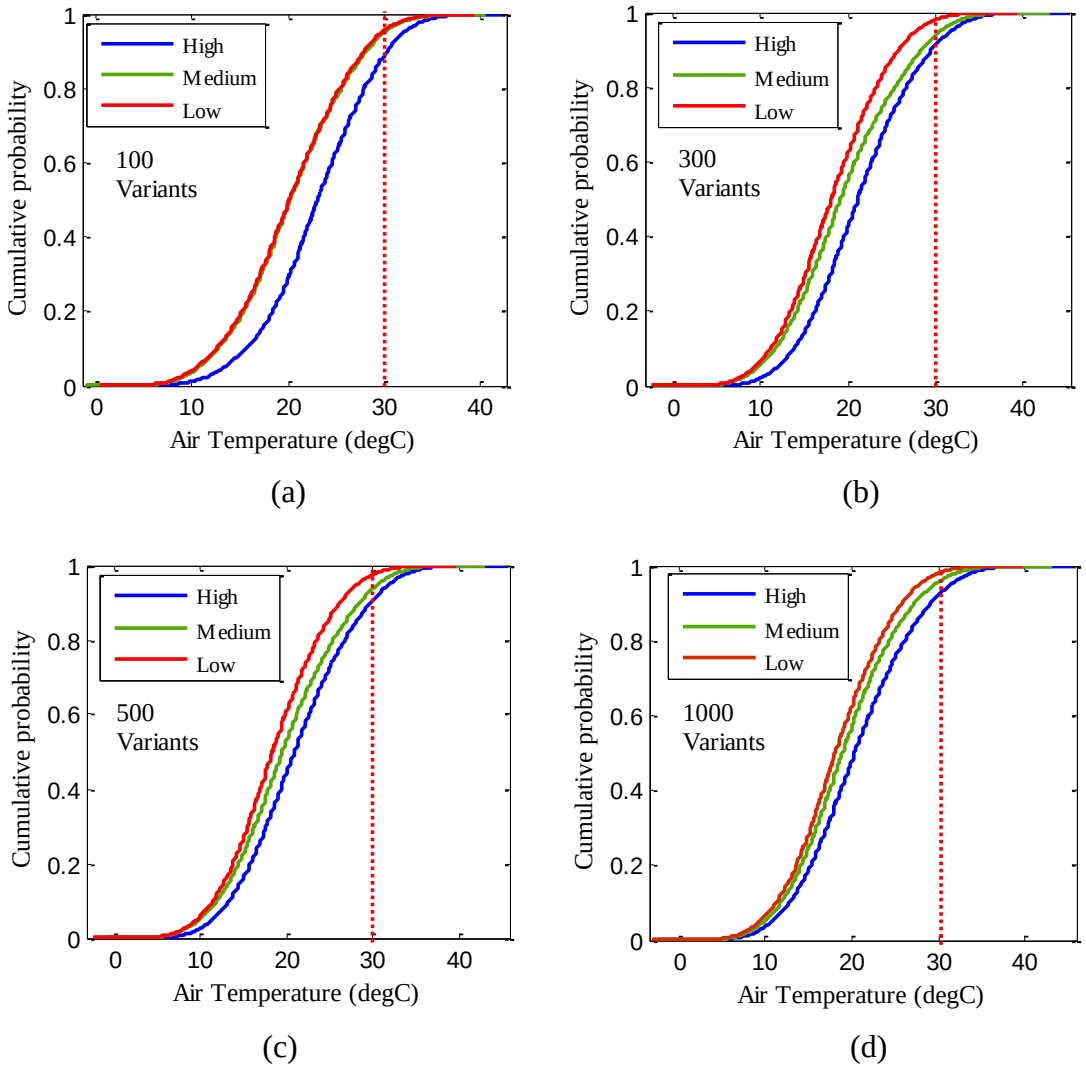

Fig. 2-9: Improvement of consistency of extreme high temperatures by increasing number of variants

2.3.3 Example Outputs

Each run of WG outputs two types of simulated weather data: control data and scenario data. The control data is taken as the baseline weather without any change factors applied. It should be noted that the control data is different from the historical record data. The historical data are certain as they are actually observed data. The control data are generated from weather generator in a stochastic method (variant based), which

provides a minor variation from the historical data. The simulated scenario data are the variant from the control data and present the future climate by introducing change factors corresponding to the emission scenario assumptions. The difference between these two types of data is defined as climate change.

Both control data and scenario data present all the weather variables, including air temperature, solar radiation, etc, in the form of daily and hourly absolute values in a synthetic 30-year time series. The example UKCP09 WG outputs based on the simulated weather in Slough in high emission scenario is presented and analysed in this section.

Fig. 2-10 gives an example of the simulated daily maximum air temperature for a high emission scenario in Slough over one year in the 2080s. The figure simply confirms the correct operation of the WG by showing that the summer months are warm whilst the winter months are cold.The fluctuations of temperature throughout the days are caused by rainfall or cloud cover.

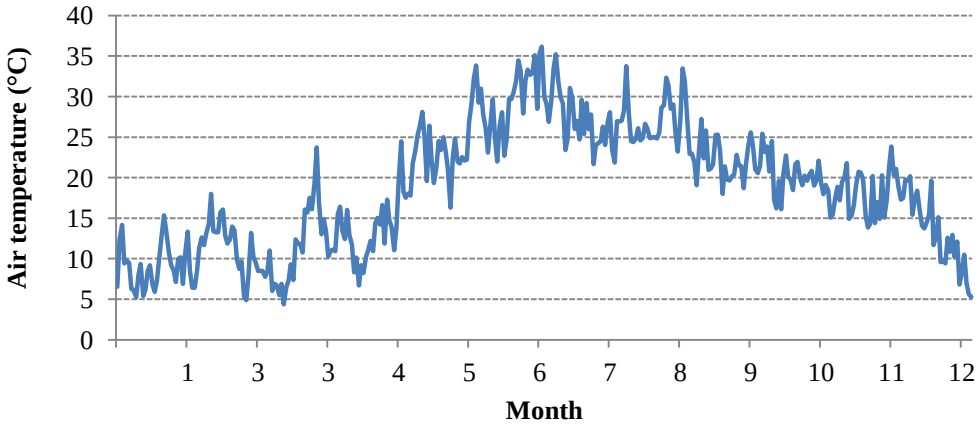

Fig. 2-10: An example of one-year simulated daily maximum air temperature in Slough in the 2080s in high emission scenario

Furthermore, Fig. 2-11 shows an example of one year of daily total solar radiation in the 2080s with a high emission scenario in Slough. The amount of solar radiation is higher

in the summer months than in other months. The amount of solar radiation drops in May and June when there is significant rainfall.

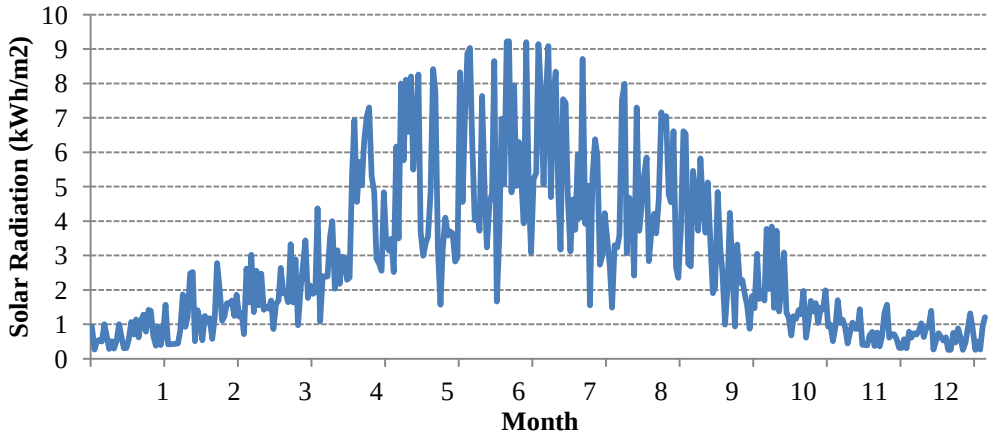

Fig. 2-11: An example of one-year simulated daily total solar radiation in Slough in the 2080s in high emission scenario

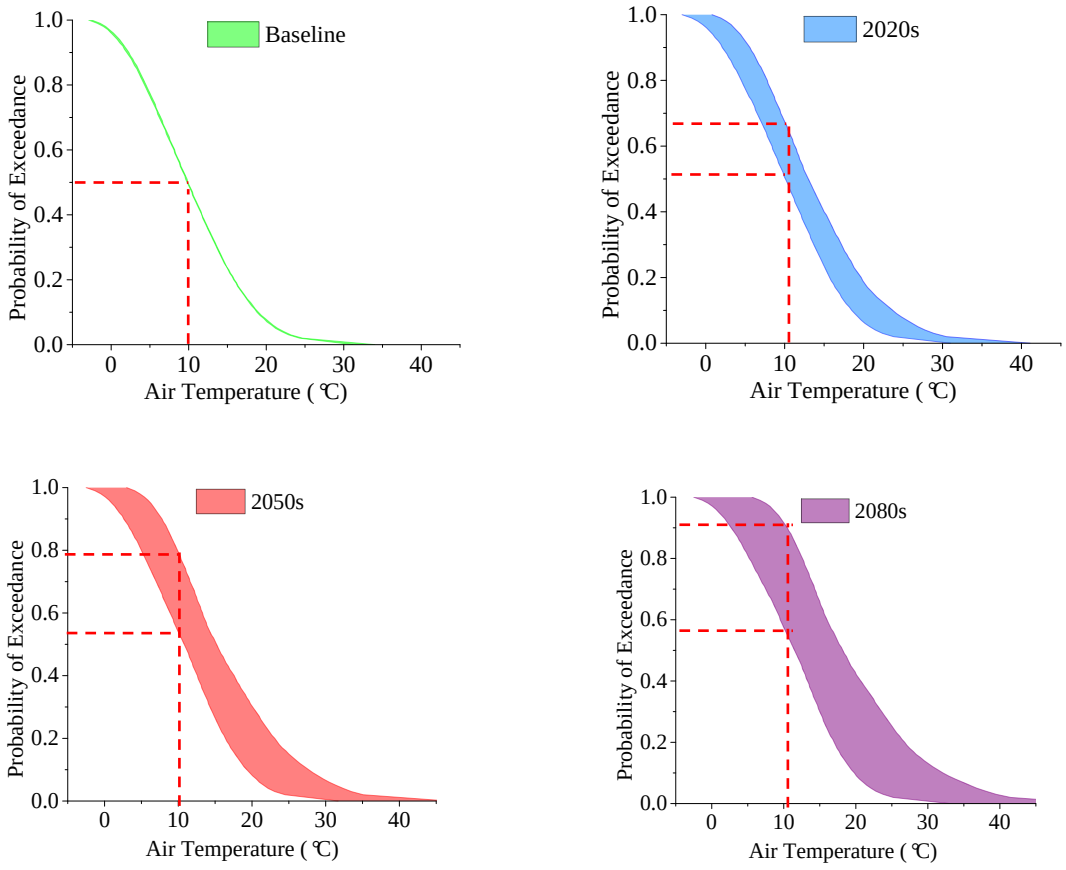

Fig. 2-12: Simulation results of annual air temperature distributions in Slough in high emission scenario.

Within each timeframe of 30 years, the hourly air temperatures can be presented as a probability distribution of exceedence of air temperature. The simulated air temperatures presented in such a distribution including the baseline and moving through to the 2080s are shown in Fig. 2-12. Each variant provides one such probability distribution. As 1,000 variants of future climate projections are used, the shaded areas illustrate the range of these probability distributions in each period. As shown in Fig. 2-12, the air temperatures in the future are likely to increase. For example, there is about a 50% probability that the temperature is over 10 ℃ in the baseline climate. The probability of exceeding 10℃ becomes 51%-68% and 54%-80% in the 2020s and the 2050s. In the 2080s, there is a 58%-92% probability that the hourly air temperature will exceed 10 ℃. Combining all central prediction estimations that are used to make up Fig. 2-12 produces the projections for each period shown in Fig. 2-13. It can be seen that the temperature distribution remains the same shape but shifts to the right side.

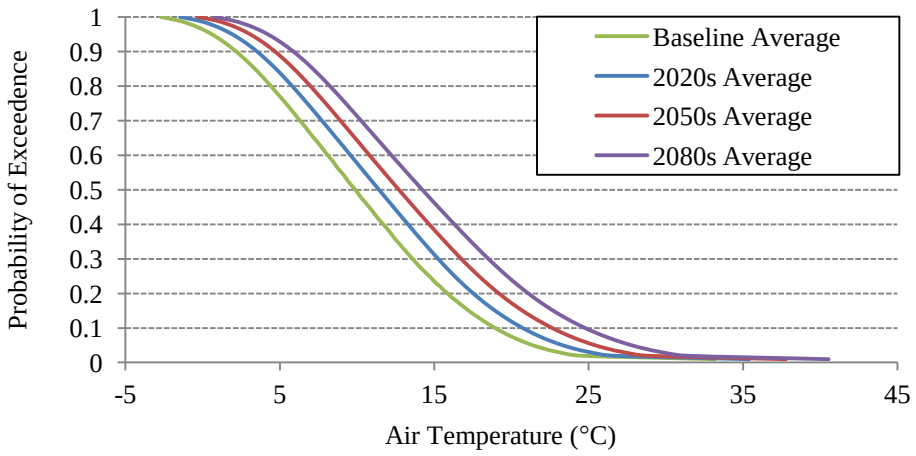

Fig. 2-13: Central estimation of annual air temperature distributions in Slough in high emission scenario in different periods.

2.4 Wind Model

Since the wind information generated from the climate models is usually considered as unreliable by the Met Office, it is not included in the UKCP09 climate projections. At the same time, wind speeds are not thought to vary in the future climate scenarios as there is no solid evidence to suggest how they will change. Therefore, the wind speed

used in this thesis is a resample of the historical records provided by British Atmospheric Data Centre (BADC) [61].

2.4.1 Wind Re-sample Method

The re-sampled wind data is taken from three observation stations across the UK: Leuchars (North Scotland), Leeming (Northwest England) and Heathrow (Southeast England) [62]. It should be noted that these three locations are not the same as those chosen for data simulation in UKCP09 WG. They are selected since the wind re-sampling requires at least 30 years of complete historical hourly wind records, and they should all have a full simultaneous hourly record between 1973 and 2010. For the purposes of this study, the wind profiles at Leuchars, Leeming and Heathrow are used as reasonable substitutes for those at Edinburgh, Manchester and Slough, respectively.

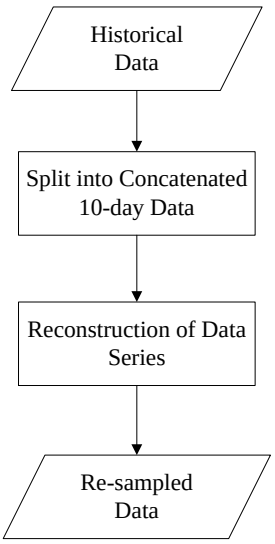

Fig. 2-14: Illustration of wind re-sampling process

The re-sampling process is illustrated in Fig. 2-14. Firstly, the historical wind records are split into 10-day concatenated hourly data series tagged with the date at which the winds were recorded. The choice of 10-day record lengths ensures that the temporal correlation structure of the re-sampled record is close to that of the historical record. The new wind series are then reconstructed by sampling the 10-day concatenated data randomly and are fitted into the new series according to the time tags. This preservation

of time of day and year ensures that the mean re-sampled wind speed corresponds to the historical mean wind speed. With such a process, a 30-year hourly re-sampled wind series is produced for each location.

The re-sampling process is repeated 100 times to generate 100 versions of wind series which will be used later and will be combined with the air temperature and solar radiation series from UCKP09 WG to produce different possible weather scenarios. It should be noted that the re-sampled wind is not in consistent with the data from WG. However, the worst case combinations can be reasonably expected to be seen owing to the number of combinations used in this thesis.

2.4.2 Example Re-sampled Wind Profile

The probability distribution of the wind speeds recorded at Leuchars, Leeming and Heathrow are presented in Fig. 2-15, Fig. 2-16 and Fig. 2-17, respectively. The re-sampled data have exactly the same probability distributions at each location as the original regions. It can be seen that Leuchars is the most windy whilst Heathrow is the least. The wind speeds at Leuchars and Leeming rarely exceed 15 m/s. The wind speeds at Leuchars have more probability over 10 m/s than those at Leeming. At Heathrow, the wind speeds are rarely over 10 m/s.

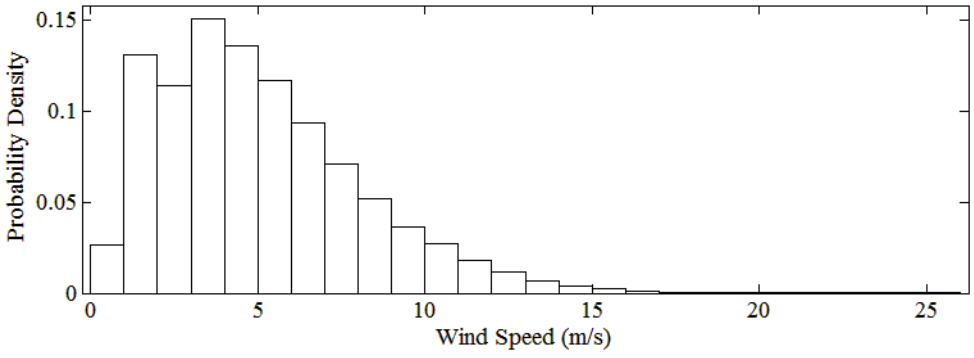

Fig. 2-15: Probability density distribution of wind speed at Leuchars.

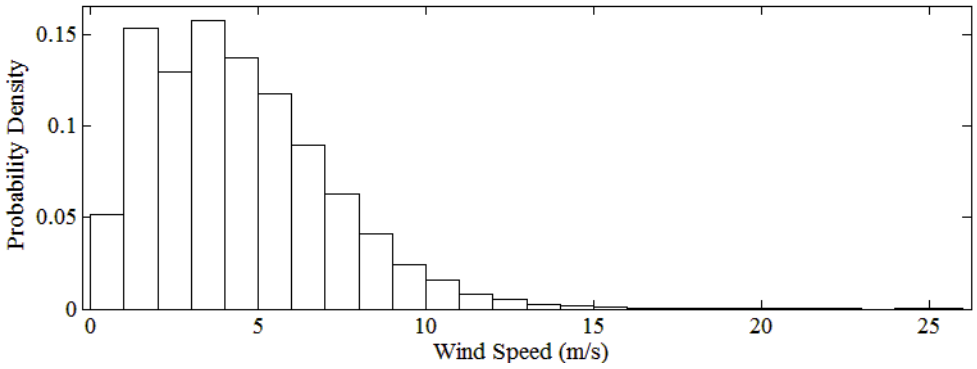

Fig. 2-16: Probability density distribution of wind speed at Leeming.

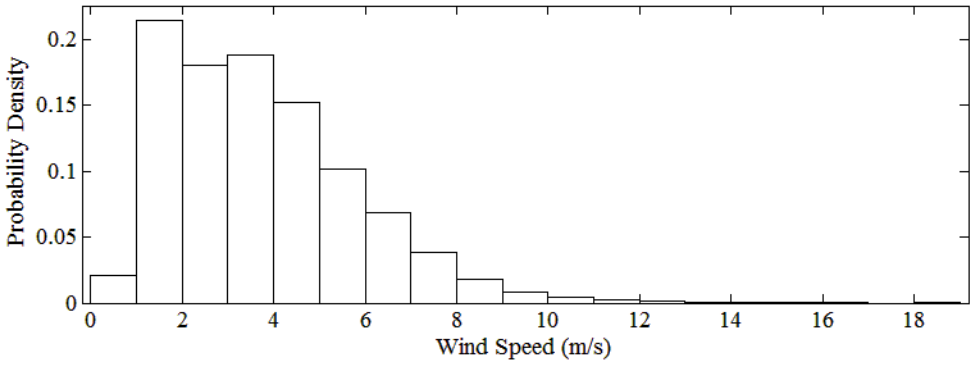

Fig. 2-17: Probability density distribution of wind speed at Heathrow.

The examples of re-sampled one-year hourly wind speeds at Leuchars, Leeming and Heathrow are given in Fig. 2-18, Fig. 2-19 and Fig. 2-20, respectively. Each presented wind series contains 8760 hours of wind speeds from 1st January (hour number 0) to 31st December (hour number 8759). As shown in the figures, the high wind speeds can occur throughout the year but the extremely high wind speeds (as highlighted in red circles) are more likely to take place in the winter months.

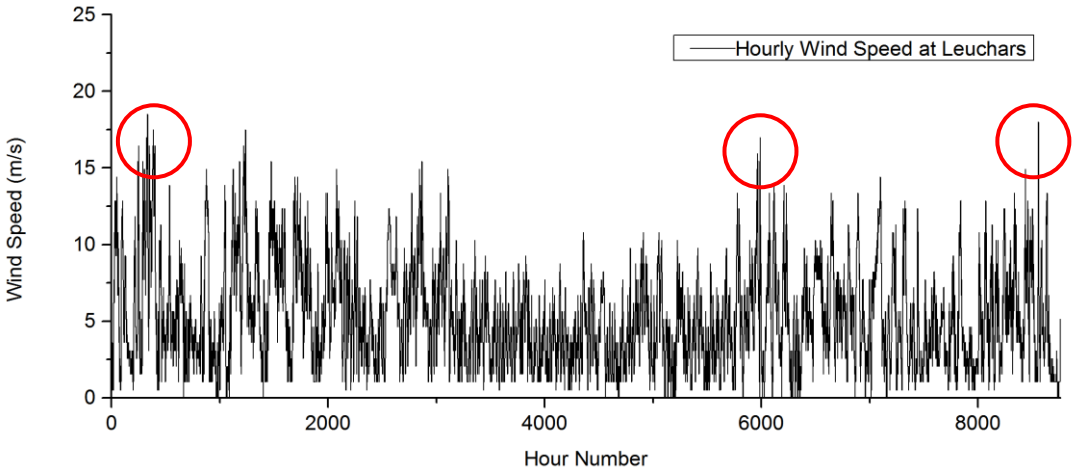

Fig. 2-18: Example of one-year wind speed series at Leuchars.

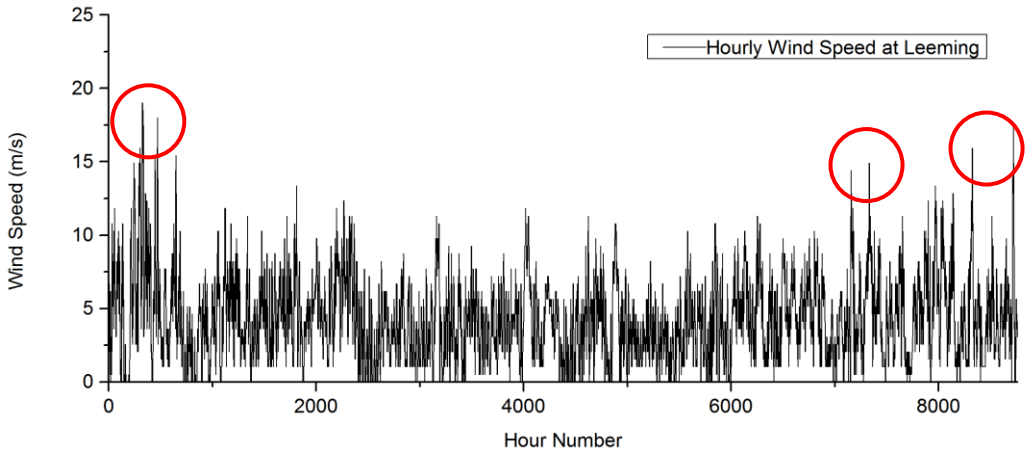

Fig. 2-19: Example of one-year wind speed series at Leeming.

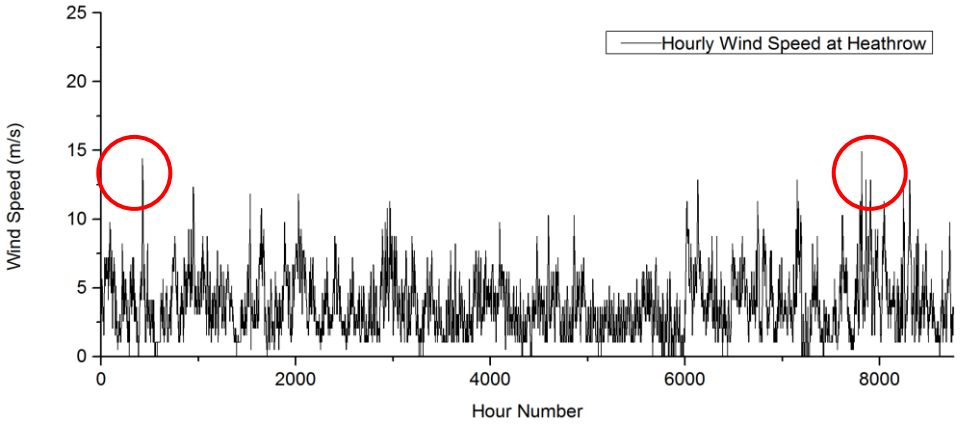

Fig. 2-20: Example of one-year re-sampled wind speed at Heathrow.

2.5 Soil Temperature Model

2.5.1 Model Description

To calculate cable ratings, the temperatures of soil layers at different depths are obtained from the modified dynamic model based on [63]. Unlike most of the models using the experimental approach, this model is derived from physical laws to ensure that it is compatible with different soil environments.

As illustrated in Fig. 2-21, the model simulates the process of the heat transfer on the surface of the soil and in the ground. The temperature of the soil at the deepest layer (20 m depth) is assumed to be 12 °C and remains constant, irrespective of weather conditions or the time of the year. At the ground surface, the heat transfer depends on solar radiation heat gain and convection heat loss. The heat flux is determined by the thermal capacity and thermal resistance of the soil as well as the temperature difference between layers.

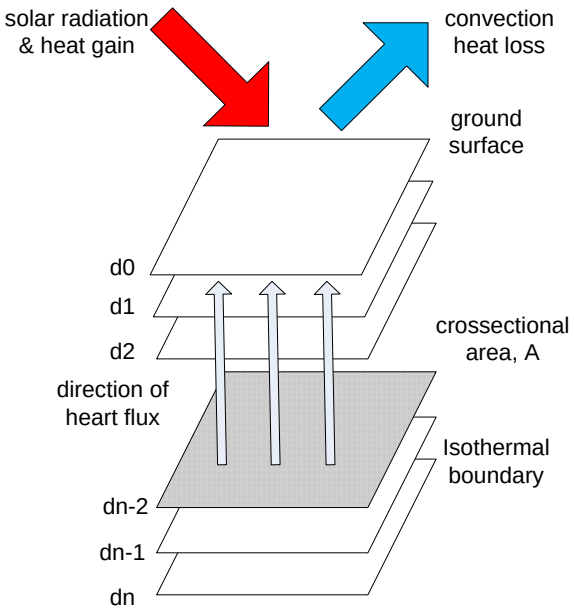

Fig. 2-21: Illustration of heat transfer in soil temperature model.

2.5.2 Model Operation

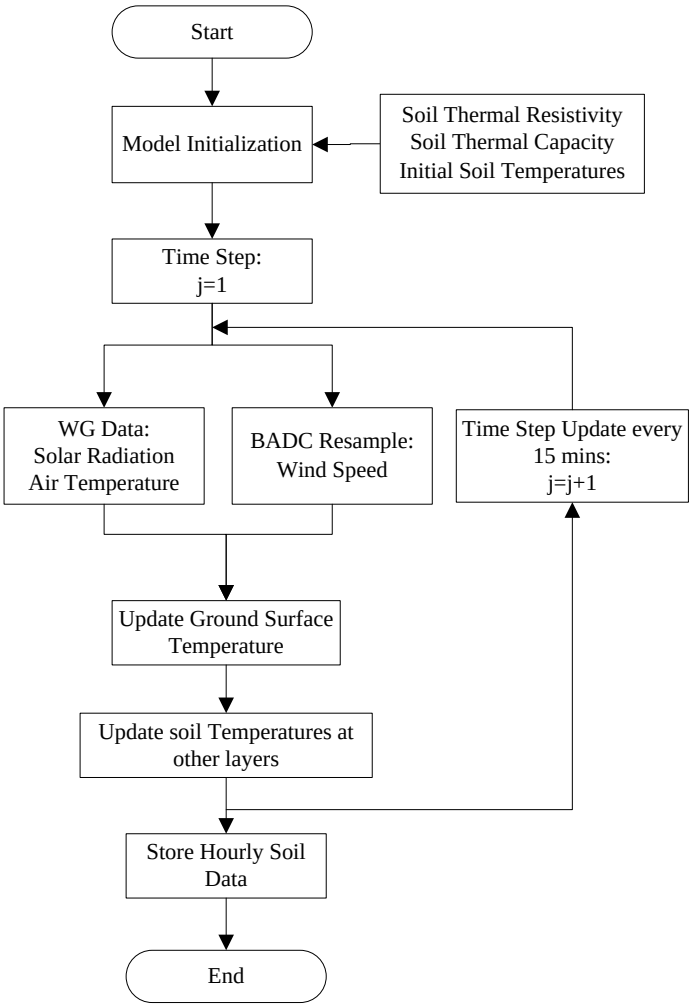

Fig. 2-22: Flow chart of soil temperature model operation.

The soil temperature model operates as a dynamic model updating the soil temperatures with the time steps. Fig. 2-22 shows the flow chart of the model's operation. The soil properties, such as initial soil temperatures at different layers, thermal resistivity and thermal capacity, are set as the constant at the model initialization stage. After initialization, the model calculates the soil temperatures with a time step of 15 minutes. In each time step, the ground surface temperature is firstly updated based on the weather data extracted from WG and BADC resample. The soil temperatures at other layers are then updated following the heat flow between the ground surface and constant deepest soil layer. As the soil temperature does not change much within 15 minutes, only the

temperature at the end of each hour is stored to minimize the dataset size and save the computational time of cable rating calculation at the next stage.

2.5.3 Modeling of Heat Flow Process

A series of equations derived from the physical laws are used to describe the heat flow process in this model and to calculate the soil temperature. The details of the equations can be found in [52].

2.5.3.1 Heat Exchange at Ground Surface

The ground surface is defined as the first layer of the soil. The net heat exchange at the ground at the jth time step can be defined as

$$q_{j,1=}q_{sr_j} + q_{cr_j} \tag{2-1}$$

where q_{sr} is the heating due to solar radiation and q_{cr} is the convective heat flux.

The value of q_{sr} can be gained from the WG and is a sum of the diffuse irradiation and the direct irradiation. The convection heat flux, q_c, can be calculated with (2-2) below

$$q_c = h_c(\theta_{gr} - \theta_{air}) \tag{2-2}$$

where θ_{gr} and θ_{air} are the temperature of ground surface and air at the previous time step. h_c is the convective heat transfer coefficient given by

$$h_c = 6 + 4.6v \tag{2-3}$$

where v is the wind speed with unit m/s.

The expression of h_c is obtained from experimental data measured at Poona, India [52]. For UK conditions, (2-3) may lead to an overestimation of h_c since the difference between ground and air temperatures are likely to be larger with a warmer climate in India. However, no significant error is observed in the sensitivity analysis with the proposed expression [63]. It should be noted that the convective heat flux can be both positive and negative depending on the relative temperatures of the ground and the air.

2.5.3.2 Heat Flow Underground

The soil is modelled as a series of n horizontal layers at different depth, d, each of cross-sectional area A as shown in Fig. 2-21. The temperature of the kth layer can be determined every Δt seconds at jth time step as

$$\theta_{j,k} = \theta_{j-1,k} + \frac{\Delta t}{C_k}\left\{\frac{\theta_{j-1,k-1}-\theta_{j-1,k}}{R_{k-1}} + \frac{\theta_{j-1,k+1}-\theta_{j-1,k}}{R_k}\right\} \quad (2\text{-}4)$$

$for\ 2 \le k \le n-1$

where C_k is the thermal capacity of the kth layer which can be defined as

$$C_k = C_v A(d_k - d_{k-1}) \quad (2\text{-}5)$$

C_v is the volumetric heat.

R_k is the thermal resistance of the kth layer which can be defined as shown in (2-6), and θ is the temperature. ρ is the thermal resistivity.

$$R_k = \frac{\rho(d_k - d_{k-1})}{A} \quad (2\text{-}6)$$

For the ground surface (the first layer), the temperature is calculated with the equation below where $q_{j,1}$ is the net heat exchange given in (2-7).

$$\theta_{j,1} = \theta_{j-1,1} + \frac{\Delta t}{C_0}\left\{\frac{\theta_{j-1,2}-\theta_{j-1,1}}{R_0} + Aq_{j,1}\right\} for\ k = 1 \quad (2\text{-}7)$$

As introduced in Section 2.5.1, the temperature of deepest layer, $\theta_{j,n}$, is 12 °C constantly.

2.5.4 Model Validation with BADC Historical Data

2.5.4.1 BADC Historical Data

As the model was developed based on the observed data in India, it is important to verify the accuracy of the model with UK weather conditions. The UK weather data used for the validation is obtained from "Met Office – MIDAS Land and Marine Surface Station Data [62]" on the BADC website, the details of which are listed in Table 2-2. The observed air temperature, wind speed and global solar radiation are fed into the model to calculate the soil temperatures at the specified depths. The calculated soil temperatures are then compared to the observed soil temperature data to evaluate the accuracy of the model.

Table 2-2: Details of BADC data

Weather Parameter	Form	Unit	BADC Table Name
Air temperature	Hourly data	℃	WH
Wind speed	Hourly data	Knot/s	WH
Global solar radiation	Hourly data	KJ/m^2	RO
Soil temperature	Daily data. Measured at 0.3 m and 1 m at 9 a.m.	℃	ST

BADC deploys a number of observation stations covering the whole UK. To select an appropriate station for the validation, the criteria are set as follows:

- The selected station should have the sensors installed to measure all of the above four parameters.

- The station should not be located in an urban area, where the constructions and human behaviour can affect the soil temperatures, and the transmission cable system is not installed.
- As the model is iteration based, the input weather data stream should be continuous.
- A minimum data length of two years is desired as the model requires an initialization period of one month approximately. The two-year data can ensure the results cover all the seasons for a further study.
- The location of the selected station should be as near as possible to Slough, the key studied location in the project.

The observation station located in the Beaufourt Park, Bracknell, which matches all the listed criteria, is selected. The weather data observed from 1990 to 1991 at this station is used for the validation.

2.5.4.2 Model Validation

The validation process is as follows: firstly, the observed weather variables from BADC along with the assumed values of the soil thermal resistivity from National Grid are fed into the soil temperature model as inputs. Secondly, the simulated soil temperature at 0.3 m and 1 m depth are compared to the observed data. The model is validated only when the error between the simulation results and the observed data is within the acceptable range.

a) Assumption of the soil thermal resistivity

Soil thermal resistivity and volumetric heat capacity are two important soil properties which have a large influence on the thermal behaviour of the soil. Both of these two parameters are determined on the soil moisture level. For the same type of soil, the drier one has a higher thermal resistivity and a lower volumetric heat capacity and vice versa. However, these two parameters are very hard to calculate since they are different

according to the soil type and they change frequently with the complicated interaction of the atmospheric and geographic conditions.

The soil thermal resistivity and volumetric heat capacity used in this model are obtained from TGN(T) 67 [51]. The former is taken as 1.2 Km/W as a conservative consideration. The latter is assumed to be 1.7 MJ/m^{3}K which corresponds to a dry density of 1795 Kg/ m^3 and a moisture content of about 3 % by dry weight.

b) Validation Results

The validation results for the soil temperatures at 0.3 m and 1 m are shown in Fig. 2-23 and Fig. 2-24, respectively. It can be seen that the output from the model is in very good agreement with the observed 9 a.m. data after an initialization period, which is caused by the assumption that all the soil layers are at 12 °C at the beginning. The initialization periods for 0.3 m and 1 m soil layers are around half a month and one month respectively. The initialization period is shorter for the soil temperatures at 0.3 m as it is closer to the ground layer and has a faster heat flow rate, whilst the deeper soil layer at 1 m is better isolated by the other soil layers above it and its temperature changes more slowly.

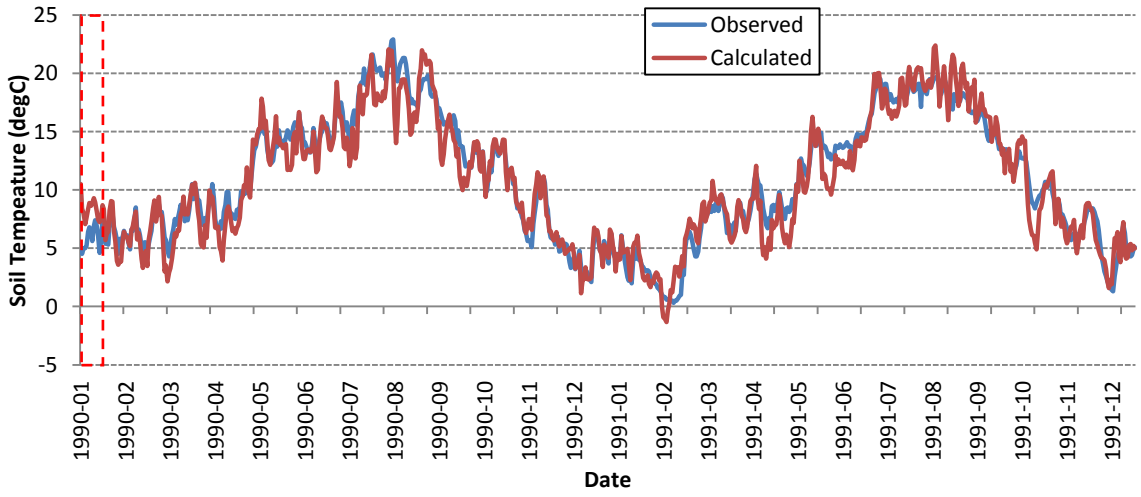

Fig. 2-23: Validation of the soil temperature model at 0.3 meter depth.

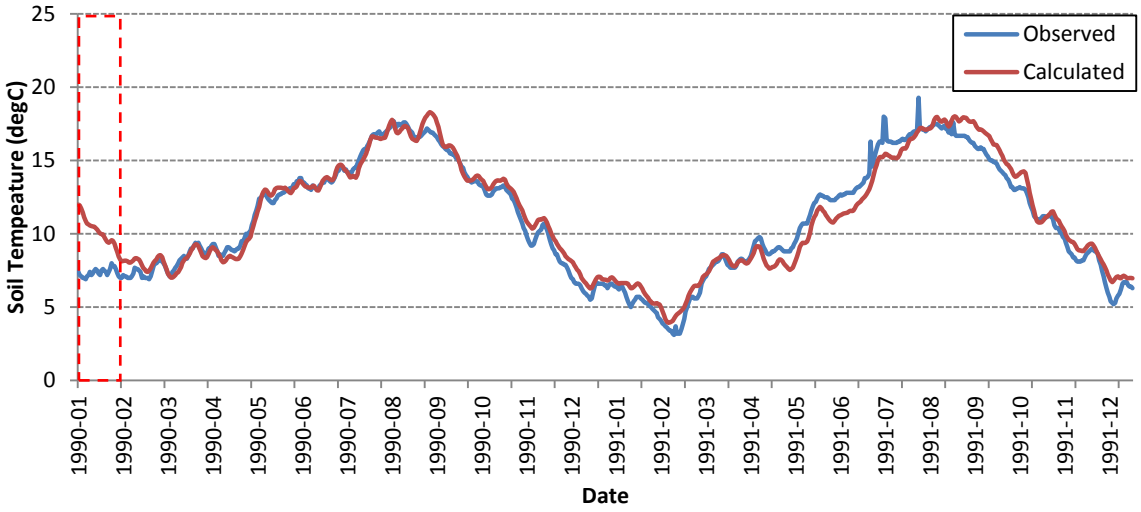

Fig. 2-24: Validation of the soil temperature model at 1 meter depth.

In each month, the average error is calculated from the absolute values of the difference between the observed data and calculated data, and is listed in Table 2-3. As highlighted in the table, the maximum value of average error, 1.91 ℃, occurs in 1990-8 at the depth of 0.3 m. However, the average error at 1 m depth in the same month is only 0.36 ℃. This is because the top soil layers' thermal resistivity and heat capacity change more frequently than the deeper layers. As these soil properties are set as constant in the model, the greater mismatches exist between the set properties and the real ones at the top layers, and therefore cause greater errors.

Table 2-3: Error between observed data and output data

Month	Average Error at 0.3 m (℃)	Average Error at 1 m (℃)
1990-1	1.68	2.73
1990-2	0.62	0.64
1990-3	1.10	0.23
1990-4	1.04	0.45
1990-5	1.05	0.37
1990-6	0.70	0.13
1990-7	1.68	0.32
1990-8	1.91	0.36
1990-9	1.41	0.48
1990-10	0.44	0.46

Month	Average Error at 0.3 m (℃)	Average Error at 1 m (℃)
1990-11	0.71	0.82
1990-12	0.56	0.71
1991-1	0.72	0.65
1991-2	1.31	0.75
1991-3	0.80	0.30
1991-4	1.28	0.54
1991-5	1.37	1.10
1991-6	1.34	1.27
1991-7	0.85	1.05
1991-8	1.22	0.40
1991-9	1.05	1.30
1991-10	1.35	0.77
1991-11	0.63	0.59
1991-12	0.97	0.75

2.5.5 Example Outputs

The model described in this section can be used to calculate the future soil temperature based on future air temperature and solar radiation simulated from WG and re-samples of wind from historical records. The example of a time series of simulated soil temperature has been shown in the last section compared to the observed data for the model validation. In this section, the simulated soil temperature at Slough is taken as an example to show how the future soil temperature changes.

The simulated hourly soil temperatures at 1 m depth are presented in the form of probability of exceedance in Fig. 2-25. The soil temperature simulated based on each UKCP09 WG variant provides one such probability distribution. The shaded areas illustrate the range of the soil temperature distributions from soil temperature model outputs based on 1000 WG variants. As shown in Fig. 2-25, the soil temperatures are likely to increase in the future. For example, there is about a 25% probability that the temperature is over 15 ℃ in the 1000 baseline climate projections. The probability of exceeding 15℃ becomes 25%-50% and 33%-67% in the 2020s and the 2050s. In the

2080s, there is a 38%-98% of probability that the hourly soil temperature will exceed 15 ℃.

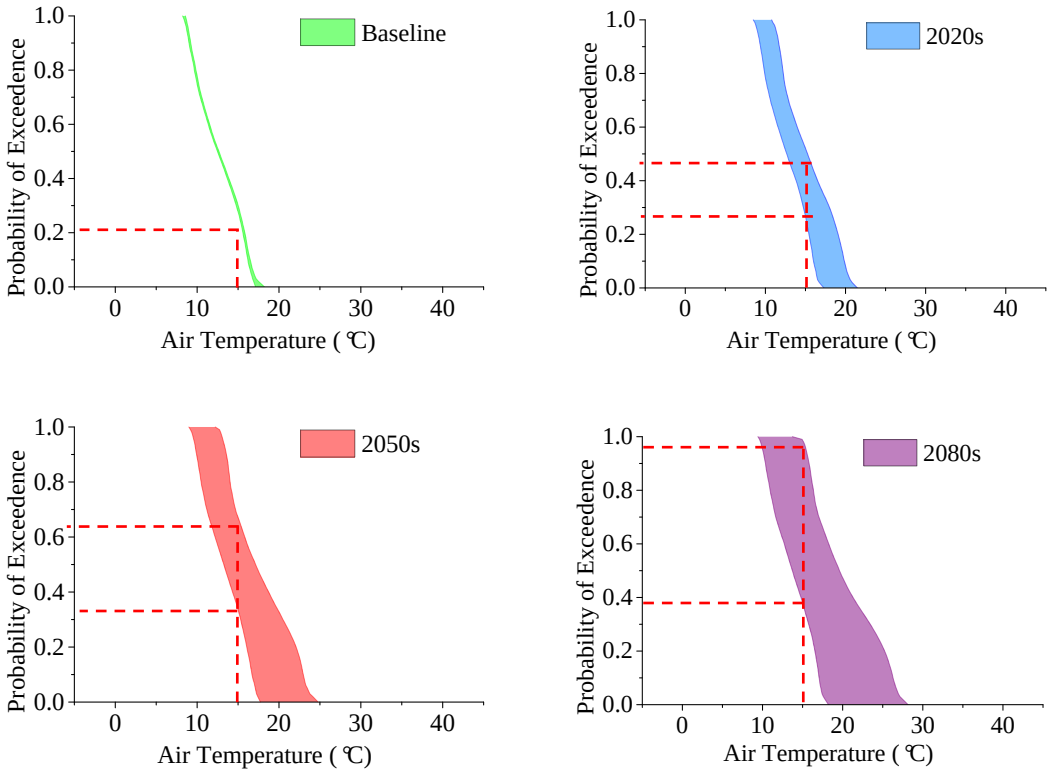

Fig. 2-25: Simulation results of annual soil temperature distributions at 1 meter depth in Slough in high emission scenario

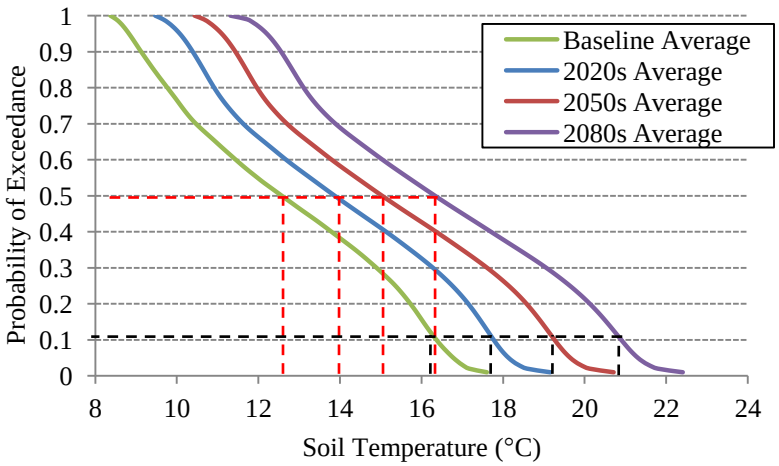

Fig. 2-26: Central estimation of annual soil temperature distributions at 1 meter depth in Slough in high emission scenario in different periods

Fig. 2-26 shows the central estimation of the soil temperature distributions taken from Fig. 2-25 in four periods. The distribution of soil temperature shifts to the right from the baseline through to the 2080s. The 50% probability of exceedance of soil temperature increases from 12.57 ℃ to 16.33 ℃ (by 29.91%) from baseline to the 2080s. For the same period, the 10% probability of exceedance goes up from 16.37 ℃ to 20.90 ℃ by 27.67%.

2.6 Soil Moisture

The soil moisture can affect the surrounding environment of an underground cable by changing the soil thermal resistivity and thermal capacity. Unfortunately, the moisture migration is an extremely complex process involving precipitation, vegetation, solar radiation, soil type and temperature, underground water system, etc. This makes it very difficult to be modelled.

The only information about the future changes in soil moisture is the outputs from UKCP02 RCM runs [64]. These outputs are also based on A1B IPCC SRES emission scenario A1B, namely medium emission scenario, as that used in UKCP09. However, unlike UKCP09, the climate projections provided by UKCP02 were not probabilistic. Only 11 variants are used to configure the UKCP02 RCM and produce 11 projections. Among these 11 projections, the one configured by the variant, HadRMQ16, provides the greatest climate changes with an estimation of temperature rise of 7.1 ℃ which is even higher than that rise of 5 ℃ given in UKCP09 for the southeast of UK at 50% probability level, in the same emission scenario. Since a higher temperature usually leads to a drier soil condition, the projection of moisture changes based on the HadRMQ16 variant is considered as the most unfavourable case.

In this section, silty clay is taken as an example to demonstrate the change of soil moisture content from the 2000s to the 2080s. The change of soil thermal resistivity, as an important property of soil which depends on the moisture content and is crucial for the later use of cable rating calculations, is also explored based on the UKCP02 moisture data.

2.6.1 Moisture Changes

Fig. 2-27 presents the daily soil moisture simulated from the HadRMQ16 variant in cumulative probability. The soil moisture data are provided in weight of water in per cube meter of soil at1m depth and 2m depth, respectively. It can be seen that the soil is wetter at 2m depth than that at 1m depth. It can also be observed that soil is drier in the 2080s than that in the 2000s. The average moisture (at 50 percentile) will decrease from 28.50 kg to 27.37 kg by 3.95% at 1m depth. At 2m depth it will decrease from 69.04 kg to 67.09 kg by 2.83%. The decreases of moisture are 4.46% and 1.01% at 1m and 2m depths, respectively, at 10 percentile at which the soil is dry and considered to be in a relatively worse case.

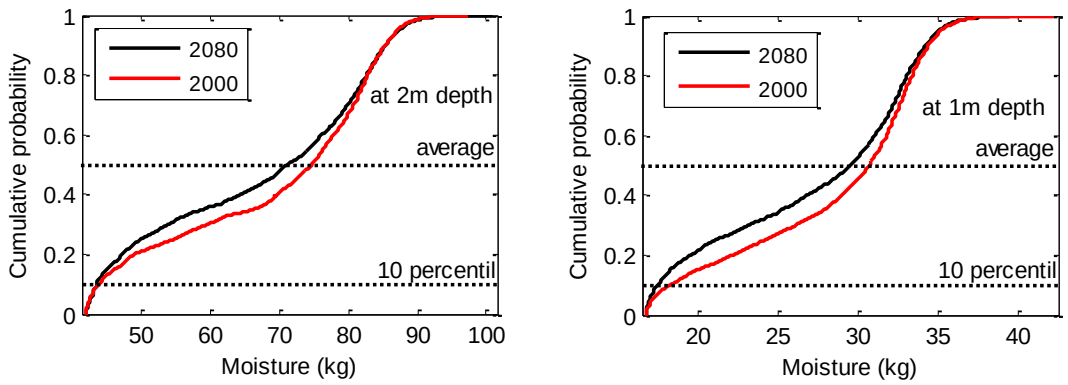

Fig. 2-27: Cumulative probability of daily soil moisture at 1m and 2m depths in the 2000s and 2080s

Silty clay is taken as an example to demonstrate its changes in soil moisture content. The density of silty clay is 1601kg/m^3. Given the density of the soil, the soil moisture content can be calculated as the percentage of the weight of water over the sum of the weight of soil and water and is presented in Fig. 2-28. As shown in the figure, the soil moisture content at 1m depth will decrease from 1.78% to 1.71% on average, and from 1.14% to 1.09% at 10 percentile, from the 2000s to the 2080s. At 2m depth, the decreases will be from 4.31% to 4.19% on average and will be from 2.74% to 2.71% at 10 percentile.

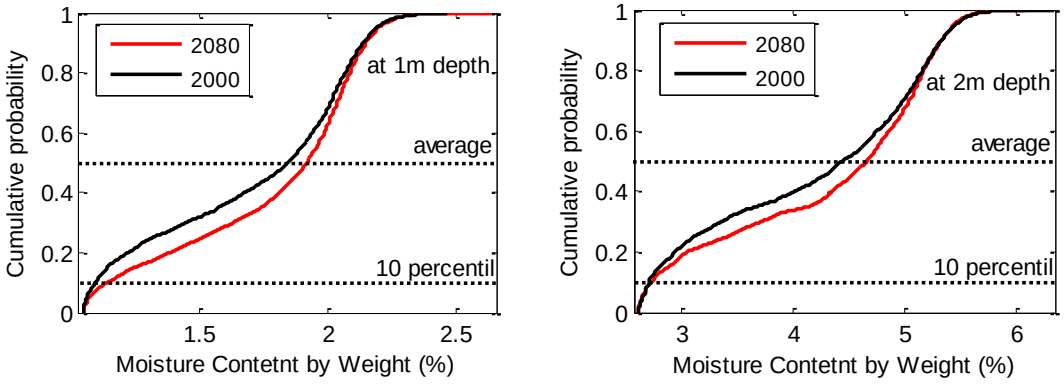

Fig. 2-28: Cumulative probability of daily soil moisture content by weight at 1m and 2m depths in the 2000s and 2080s

2.6.2 Soil Thermal Resistivity Changes

Given the soil moisture content in Section 2.6.1, the soil thermal resistivity is calculated according to the thermal resistivity curves provided in IEEE Std 442-1981 [65]. These curves are measured with an experimental approach and are shown as the discrete data points. To obtain the soil thermal resistivity as a continuous function of moisture content, the curve fitting technique is applied. As shown in Fig. 2-29, the polynomial fitting is adopted and shows a perfect fitting for Silty Clay's thermal resistivity curve.

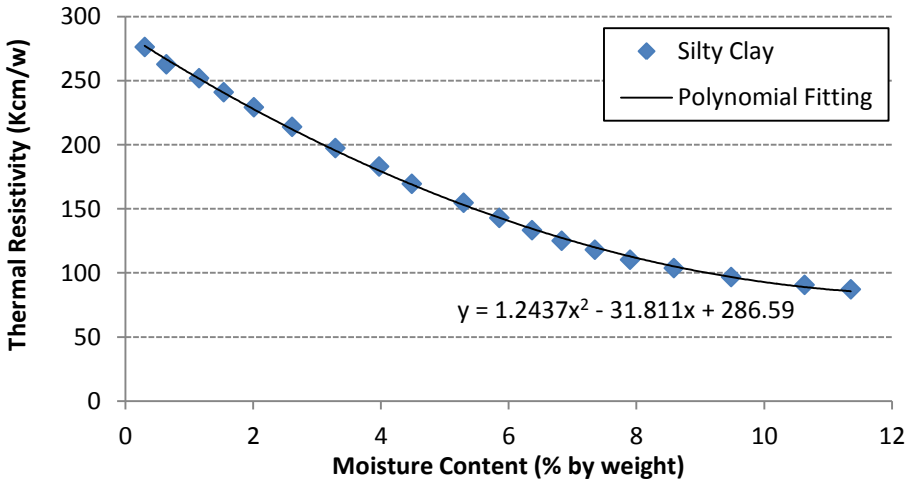

Fig. 2-29: Soil thermal resistivity of Silty clay as a function of moisture content by polynomial fitting.

The soil thermal resistivity is obtained by mapping the soil moisture content present in Section 2.6.1 to the thermal resistivity curve described in Section 2.6.4. The higher the thermal resistivity is, the drier the soil. As presented in Fig. 2-30, the change in the soil thermal resistivity is very small even with a great climate change level from the UKCP02 HadRMQ16 variant. On average, the soil thermal resistivity only has a slight increase from 234 to 236 K.cm/W by 0.84% at 1m depth, and from 174 to 176 K.cm/W by 1.54% at 2m depth. In the worse cases in which soil thermal resistivity is at 95 percentile, the increase is even smaller, i.e. by 0.58% and 0.34% at 1m depth and 2m depth, respectively. The results indicate that the soil thermal resistivity will be affected very slightly in the future climate. This can be explained by the effect of temperature rises which force a drier soil condition to be offset by the increase in rainfall. In conclusion, the existing soil thermal resistivity adopted for cable rating calculations can still be used in the future cases even in the context of climate change.

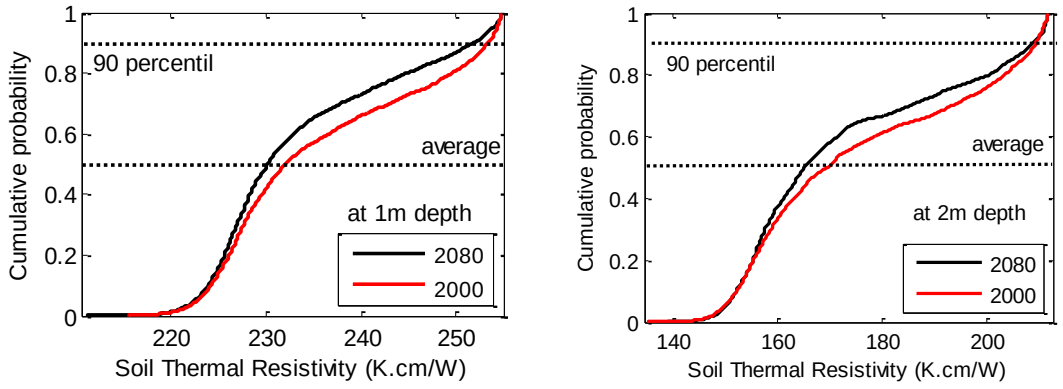

Fig. 2-30: Cumulative probability of daily soil thermal resistivity at 1m and 2m depths in the 2000s and 2080s

2.7 Summary

This chapter presented the climate simulation methodologies and simulation results which will be used throughout the thesis for the assessment of impacts of climate change on power systems and components.

The chapter began with an overview of the climate simulation process used in this thesis.

In this process, the future projections of six weather variables, including air temperature, solar radiation, wind speed, wind direction, soil temperature and soil moisture, are generated from five sources, namely UKCP09 projections, UKCP09 Weather Generator, wind model, soil temperature model and constants assumptions made for soil moisture and wind direction. Five separate sections are used to describe each of the sources. Each section of the first four sources starts off by introducing the principles of the models, then describes the implementation of them for the studies in this thesis, and finally gives example simulation results of the future climate projections. The last section of this chapter presents the study on the soil moisture and thermal resistivity based on UKCP02 RCM runs. The results show that they will experience minor changes even in the worst scenarios. Therefore, they are assumed to be constants and use the same values as the existing ones. Values suggested by the industrial standards that are based on the practice of historical observation.

In the remaining chapters, the air temperature, solar radiation, and wind speed and direction will be used to calculate the ratings of overhead lines. Soil temperature and moisture will be used to calculate the cable ratings. Furthermore, air temperature will be used as the only weather parameter for the calculation of transformer rating and ageing.

Chapter 3 Power System Components Modelling

In this chapter, the thermal modelling of the three power system components, overhead line, cable and transformer, are presented. For each of these components, the thermal model is well developed and verified in various published standards, including IEEE, IEC and CIGRE. Difference exists in the models among different standards depending on the choices of parameters, values of coefficients, complexity of the models and etc. This chapter reviews and compares the models in different standards and select the ones for the use of this research according to data source availability and suitability of the system development.

3.1 Overhead Line

Overhead lines are air insulated transmission lines suspended between towers or poles. To avoid the flashover between overhead lines and other objects (e.g. ground, roof, trees and etc.), the safety regulations set the minimum clearances according to different voltage levels. This clearance is defined as the distance between the lowest point of line sag, which is usually at the mid-span, and other objects.

The overhead line sag (L_{sag}) are affected by three factors: the span length (L_{span}), the tension (F_t) and the perpendicular force (F_p) applied to the conductor which is the sum of the weight of conductor itself, the wind pressure and ice or snow covered. It can be roughly calculated with Equation (3.1) as below:

$$L_{sag} = \frac{F_t}{F_p}\left[cosh\left(\frac{F_p L_{span}}{2F_t}\right) - 1\right] \cong \frac{F_p L_{span}^2}{8F_t} \tag{3.1}$$

Moreover, the tension (F_t) is affected by the overhead line conductor temperature. When the conductor temperature rises, it is increased as a result of thermal expansion. Therefore, it is necessary to solve the thermal-tensional equilibrium of the overhead line conductor shown in Equation (3.2):

$$E_c A_c \beta_c (T_{c2} - T_{c1}) + \left(\frac{F_{p_1}^2 L^2 E_c A_c}{24 F_{t_1}^2}\right) - F_{t_1} = \left(\frac{F_{p_2}^2 L^2 E_c A_c}{24 F_{t_2}^2}\right) - F_{t_2} \tag{3.2}$$

3.1.1 Thermal Modeling

The rating of an overhead line is defined as its maximum current carrying capacity which is constrained by the designed rated conductor operating temperature and the ambient weather conditions. The exceedence of this rated temperature will cause an unexpected excessive elongation of overhead line. This will lead to an increase of sag violating the safety regulations. To maintain the line working at this rated temperature, the heat balance equation needs to be solved to calculate the rating of an overhead line at the given environmental conditions. The heat balance equation is given in (3.3) as below:

$$I^2 R(T_c) + q_s = q_c + q_r \tag{3.3}$$

It can be seen from Equation (3.3) that the conductor gained heat from two sources which are Joule heating ($I^2 R(T_c)$) and solar heating (q_s). Joule heating is the main source of heat gain and is depended on the current and resistance of the conductor. Solar

radiation varies through the day and seasons and is affected by the cloud covering condition. The abosorptivity of the conductor surface also have an influence on solar radiation heating gain. In the meantime, the conductor is cooled through two ways. One is forced convection heat loss (q_c) which is caused by the wind and can be affected by wind speed and direction. The other is radiated heat loss (q_r) depending on the emissivity of the conductor and ambient air temperature.

3.1.2 Comparison of Rating Standards

The thermal models are developed to calculate overhead lines' rating according to its specifications and environmental conditions. These models are described in standards to provide guidance to manufacturers and power system designers. Two standards and one technical guide currently used in the industry are compared within this section, including:

- IEEE Std 738-2006 [66]
- IEC TR 61597-1995 [67]
- CIGRE WG 22.12, ELECTRA No. 144 [68]

The models in all the three standards are built based on the heat balance equations. IEEE and IEC standards use the equation (3.3) shown in the last section. CIGRE adopts a more complex equation which involves magnetic heating (q_m), corona heating (q_i) and evaporative cooling terms (q_w). The CIGRE heat balance equation is shown below:

$$I^2R(T_c) + q_m + q_s + q_i = q_c + q_r + q_w \tag{3.4}$$

a) Common Terms

All the balance equations in these three standards contain the four terms in: Joule heating, solar heating, radiated cooling and convection cooling.

Regarding the electric resistance (R) at conductor temperature (T) in the Joule heating calculation, all the three standards use a linear correction equation to present the relationship between conductor resistance and its temperature, as shown in Equation

(3.5). The coefficient $\propto_R$ varies depending on different material of the conductor. The values of $\propto_R$ are suggested in [69].

$$R(T_c) = R(T_0)[1 + \propto_R (T_c - T_0)] \tag{3.5}$$

In terms of the solar heating (q_s), all the three models propose the similar calculation method described in Equation (3.6), where $\propto_{abs}$ is absorption factor, D_c is conductor diameter, and S_r is solar radiation. Absorption factor $\propto_{abs}$ is in the range from 0 to1 and typically varies from 0.3 to 0.9 for new and old conductors respectively. Both IEEE and CIGRE standard provide the method for calculating the solar radiation (S_r) based on latitude, altitude, atmosphere condition, time and date. IEEE standard only considers the heat directly from the sun, whilst CIGRE standard also takes reflected radiation and defuse radiation into consideration. Therefore, the solar heating calculated from CIGRE standard is slightly higher (10% - 15%) than that from IEEE [70].

$$q_s = \propto_{abs} D_c S_r \tag{3.6}$$

The radiated cooling (q_r) is calculated with the same formula suggested in three standards which is shown in Equation (3.7). From the equation, it can be seen that it is proportional to the Stephen-Boltzmann constant ($\propto_{em}$) and an emission constant (σ_{sb}). The value of σ_{sb} is in the range from 0.23 to 0.91 for new and old conductors, respectively, based on the empirical practice. The difference between conductor temperature (T_c) and air temperature (T_a) can also affect the radiated cooling.

$$q_r = \propto_{em} \sigma_{sb}[T_c^4 - T_a^4]\pi D_c \tag{3.7}$$

The convection cooling (q_c), is determined by both wind speed and wind direction. The three standards provide different models for its calculation. The major differences are the Nusselt number used for the different divisions of the wind speeds. The model in IEC standard is the simplest which only considers the laminar convection. IEEE standard and CIGRE standard take both laminar convection and natural convection into

consideration. In the IEEE standard, two formulas are provided to calculate the laminar convection cooling for low and high wind speeds respectively. However, no boundary has been set to distinguish the low and high speeds. Both formulas will be applied and the higher value will be taken as suggested. CIGRE model is the most complex one. It adds the turbulent convection cooling which is neglected in IEEE standard due to its minor importance in conductor temperature calculations. Apart from turbulent convection, the difference between the convection cooling calculated from IEEE and IEC standards is less than 4% at all laminar wind speeds [70]. When wind speed is less than 5 fps, CIGRE calculates a slightly higher convection cooling.Wind direction also plays an important role in the convection cooling calculation. The wind blowing in perpendicular to conductor is expected to bring more cooling than that in parallel to conductor. The effect of wind speed on forced convection Nusselt number is not considered in IEC standard. IEEE and CIGRE provide different formulas to calculate the Nusselt number as a function of wind direction. However, the differences between results from IEC and IEEE are very minor [70]. More details of these formulas and coefficients adopted can be found in the standards.

b) Different Terms

As mentioned previously, the heat balance equation in CIGRE model has three extra terms comparing to IEEE and IEC standards: magnetic heating, corona heating and evaporative cooling.

The magnetic heating term (q_m) is used to reflect the magnetic and skin effects on ferrous conductors only. As a result, this extra heating term causes a minor rating reduction typically between 0 and 3% [70].

Corona heating (q_i) is another term added to the heat balance equation in CIGRE model. This term is usually neglected when determining overhead lines ratings because that corona heating is only obvious when high voltage gradients exist on the conductor surface, which normally occurs only under a condition of high wind and heavy precipitation. Furthermore, the corona heating is offset by the high convective and evaporative cooling which also takes place at the same weather condition.

Even though the evaporative cooling term is presented in the CIGRE model, no calculation method is provided in the CIGRE standard. CIGRE states that evaporative cooling can be ignored generally because it is only significant when the conductor is totally wet. The evaporative cooling is minor from air born water vapor or water droplets flowing around the conductor under general environmental conditions.

IEEE Std 738-2006 [66] is chosen for overhead line rating calculation as CIGRE model [68] requires more weather parameters which can't be obtained, especially from climate change perspective, and IEC model [67] is short of convection cooling calculation under different wind conditions.

3.2 Cable

A cable conductor is insulated and protected by a series of layers of insulating materials and metallic protections. The structure of a cable usually consists of five layers: conductor, insulation, sheath, armouring and over-sheath. Conductor is used to carry the current; insulation prevents current flow from conductor to the earthed cable sheath; sheath provides a fault current path and mechanical protection for the insulation; armouring provides the strength of the cable; and over-sheath protects the cable against ingress and corrosion.

3.2.1 Thermal Modeling

The rating of a cable is defined as the current carrying ability at its maximum conductor operating temperature. This maximum operating temperature is constrained by the temperature limit of insulation layers which can be damaged when they are overheated. Furthermore, from the perspective of insulation ageing, the determination of the operating temperature also takes the service life expectation into consideration. The case in which the soil surround a buried cable is dried-out should be avoided, since overheat of conductor may occur because of an unexpected high soil thermal resistance and may damage its insulation.

The thermal ladder scheme is widely used in the cable thermal modeling as illustrated in Fig. 3-1. There are four heat sources in a cable thermal model. W_C is Joule heating generated by current in the conductor. W_d is the dielectric loss of the cable. W_s and W_a are the sheath loss and armour loss caused by circuit current and eddy current when the sheath and armour are made of metallic material.

Four thermal resistances are analogised in this model according to the layers of cable structure and surrounding environment. As shown in Fig. 3-1, T_1 is the thermal resistance between the conductor and the sheath. T_2 is the thermal resistance between the sheath and the armour. T_3 is the thermal resistance of external serving of the cable. T_4 is the thermal resistance between the cable surface and the surrounding environment.

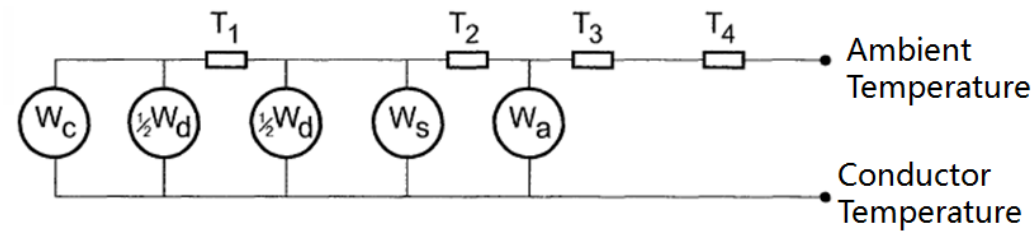

Fig. 3-1: The thermal ladder scheme used in the cable thermal modelling

Given the gradient between the rated conductor temperature and ambient temperature ($\Delta\theta$), the current rating of a conductor can be calculated by solving Equation (3.8) by neglecting the sheath and armour loss as shown below, where λ_1 and λ_2 are the ratios of total losses in metallic sheaths and armour respectively to the total conductor loss. W_s and W_a can therefore be expressed as $\lambda_1 I^2R$ and $\lambda_2 I^2R$ and contained in (3.8).

$$\Delta\theta = (I^2R + 0.5W_d)T_1 + [I^2R(1+\lambda_1) + W_d]nT_2 + [I^2R(1+\lambda_1+\lambda_2) + W_d]n(T_3+T_4) \quad (3.8)$$

Within Equation (3.8), electric resistance (R) is influenced by conductor temperature, skin effect factor (y_s) and proximity effect factor (y_p), and can be calculated with Equation (3.9). Similar to overhead line conductor, the resistance of cable conductor varies with temperature as shown in Equation (3.10). Skin effect factor and proximity factor are affected by frequency. Furthermore, proximity factor is also affected by the

diameter of conductor and the distance between conductor axes. The details of calculations of these two factors can be found in [71].

$$R(T_c) = R'(T_c) \cdot (1 + y_s + y_p) \tag{3.9}$$

$$R'(T_c) = R(T_0)[1 + \propto_R (T_c - T_0)] \tag{3.10}$$

Dielectric loss W_d is determined by current frequency (f), voltage to earth (V), insulation capacitance (Cap) and insulation factor (tan (δ)), as calculated by Equation (3.11). Furthermore, insulation capacitance is calculated with Equation (3.12) given insulation relative permittivity (ε), and insulation internal diameter (D_i) and external diameter (D_e).

$$W_d = 2\pi f \cdot Cap \cdot V^2 \cdot \tan(\delta) \tag{3.11}$$

$$Cap = \frac{\varepsilon}{18 \cdot ln\frac{D_e}{D_i}} \cdot 10^{-19} \tag{3.12}$$

Thermal resistances T_1, T_2 and T_3 are dependent on the thermal resistivity (ρ_j) and thickness of the layers. They can be calculated with Equation (3.13). The calculation of external thermal resistance T_4 is more complicated as it varies with different situations such as cables buried directly or in ducts, trefoil or flat configuration used, soil dried-out or not. The Equations for the calculation of external thermal resistance (T_4) are not provided in this thesis but can be found in [72].

$$T_{i=1,3} = \frac{\rho_{i=1,3}}{2\pi} ln\left(1 + 2 \cdot \frac{D_e - D_i}{D_i}\right) \tag{3.13}$$

3.2.2 Comparison of Rating Standards

The one industrial standard and one guide published by IEC and CIGRE to guide the cable rating calculation are:

- IEC 60287-1-1 standard [50]

- CIGRE SC WG B1.35, "Guide for rating calculations"

Both of the standards adopt the model based on thermal ladder scheme described in the previous section. The IEC 60287 standard series was published in 2006 and is generally used to determine cable rating. CIGRE WG B1.35 "Guide for rating calculations" was delivered in 2013. This CIGRE guidance is developed based on IEC 60287 and aims to provide the rating calculation methods under the situations which are not covered in IEC standard, such as HVDC cables, deep burial, horizontal drilling and multiple circuits.

In addition to cable modeling method provided in IEC 60287-1-1 [50], IEC 60287-2-1 [73] gives details of thermal resistance calculations in different cases. The methods for the calculation of cyclic and emergency current rating of cables is given in IEC 60853 [74]. In this thesis, the model in IEC 60287-1-1 standard [50] is taken for cable rating calculation since CIGRE SC WG B1.35 was not available when this project started.

3.3 Transformer

Transformers are utilized to transform the voltage between different levels. According to ratings, they are classified as distribution transformer, medium power transformer and large power transformer.

Different insulation material is used for distribution transformers and power transformers. Oil-immersed transformer in which insulation is provided by mineral oil and cellulose paper are mostly commonly used. Some of distribution transformers use cast-resin as the main insulation material and are known as dry-type transformers.

As this thesis focuses on the transmission system, the oil-immersed power transformers are mainly considered. Inside this type of transformer, a magnetic circuit is made up of iron core and windings. Both the iron core and the windings are immersed in coolant oil. Oil pumps and fan-cooled heat sinks can be used in larger transformers to improve cooling performance.

3.3.1 Thermal Modeling

The maximum operating rating of a transformer is limited by hot-spot temperature at its winding. The exceeding of the rated hot-spot temperature may cause damage to transformers in two ways. Firstly, when the hot-spot temperature is over 140℃, bubbles may form in the oil and reduce the dielectric insulation strength. (It should be noted that the formation of bubble is also affected by moisture content and gas condition [75]). Secondly, a high oil temperature can increase the ageing rate of the winding insulation exponentially. To guarantee the expected life span, the transformers are operated below the rated temperature useless in an emergency occasion.

The losses in the iron core, q_{fe}, caused by eddy currents, and the losses in the windings, q_{cu}, caused by Joule heating are the two heat sources in this model. The ratio between these two losses is defined as loss factor as shown in Equation (3.14). The total heat dissipated from these two heat sources (q_{cu+fe}) can therefore be presented in Equation (3.15) where R_w is the electric resistance of windings.

$$K_{loss} = \frac{q_{fe}}{q_{cu}} \tag{3.14}$$

$$q_{cu+fe} = q_{cu} + q_{fe} = q_{cu}(1 + K_{loss}) = I^2 R_w (1 + K_{loss}) \tag{3.15}$$

According to the structure of transformer and its cooling system, the transformer thermal model can be split into two parts which are winding-to-oil model and oil-to-air model.

a) Winding-to-oil model

The winding-to-oil model is shown in Fig. 3-2. The heat from the core and the windings then flows through the winding-to-oil thermal resistance, R_{th-wo} , which is a combination of winding thermal resistance, insulation thermal resistance and oil thermal resistance of the oil layer moving next to insulation. The thermal response time of this model is determined by the hot-spot thermal capacitance, C_{hs}. Given the oil temperature,

θ_{oil}, flowing around the windings, the hot-spot temperature, θ_{hs}, can be calculated with Equation (3.16) at steady-state.

$$\theta_{hs} = R_{th-wo} \cdot q_{cu} + \theta_{oil} \tag{3.16}$$

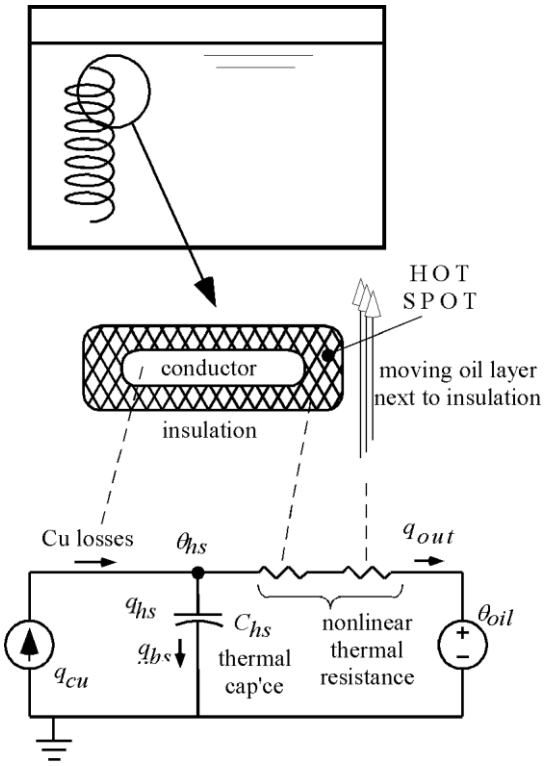

Fig. 3-2: Winding-to-Oil Heat Transfer in the Oil-Immersed Transformer [76]

b) Oil-to-air model

The oil-to-air model describes the heat transfer through coolant oil to the ambient environment as shown in Fig. 3-3. The oil-to-air thermal resistance, R_{th-oa}, in this model consists of oil thermal resistance and interface thermal which includes the tank wall and the moving air layer between than tank wall and the ambient. Oil pumps and fan cooled heat sinks can help to reduce this thermal resistance. A significant thermal response time is expected due to the large oil thermal capacitance, C_{hs}. At state-state, the oil temperature can be calculated as in Equation (3.17).

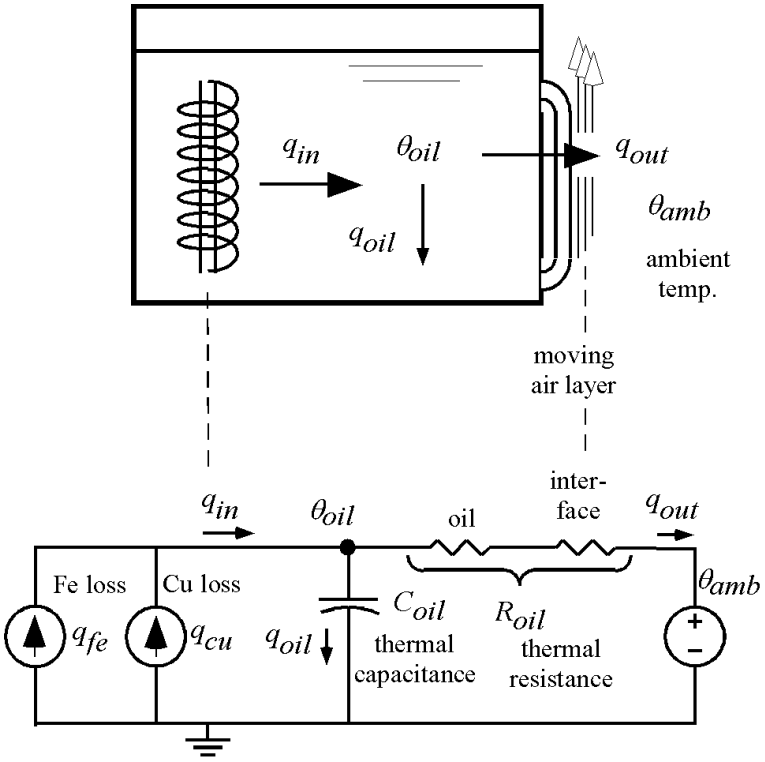

Fig. 3-3: Oil-to-Air Heat Transfer in the Oil-Immersed Transformer [76]

Combining oil-to-air model and winding-to-oil model, the temperature of hot-spot can be derived as Equation (3.18).

$$\theta_{oil} = R_{th-oa} \cdot q_{cu+fe} + \theta_{amb} \tag{3.17}$$

$$\theta_{hs} = (R_{th-wo} + R_{th-oa}) q_{cu+fe} + \theta_{amb} \tag{3.18}$$

3.3.2 Comparison of Rating Standards

Two industrial standards for transformer rating calculation are compared in this section, which are:

- IEC 60076-7 [77]
- IEEE C57.91 [78]

a) Steady-State

Both standards provide the same method for hot-spot temperature calculation by summing up the two temperature difference ($\Delta\,\theta_{hs-o}$ and $\Delta\,\theta_{o-a}$) and ambient temperature (θ_{amb}) as shown in Equation (3.19) where $\Delta\,\theta_{hs-o}$ is the maximum temperature gradient between hot-spot and oil, and $\Delta\,\theta_{o-a}$ is the maximum temperature gradient between oil and ambient air.

$$\theta_{hs} = \theta_{amb} + \Delta\,\theta_{hs-o} + \Delta\,\theta_{o-a} \tag{3.19}$$

The calculation of the maximum temperature gradients $\Delta\,\theta_{hs-o}$ and $\Delta\,\theta_{o-a}$ are provided in Equation (3.20) and (3.21), respectively. The temperature gradients at the rated condition are given as $\Delta\,\theta_{hs-o,R}$ and $\Delta\,\theta_{o-a,R}$. Load factor, K_{load}, is defined as the ratio of load current (I) and rated current (I_R) as shown in Equation (3.22). Oil exponent, C_o, and winding exponent, C_w, are constants which are empirically derived and vary with different designs of transformers. The values of these two constants are suggested in the standards.

$$\Delta\,\theta_{hs-o} = \Delta\,\theta_{hs-o,R} \cdot K_{load}^{C_w} \tag{3.20}$$

$$\Delta\,\theta_{o-a} = \Delta\,\theta_{o-a,R}\left[\frac{1 + K_{loss}K_{load}^2}{1 + K_{loss}}\right]^{C_o} \tag{3.21}$$

$$K_{load} = \frac{I}{I_R} \tag{3.22}$$

b) Dynamic State

For the determination of hot-spot temperature at dynamic state, two standards propose different calculation method. IEEE standard adopted an exponential variation based model as shown in Equation (2.23), where i and j is defined as the initial and final time.

τ is the time constant as the product of thermal capacitance and thermal resistance between different parts of transformer as shown in Equation (2.24).

$$T_f = T_i + (T_f - T_i)e^{\frac{t}{\tau}} \tag{2.23}$$

$$\tau = C_{th} \cdot R_{th} \tag{2.24}$$

IEC standard provides a more complex model by evaluating the temperatures variation at oil and the metallic part, i.e., windings and iron cores, separately with different time dependant functions $f_i(t)$. The model also gives different equations for calculating an increase in temperature as in Equation (3.25) and a decrease in temperature as in Equation (3.26). The time dependant functions are given in Equation (3.27) where C_{11}, C_{21} and C_{22} are constants suggested in IEC standard depending on the transformer type, τ_o and τ_w are oil and winding time constants which are also given in the standard.

$$\begin{aligned}\theta_{hs}(t) = \theta_a + \Delta\,\theta_{o-a,i} + \left[\Delta\,\theta_{o-a,f} - \Delta\,\theta_{o-a,i}\right]f_1(t) + \Delta\,\theta_{hs-o,i} \\ + \left[\Delta\,\theta_{hs-o,f} - \Delta\,\theta_{hs-o,i}\right]f_2(t)\end{aligned} \tag{3.25}$$

$$\theta_{hs}(t) = \theta_a + \Delta\,\theta_{o-a,f} + \left[\Delta\,\theta_{o-a,i} - \Delta\,\theta_{o-a,f}\right]f_3(t) + \Delta\,\theta_{hs-o,f} \tag{3.26}$$

$$\begin{cases} f_1(t) = 1 - e^{\frac{-t}{C_{11}\tau_o}} \\ f_2(t) = C_{21}(1 - e^{\frac{-t}{C_{11}\tau_w}}) - (C_{21} - 1)(1 - e^{\frac{-t}{\tau_o/C_{22}}}) \\ f_3(t) = e^{\frac{-t}{C_{11}\tau_o}} \end{cases} \tag{3.27}$$

c) Ageing

In both of these standards, transformer ageing rate is calculated as the relative value of ageing rate at a specified temperature to the ageing rate at rated temperature. The formula is given in Equation (3.28) and is derived from the Arrhenius equation. Furthermore, IEC standards also provides a formula, shown in Equation (3.29), based

on Montstinger approximation for ageing rate calculation for transformer with thermally upgraded insulation paper.

$$Ageing_r = 2^{\frac{\theta_{hs}-371}{6}} \tag{3.28}$$

$$Ageing_r = e^{(\frac{1500}{383}-\frac{1500}{\theta_{hs}})} \tag{3.29}$$

Regarding transformer modelling, the models proposed by IEC [77]and IEEE [78] have little difference. IEC model [77] is chosen as it is adopted by National Grid UK.

3.4 Summary

This chapter presented the thermal modelling of power system components, i.e., overhead line, cable and transformer. These models will be used to assess the components' performance (i.e., rating and ageing) in the context of climate change

The rating standards from IEEE, IEC and CIGRE for each of the three components are compared. The model in IEEE Std 738-2006, IEC 60287-1-1 Standard, and IEC are selected for OHL, cable and transformer, respectively, for the use in this thesis.

Chapter 4 Sensitivity of Component Ratings to Weather Variables

Having selected the thermal model of power system components in Chapter 3, this chapter presents a comprehensive analysis of the sensitivity of components rating to each individual weather variable. The preliminary study into the investigation of climate change in later chapters aims to reveal how the rating of components of different types can be influenced by various weather variables, and suggests: i) the variable that the component is the most sensitive to; ii) the type of component which is the most vulnerable to changes in weather variables. No climate information simulated in Chapter 2 is involved in this Chapter.

The chapter begins with the sensitivity of OHL ratings against air temperature, solar radiation, wind speed and wind direction. Soil temperature and soil thermal resistivity are the two variables which are then analysed for cable ratings. Finally, the sensitivity of transformer ratings is studied against air temperature.

4.1 Sensitivity of Overhead Line Ratings to Weather Variables

As introduced in Chapter 1, the rating of an OHL is defined as the current carrying ability at the rated conductor temperature under the given ambient weather conditions. As described in the model provided in IEEE standard [49], the conductor temperature can be affected by four weather parameters, including air temperature, solar radiation, wind speed and direction.

Various types of OHL conductors are selected to compare their rating sensitivities to weather conditions. They are designed in different materials, diameters, rated temperatures and resistances. Among the selected conductors, Collybia and Zebra are Aluminium Conductor Alloy Reinforced (ACAR) and Aluminium Conductor Steel Reinforced (ACSR), respectively, which are both rated at 75 ℃. Two Aluminium Alloy Conductors (AAAC) conductors, Rubus and Araucaria, are rated at 90 ℃. Drake Aluminium Conductor Composite Reinforced (ACCR) conductor is novel and can be rated at a much higher temperature of 240 ℃ than all the other conductors examined in this study. The key parameters of the conductors are presented in Table 4-1.

Table 4-1: Key parameters of the selected types of overhead line conductors

Type	Material	Diameter (mm)	Rated Temperature (℃)	AC Resistance (ohm/km)
Collybia	ACAR	30.33	75	0.0589
Rubus	AAAC	31.5	90	0.0558
Zebra	ACSR	28.62	75	0.0684
Araucaria	AAAC	37.26	90	0.04
Drake	ACCR	28.6	240	0.0658

The sensitivity analysis of each type of OHL conductor is carried out in four cases as shown in Table 4-2. Within each case, only one of the four weather parameters is used as a variable to examine its influence on the rating, whilst the other three parameters are set as constants.

Table 4-2: Assumptions for analysis of influence of weather on OHL ratings

Case No.	Air Temperature (℃)	Solar Radiation (W/m)	Wind Speed (m/s)	Wind Direction (degree)
1	Variable	30	0.5	17.5
2	20	Variable	0.5	17.5
3	20	30	Variable	17.5
4	20	30	5	Variable

4.1.1 Air temperature

The sensitivity of OHL ratings to air temperature is examined in case 1. As shown in Fig. 4-1, the OHL ratings keep decreasing as a result of air temperature rises. This is because the radiated cooling effect is determined by the difference between the conductor temperature and ambient air temperature. A higher air temperature will reduce this difference and cause less radiated cooling. In the figure, it is obvious that the novel Drake ACCR conduct is less affected by the temperature change since its high rated temperature (240℃) is much greater than the ambient air temperature to maintain a good radiated cooling effect. As a result, the change in air temperature is relatively less crucial for ACCR conductors.

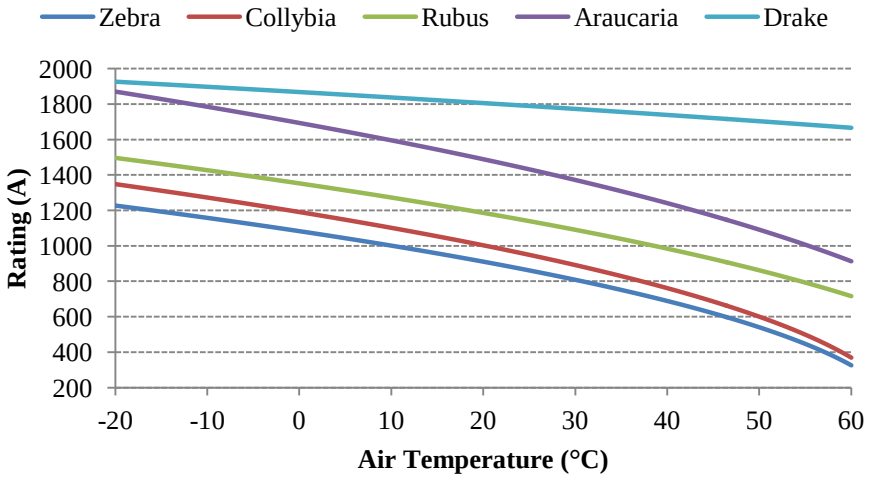

Fig. 4-1: Influence of air temperature on OHL ratings

To quantify the influence on all types of conductors, the rating change rates at different air temperatures are shown in Fig. 4-2. The negative rates describe the de-ratings of the conductors as a result of temperature rises. It can be seen that the de-rating rate is not linear to the temperature. When the air temperature is over 30 ℃, each 1 ℃ of temperature rise can cause significant de-ratings of OHL conductors. The rated conductor temperature again plays an important role in affecting the rating change rate. Higher rated temperatures lead to a less de-rating rate. For example, Drake conductor has a very low de-rating rate around 4 A/℃. Zebra and Collybia conductors with a rated temperature of 75℃ have a faster de-rating rate than Rubus and Araucaria conductors rated at 90℃.

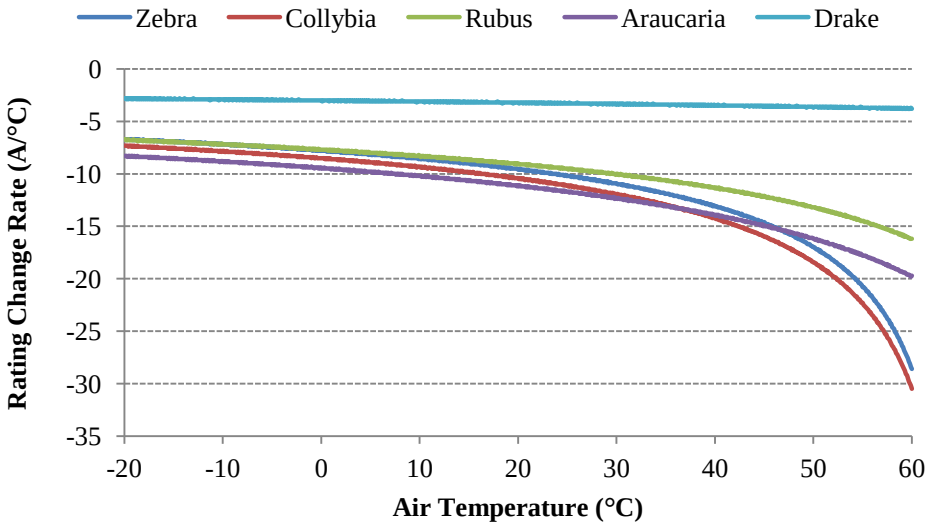

Fig. 4-2: Influence of air temperature on OHL rating change rates

4.1.2 Solar radiation

Case 2 looks into the sensitivity of OHL ratings to solar radiation. As shown in Fig. 4-3, the increasing solar radiation will cause decreases in ratings as more solar heating is gained by conductors. Fig. 4-4 gives the rating change per 1 W/m increase in solar radiation at different solar radiation levels. Because a conductor with a bigger diameter (i.e., a bigger projection area) can gain more solar radiation, for the OHLs at the same rated conductor temperature, the one with the bigger diameter has a faster rating change

rate at the specified solar radiation level, e.g., the ratings of the Collybia conductor decrease faster than those of the Zebra conductor as the solar radiation increases.

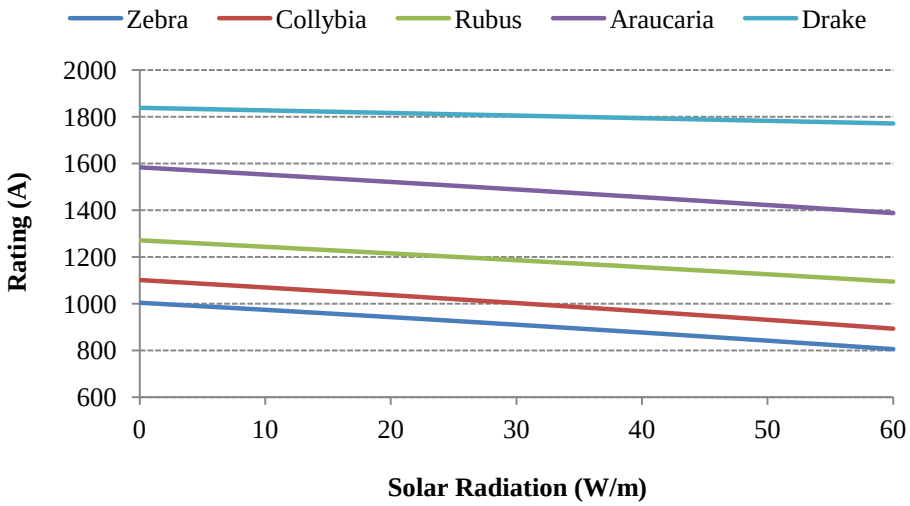

Fig. 4-3: Influence of solar radiation on OHL ratings

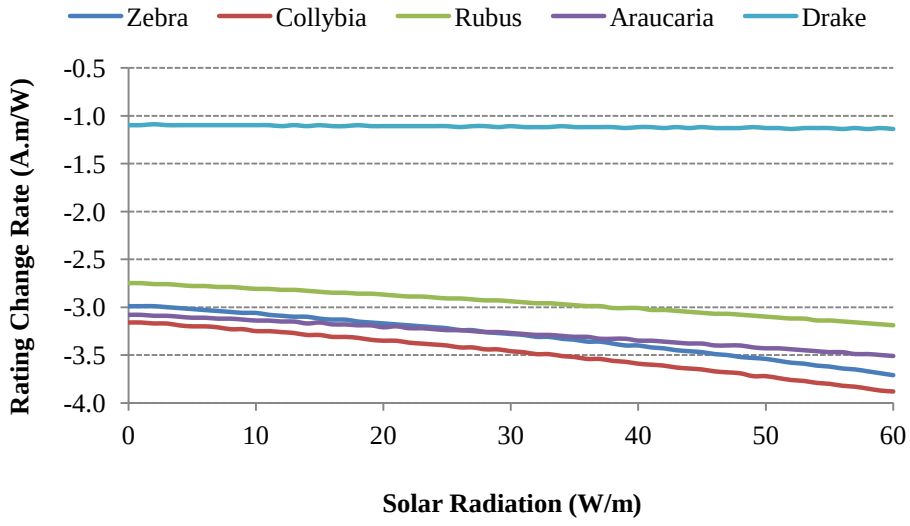

Fig. 4-4: Influence of solar radiation on OHL rating change rates

4.1.3 Wind speed

The sensitivity of OHL ratings to wind speed is presented in Fig. 4-5 and Fig. 4-6. The OHL ratings are examined by varying the wind speed from 0 m/s to a maximum of 25

m/s. Other weather parameters are set as constants as shown in Table 4-2. Benefiting from the massive convection cooling effect, the OHL ratings go up significantly with the increasing wind speed as shown in Fig. 4-5.

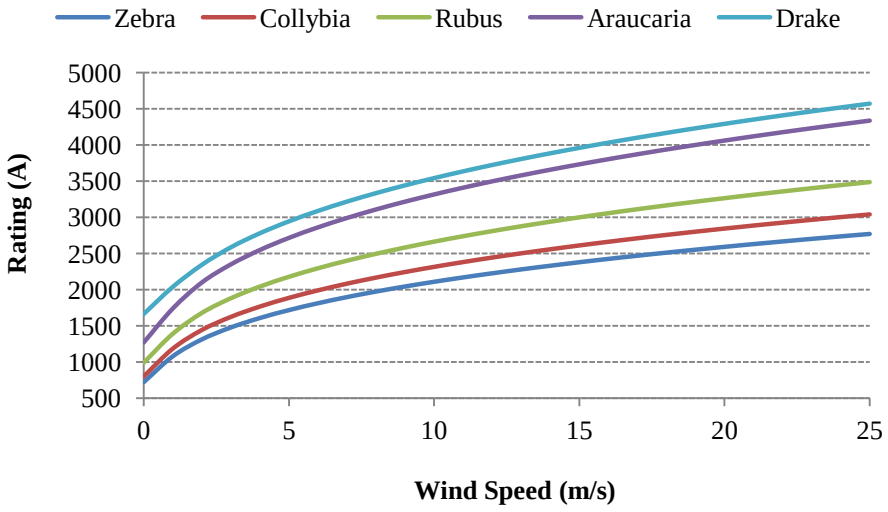

Fig. 4-5： Influence of wind speed on OHL ratings

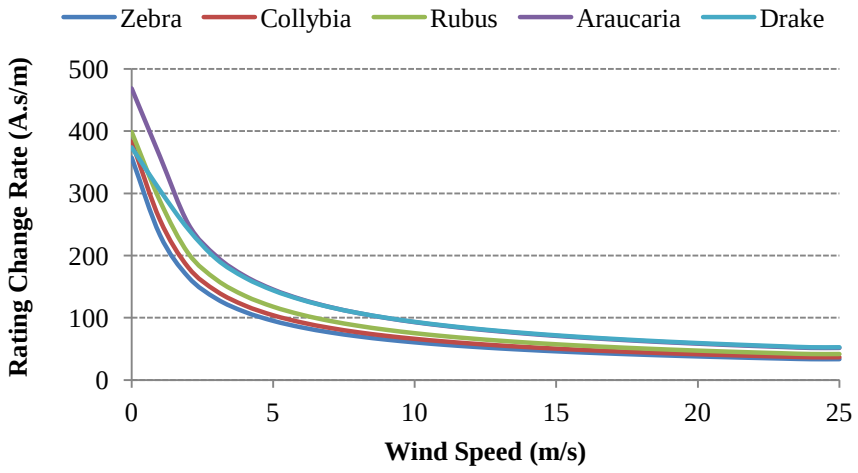

Fig. 4-6: Influence of wind speed on OHL rating change rates

The rating change rates of different types of conductors are shown in Fig. 4-6. They are calculated as the change of rating as a result of 1 m/s increase in wind speed. The figure shows that at lower wind speeds, the rating increases faster. It can also be seen in the

figure that the conductor with a greater diameter can take more advantage from high wind speeds, e.g., Araucaria conductor with a greater diameter of 37.26 mm has a faster rating increasing rate than that of a Zebra conductor with a diameter of 28.62 mm.

4.1.4 Wind direction

Wind direction is another weather parameter which can affect an OHL conductor's rating. It is taken as the wind injection angle to the conductor. An injection angle of 0^o indicates that wind direction is parallel to the conductor whilst an injection angle of 90^o indicates that wind direction is perpendicular to it. In this study, the OHL ratings are tested with a wind injection varying from 0^o to 90^o, whilst other weather parameters remain as constants as given in case 4 in Table 4-2.

Fig. 4-7 shows that the ratings go up as the wind inject angle increases. Under the same conditions of other weather parameters, the OHL rating has the maximum value when the wind is perpendicular to the conductor and has the minimum value when the wind is parallel to the conductor. Fig. 4-8 indicates that the ratings have a faster change rate at a lower wind injection angle. For example, the rating change rate is higher when the wind injection angle is less than 45^o than when the angle is more than 45^o. The changing rate is the smallest around 70^o and increases slightly from 70^o to 90^o due the use of wind factor equation used in [49].

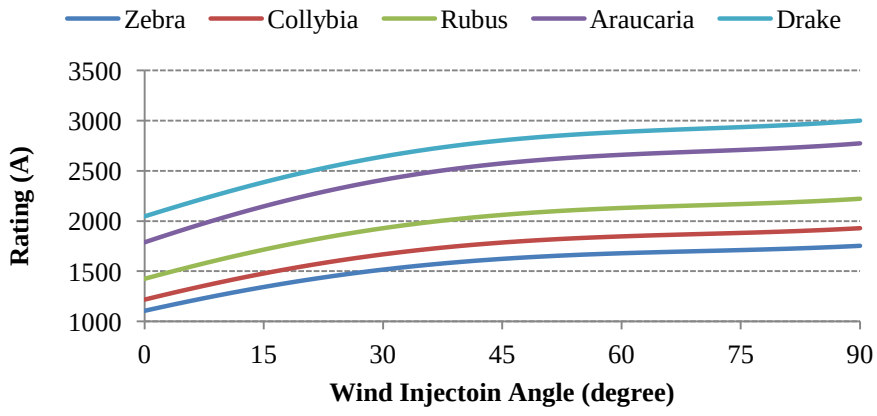

Fig. 4-7: Influence of wind direction change on OHL ratings

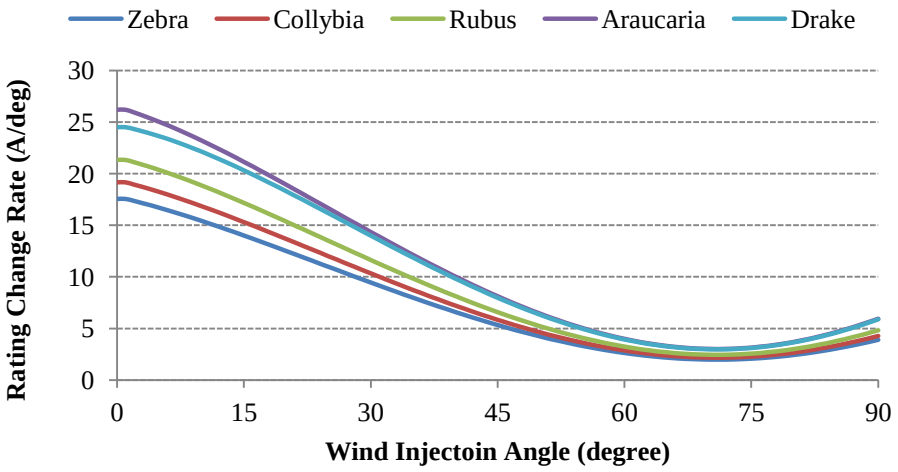

Fig. 4-8: Influence of wind direction on OHL rating change rates

4.1.5 Discussion

Most importantly, it can be concluded that the rating of the OHL conductor is the most sensitive to the wind speed. A variation of 1 m/s in wind speeds can result in a rating change of hundreds of amperes when the wind speed is below 5m/s. This is a much larger rating change than those caused by other weather parameters (i.e., air temperature, solar radiation and wind direction).

4.2 Sensitivity of Cable Ratings to Weather Variables

Cable ratings are defined as the maximum current carrying ability of its conductor that is limited by the rated conductor temperature. The overheated cable conductor will damage its insulation layers and quicken insulation aging. Unlike the OHL conductor surrounded by flowing air, cables are buried under ground surrounded by soil with massive thermal resistance. Soil temperature and soil thermal resistivity are the two ambient environment parameters which can affect a cable's conductor temperature by influencing its cooling effect. The worst case in cable operation is that soil is dried out as a result of continuous heat from cables combined with severe weather conditions, i.e., seldom precipitation, high air temperature and low wind speed.

As discussed in Chapter 3, cable ratings in this study are calculated using the method

provided in IEC 60287 [79]. This method analytically solves a thermal resistance ladder network to give the current at which the rated conductor temperature is reached.

Four types of cables are examined, including two XLPE cables and two fluid-filled cables. All of them are rated at the conductor temperature of 90℃. The cables are assumed to be directly buried in parallel at 2 m depth. The key parameters and calculated thermal resistances of these cables are given in Table 4-3. As listed in the table, comparing the XLPE cables and fluid-filled cables, the former have greater dielectric losses whilst the latter have higher T1 (thermal resistance between conductor and sheath) and T3 (thermal resistance of external serving of cable). As all the cables are assumed without armour, T2 (thermal resistance between sheath and armour) is taken as 0.

Table 4-3: Key parameters of the selected types of cables

Conductor Type	Conductor Area (mm^2)	Dielectric Loss (W/m)	T1	T2	T3
XLPE1600	1600	3.31	0.4025	0	0.0267
XLPE2500	2500	3.90	0.3397	0	0.0241
Fluid-Filled1600	1600	14.08	0.4499	0	0.0338
Fluid-Filled2500	2500	15.35	0.3526	0	0.0303

4.2.1 Soil temperature

Cable ratings are calculated based on the soil temperature varying in the range between -20℃ and 40℃ and the soil thermal resistance remaining as a constant of 1.2 Km/W. It can be seen in Fig. 4-9 that the rating of a cable decreases when the soil temperature increases. Fig. 4-10 gives the change rates of the cable ratings as a result of per 1℃ increase in soil temperature. The figure shows that the change in ratings is non-linear. The rating has a bigger de-creasing rate at a higher temperature. For example, the fluid-filled 2500mm^2 conductor has a de-rating rate of 8 A/℃ at soil temperature of -10℃ which is lower than that of 12 A/℃ at a soil temperature of 30℃. Moreover, for the cable made of the same material, the one with a bigger diameter is more sensitive to the soil temperature change as it has a thicker outer layer which provides more thermal

resistance, e.g. the XLPE 1600 mm^2 cable has a lower rating change rate than XLPE 2500 mm^2 cable.

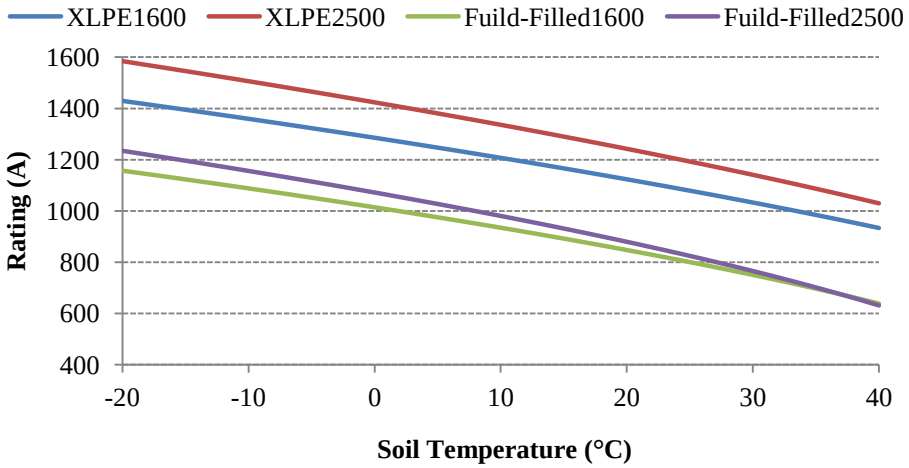

Fig. 4-9: Influence of soil temperature on cable ratings

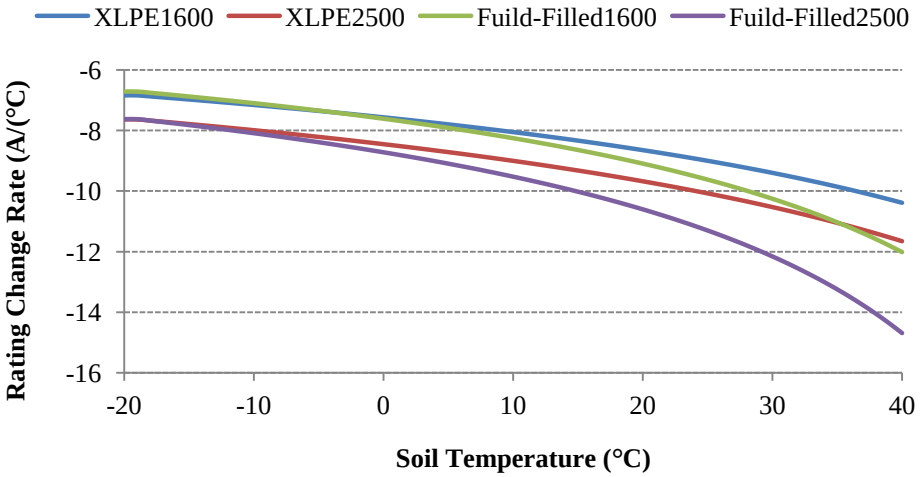

Fig. 4-10: Influence of soil temperature on cable rating change rates

4.2.2Soil thermal resistivity

The soil thermal resistivity is dependent on not only the soil moisture content but also

the soil type. For the same type of soil, the drier it is the greater thermal resistivity it has. As shown in Fig. 4-11, the cable ratings decrease when the soil thermal resistivity goes up. This is because the greater thermal resistance of drier soil weakens the dissipation of the heat generated in the conductor through the soil to the ambient environment. The soil is considered to be dry when the soil thermal resistivity is over 1.5 Km/W. It can be seen that the ratings drops dramatically in dry soil. At 2.7 Km/W, the rating of fluid-filled cable falls to less than 400 A.

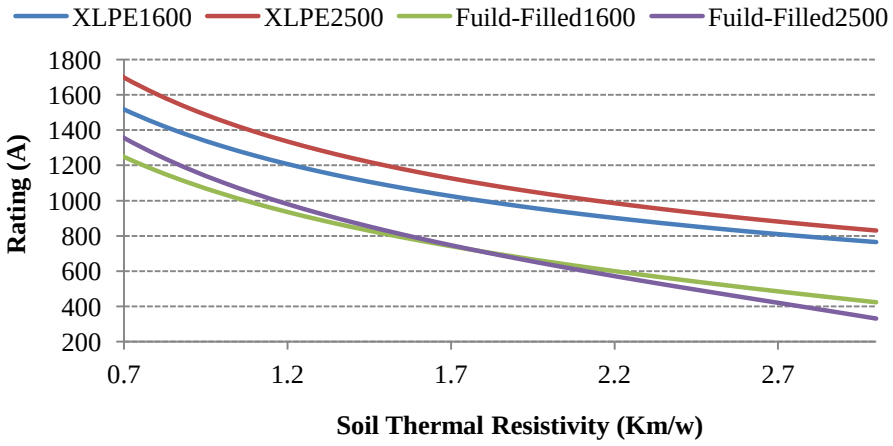

Fig. 4-11: Influence of soil thermal resistivity on cable ratings

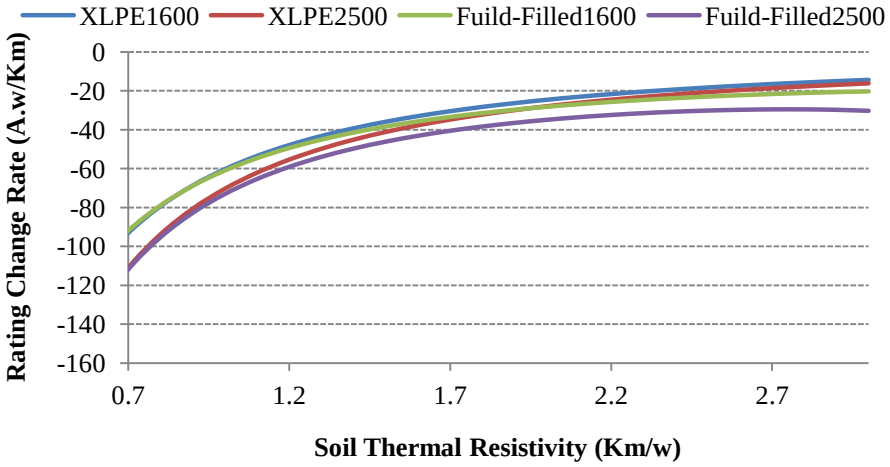

Fig. 4-12: Influence of soil thermal resistivity on cable rating change rates

Fig. 4-12 shows the rating change rates at different soil thermal resistivity measured as the rating change over per 0.1 Km/W increase of the thermal resistivity. It can be seen

that the rating change rate is higher at a lower thermal resistivity than that at higher ones. At the thermal resistivity of 0.7 Km/W, an increase of 0.1 Km/W thermal resistivity can cause about 110 A de-ratings on a XLPE 2500 mm2 cable. This figure also shows that different types of cables have similar rating change rates, especially at higher soil thermal resistivity. This indicates that the size and material of the cables do not have significant impact on rating change rates compared to the soil moisture change. This is because the surrounding soil provides a much greater thermal resistance than the resistance in the cable layers.

4.2.3 Discussion

In conclusion, the cable rating is more sensitive to the change in soil thermal resistivity. However, it is indicated in [12] that the large variation of soil thermal resistivity takes place only in the ground surface layer of soil, and the variation below 1.2m depth remains small. Besides soil thermal resistivity, soil temperature is another weather variable which can notably affect a cable's rating.

4.3 Sensitivity of Transformer Ratings to Weather Variables

Air temperature is the only weather parameter considered in the transformer rating calculation as described in IEC standard [29]. The transformer rating is constrained by its rated temperature at hot-spot, i.e., winding. Given the ambient air temperature, the transformer rating at rated hot-spot temperature can be calculated through the thermal model.

The sensitivity analysis of transformer ratings to air temperature are carried out on three types of large power transformer which are widely used in transmission systems: Oil-Nature-Air-Force (ONAF) transformer, Oil-Directed (OD) transformer and Oil-Forced (OF) transformer. They have different cooling system designs. The ONAF transformer uses the natural convectional flow of the oil for cooling. The oil in the OF transformer is forced to flow inside the tanks by the use of oil pumps. The OD transformer can be

regarded as an improved version of OF transformer, in which the oil is forced to flow through a predetermined route to enhance the cooling effect. In the thermal model provided in the IEC standard, the different types of transformer are parameterized with different factors and coefficients as shown in Table 4-4 [29].

Table 4-4: Key parameters, factors and coefficients of the selected types of transformers [29]

Transformer Type	Oil exponent	Winding exponent	Constant k11	Constant k21	Constant k22	Rated Winding temperature (℃)
ONAF	0.8	1.3	0.5	2	2	120
OD	1	1.3	1	1.3	1	120
OF	1	2	1	1	1	120

4.3.1 Air temperature

The transformer rating is presented as a load factor which is the ratio of the current load over the rated load on the nameplate. The rated load of a transformer is the rating at the designed ambient air temperature of 10 ℃. At this air temperature, the transformer rating (i.e., loading factor) is shown as 1. Fig. 4-13 shows that the transformer rating decreases when the air temperature rises. The transformer rating over 1.0 p.u. means that it can be operated over the rated load under a cooler ambient condition.

The transformer rating change rate at different air temperature is shown in Fig. 4-14. It is calculated as the rating reduction as a result of per 1 ℃ rise in air temperature. The figure shows that the rating change rates are not linear. A greater de-rating rate is expected at a higher air temperature. Furthermore, the ONAF transformer has the greatest rating change rate which indicates that it is the most sensitive to the air temperature change as its cooling system is less effective than the other two types of transformer.

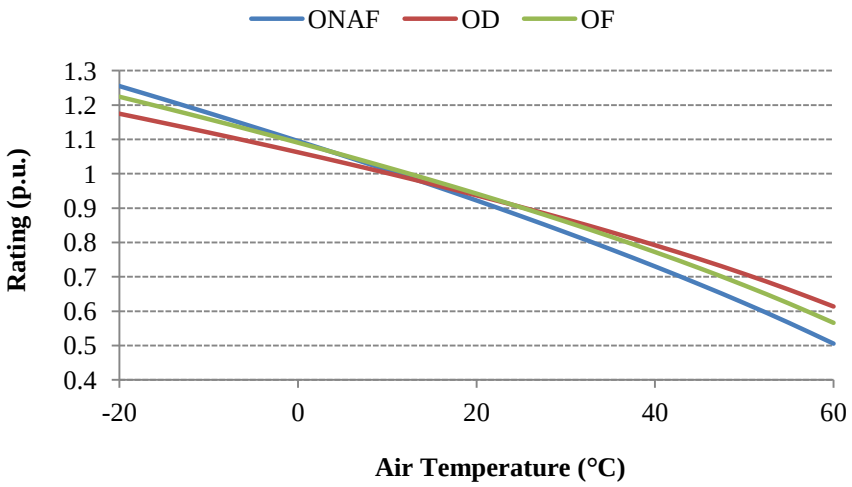

Fig. 4-13: Influence of air temperature on transformer ratings

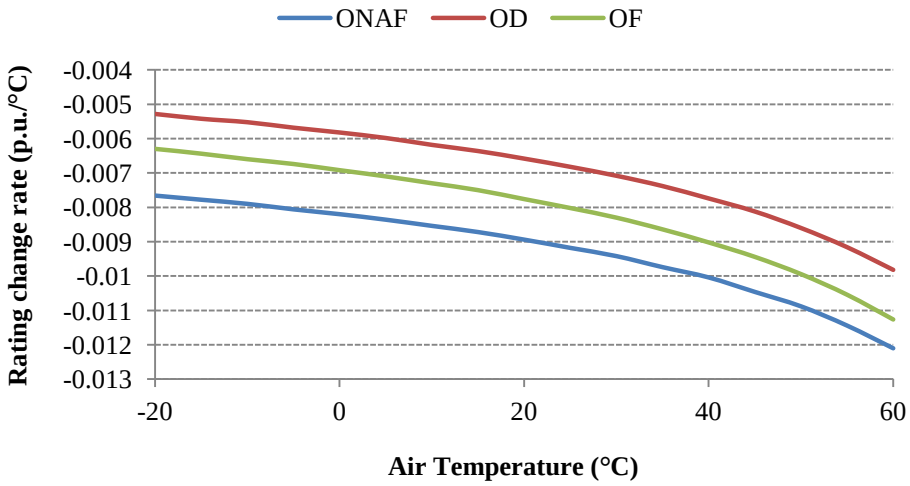

Fig. 4-14: Influence of air temperature on transformer rating change rates

4.4 Summary

An extensive sensitivity analysis of the rating of power system components to weather variables has been completed. This has involved investigations of air temperature, solar radiation, wind speed and wind direction for OHL rating, soil temperature and soil thermal resistivity for cable rating, and air temperature for transformer rating. For each component, one weather parameter is taken as a variable at a time, with other weather parameters set as constants, to present both the change and changing rate of the

component rating. Different types of components are also compared, including Collybia, Rubus, Zebra, Araucaria and Drake for OHLs, XLPE1600, XLPE2500, Fluid-Filled1600 and Fluid-Filled2500 for cables, and finally ONAF, OD and OF type of transformers.

This chapter is a preliminary study to suggest the weather variable that the power system components are more sensitive to, and the types of components that are more vulnerable to changes of weather parameters. The results will be considered in the later chapters when investigating the impact of climate change.

Chapter 5 Impacts of Climate Change on Component Ratings

In the previous chapter, a preliminary study of the sensitivity of power system component ratings to individual weather variables was established. Using the climate models and simulation tools described in Chapter 2, this chapter presents the impacts of climate change on component ratings, which is the *second original contribution* of this thesis.

The methodologies to determine both the static and dynamic rating are first provided in this chapter. For the static rating, the probabilistic approach to assess the impacts of climate change is described, followed by the detailed results on OHL, cable and transformer. Among the three types of components, OHL can derive more benefit from the use of the dynamic rating than that of the other two. In this study, only the dynamic ratings of OHL are being assessed with the probabilistic method developed.

5.1 Determination of Static and Dynamic Ratings

As introduced in Chapter 1, considering both safety and economic issues, there are

generally two types of ratings that are implemented on power system components: static rating and dynamic rating. Both of them are used to prevent a component to exceed its rated temperature under most weather conditions. The static rating is determined based on historical weather records, and is taken as a fixed transfer limit of component to ensure that the component does not exceed its safety margin in most of the time period, typically a season. In contrast, the dynamic rating is determined based on the real-time ambient weather conditions provided by the sensor to fully use the capacity of a component and therefore improve the utilization of the existing system. It can be updated from every minute to a few hours depending on the requirements of system operators.

5.1.1 Static Rating Determination

Traditionally, the ratings of power system components widely implemented by system operators are static. Due to the limitation of weather monitoring and communication techniques, the ambient environment and the operating conditions of a component, such as the operating temperature, are unknown. It is very difficult to rate a component in real time. In this context, the current carrying ability (i.e., rating) of a component is determined to be a fixed and conservative value so that the component does not exceed its safety margin for most of the time. The ratings obtained in this way are called "static ratings".

To determine the static rating for a component, the first step is to calculate the actual hourly ratings according to the historical weather data. An "exceedence probability" curve can then be obtained from the actual hourly ratings, as illustrated in Fig. 5-1. The "exceedence" referes to the exceedence of the component' rated temperature. In this figure, if the component is continuously operated at the chosen static rating, the proportion of time for which the component exceeds its rated temperature is the exceedence probability. For example, the red dot ***A*** on the curve indicates that if the static rating is selected to be the value of ***a***, there is a 20% probability that the actual rating is lower than ***a***. Based on this curve, the static rating is determined as the rating at the chosen " exceedence probability" level. The most conservative method is to set the “exceedence probability” as 0, which means that the lowest actual rating is chosen as

the static rating. In such a case, there is no probability that the component will exceed the rated temperature. However, this is not an economic efficient as this lowest rating has a very slight probability of occurrence. A reasonably low "exceedence probability" is therefore adopted at a level which can be tolerated by the operators.

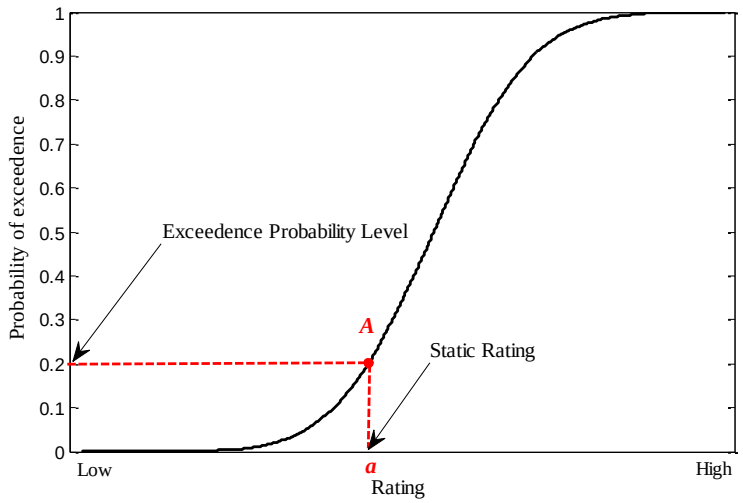

Fig. 5-1: Illustration of static rating determination on probability of exceedence curve

The static rating determination method is the same as described above for all the three types of power system components studied in this research, i.e., OHL, cable and transformer. However, the "exceedence probability" levels are different. OHLs can heat up within a short time (in minutes) when they are fully loaded because their bare conductors have low thermal capacitance. The "exceedence probability" level is therefore set to a very low value to prevent the occurrence of overheating. The other two types of components, cable and transformer, have massive thermal capacitance which effectively slow down the thermal response. It takes hours for them to reach the rated temperature even when they are operated at rated load. In the practical power system operation, the peak load, which may push the components to reach the rated load, usually lasts for less than 2 hours. This means cables and transformers rarely exceed their rated temperature. As a result, the "exceedence probability" levels for cable and transformer are usually set as a relatively high value.

In the following sections, the static rating determination method is demonstrated for

OHL, cable and transformer, respectively. In each section, the weather variables used for actual rating calculation and "exceedence probability" level use for static calculation are firstly discussed. An example of rating determination is then given for demonstration.

5.1.1.1 Overhead Line Static Rating

a) Weather variables used for actual rating calculation

As discussed in Chapter 3, the calculation of an OHL rating requires four weather variables, including air temperature, solar radiation, wind speed and direction. When calculating the actual hourly rating for OHL static rating determination, only air temperature and solar radiation are variables taken from historical records. Since OHL ratings highly depend on wind conditions because of their cooling effect, and the wind is extremely random and does not follow any pattern, it is very risky to use its historical records to determine the static rating for an OHL. As a result, the wind speed and direction are set as conservative constants. According to UK weather observations, wind speed is taken as 0.5 m/s and the wind injection angle to the OHL conductor is taken as 17.5 ° for the actual rating calculations.

b) Exceedence probability level

Different exceedence probability levels are adopted by different operators following their own safety requirements and climate patterns. The levels used by the operators in the UK, namely National Grid, are taken to determine OHL static ratings.

The OHL exceedence probability levels used by National Grid are taken from the research work carried out at Central Electricity Generating Board. According to different toleration levels and implementation occasions, there are two probability levels for the determination of static ratings. The static rating determined by the lower exceedence probability level is called a pre-fault rating. It is used for the normal operating occasion. The static rating determined by the higher exceedence probability

level is called a post-fault rating to implement an OHL during the faulty occasion but within an acceptable limited time until the line recovers to the normal condition.

The pre-fault rating is set to ensure the risk of exceeding the line rated temperature is of order 1 in 1,000, and the risk of exceeding it by more than 5°C (when sag increases start to become significant) is less than a 1 in 10,000 chance. Based on the above two criteria, the actual ratings are calculated at rated temperature and a temperature higher than the rated temperature by 5°C. Two static ratings are then determined separately from the actual rating at the above two temperatures at exceedence probability levels of 0.1% and 0.01%, respectively. The lower of the two static ratings is chosen as the pre-fault rating.

The exceedence probability level of 12% is applied to determine the post-fault rating from actually ratings calculated at the rated temperature. Thus, if the full post-fault rating is used on a continuous basis, the line temperature will exceed its profiled temperature for approximately 12% of the time [80]. This choice of the exceedence is based on the considerations of the statistical occurrence of rated post-fault continuous or short-tem loadings, reinforced by the tendency for the weather conditions to provide greater cooling during times of high load and high risk of fault. However, the continuous use of post-fault rating should be less than 12 hours. If the line remains in the post-fault condition, other actions will be taken, such as switching off the line.

Furthermore, the OHL static ratings are implemented over three seasons in the UK. The summer static ratings are used from May to August. The winter static ratings are used from December to February. The spring and autumn share the same static ratings and are regarded as one rating season that includes March, April, September, October and November.

c) Example of overhead line static rating determination

The static rating determination of a Zebra ACSR OHL based on the simulated weather data series from a WG variant in the summers of the 2020s in Slough in high emissions scenario is given as an example. Firstly, the actual hourly ratings of the Zebra OHL are

calculated at the rated temperature, i.e., 75℃, and the rated temperature plus 5℃, i.e., 80℃, based on the simulated 30-year weather series containing air and solar radiation. Then, the calculated actual ratings are placed into two distribution curves representing the probability of exceedence of the calculated ratings. As shown in Fig. 5-2, the curve calculated at the rated temperature is in black and that at the rated temperature plus 5℃ is shown in red. The determination of a pre-fault rating requires the rating in black curve at 0.1% probability level, which is 905.67 A, and the rating in red curve at 0.01% probability level, which is 870.65 A. Comparing the two ratings, the lower one, 850.65 A, is determined as the pre-fault rating. The post-fault rating is taken as the rating as 12% probability level in the black curve only. As shown in the figure, the post-fault rating is determined as 983.03 A in this example.

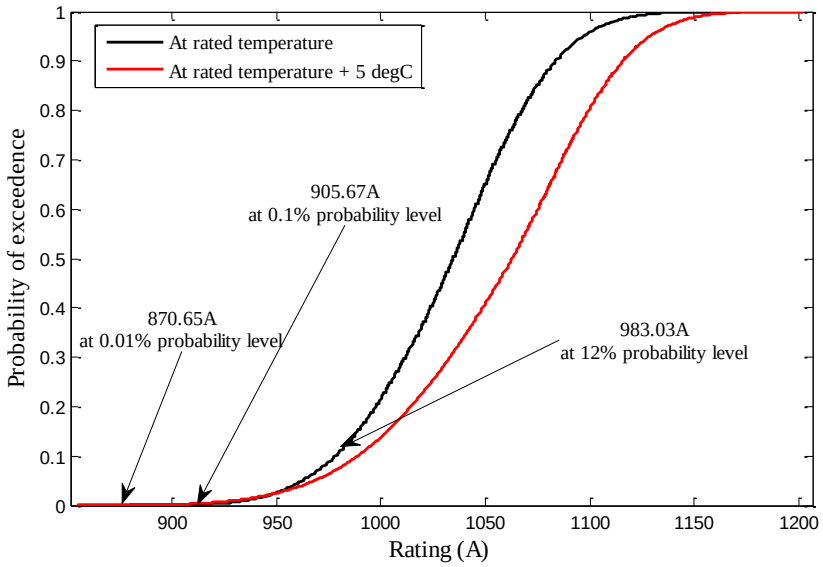

Fig. 5-2: Example of static rating determination of a Zebra ACSR OHL based on simulated summer weather from a variant of WG at Slough in 2020s, high emission scenario

5.1.1.2 Cable Static Rating

a) Weather variables used for actual rating calculation

Soil temperature and soil thermal resistivity are the two weather variables required for underground cable rating calculations. Regarding the calculation of actual ratings for the

determination of static rating of a cable, soil temperature is the only weather variable taken into consideration. The soil thermal resistivity is assumed to be constant at 1.05 Km/W and 1.2 Km/W for summer and winter, respectively, for the use of static rating calculation of a cable according to the suggestion from National Grid [51].

b) Exceedence probability level

No information about the exceedence probability level used for cable static rating determination is provided by National Grid. It only suggests that the cable should be rated at 15 ℃ and 10 ℃ in summer (May to October) and winter (November to April), respectively. The above two soil temperatures correspond to the ones at about 13% probability level in the baseline simulated from a soil temperature model. A study [81] carried out in Australia shows that a 10% probability level should be taken in determining the static rating. Since this study focuses on a future system with an unknown load profile, a relatively conservative exceedence probability level of 5% is used.

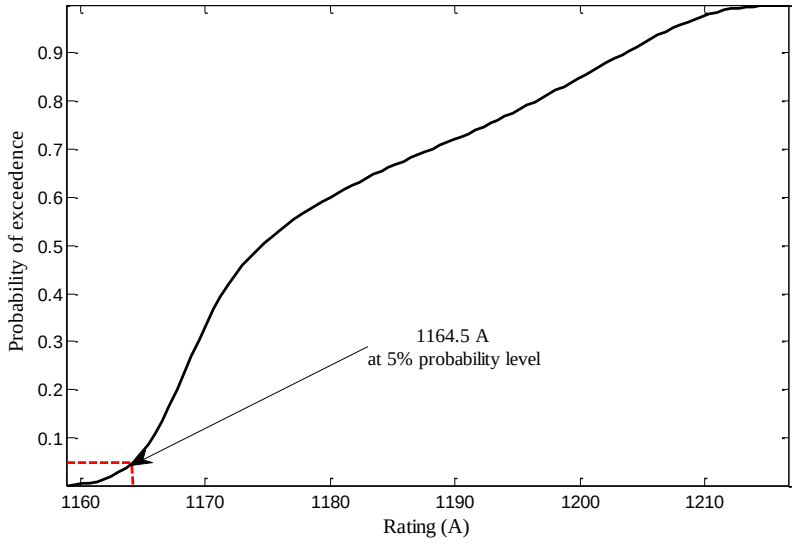

Fig. 5-3: Example of static ratings determination of an XLPE 1600 mm^2 cable based on the simulated summer weather from a variant of soil temperature model in Slough in the 2020s in high emission scenario

c) Example of cable static rating determination

The static rating determination of a XLPE 1600 mm^2 cable is given as an example. The actual hourly ratings are calculated based on the simulated 30-year hourly summer soil temperatures in high emission scenario in Slough in 2020s and are placed into a probability distribution of exceedence as shown in Fig. 5-3. The rating of 1164.5 A is then determined as the cable static rating at 5% probability level.

5.1.1.3 Transformer Static Rating

a) Weather variables used for actual rating calculation

According to the thermal model described in IEC standard [29], the calculation of the transformer hot-spot temperature, which limits its rating, requires the air temperature as the only weather variable input. The effect of solar radiation and wind are not considered in the standard. Therefore, the actual ratings are calculated purely on the hourly air temperatures.

b) Exceedence probability level

The exceedence probability level for the static rating determination of a transformer is taken as 10%. This level is adopted according to the study result of the recorded air temperature data collected in 20 observation stations over the period 1980-1989 [82]. The static ratings of a transformer are also set to be implemented over three seasons (summer, winter and spring/autumn) as those for OHL.

c) Example of transformer static rating determination

The static rating determination of an ONAF power transformer is given as an example. The transformer ratings are in load factor. The actual ratings are calculated based on the simulated 30-year hourly summer air temperatures in high emission scenario in Slough in the 2020s. After placed all the actual hourly ratings into the distribution curve of

probability of exceedence of calculated ratings, the summer static rating over this period is determined as 0.8956 p.u. at the 10% probability level.

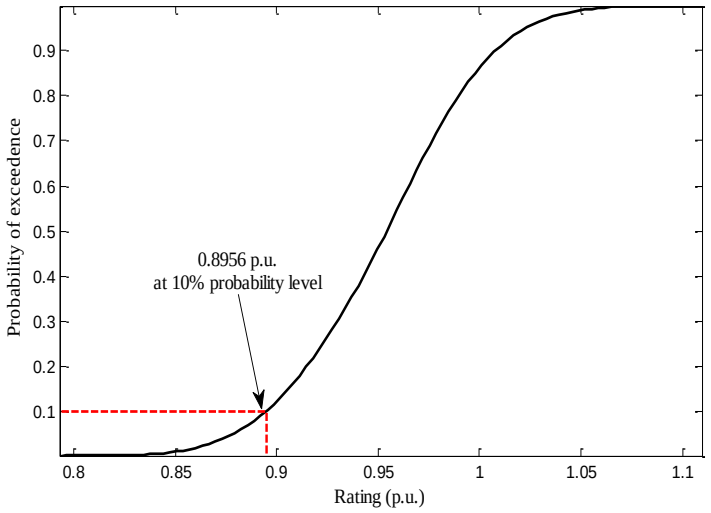

Fig. 5-4: Example of static ratings determination of a ONAF transformer based the on simulated summer weather from a variant of WG in Slough in the 2020s in high emission scenario

5.1.2 Dynamic Rating Determination

Different from the static rating, the dynamic rating can vary with weather conditions. For the implementation of the dynamic rating, both the forecasted and real-time weather conditions are used. The forecasted weather provides a rough estimation of the ratings one-day or hours ahead for the system operator to draw up an operation plan. Then the real-time weather condition is obtained by the sensors distributed along transmission lines or on site to update the real-time ratings. In such a way, the dynamic rating can maximize the power delivery ability of power system components by taking advantage of weather conditions that are more favourable than the designed conditions, and can also avoid the exceedence of the rated temperature in severe weather conditions.

There are several challenges to implementing the dynamic rating. First, it requires reliable monitoring and communication systems which are extremely expensive. Weather forecasting, especially wind forecasting, is also expected to be more accurate. As a result, the dynamic rating is currently not widely used. In recent years, however, it

has attracted much attention and been considered as a potential solution to increase the utilization of the existing system, since the future power system will become much more intense with the injection of renewable energy.

All three types of components, i.e., overhead line (OHL), cable and transformer, can be operated in dynamic ratings. The benefit of using the dynamic rating on the overhead lines is the most significant as the wind can provide a massive cooling effect. In this study, only the use of the dynamic rating on OHL is investigated. Since the simulated data are in hourly series, dynamic ratings are actually calculated as hourly ratings.

5.1.2.1 Overhead Line Dynamic Rating

To determine the OHL static rating, the hourly actual ratings are calculated based on varied air temperature and solar radiation, but a constant wind speed of 0.5 m/s and wind injection angle of 17.5^{o}. However, the calculation of dynamic ratings takes the variation of wind speeds into consideration as well. In this study, the hourly mean wind speeds simulated in the wind model described in Chapter 2 are used for the dynamic rating calculation. As wind direction can vary frequently in a short time, a wind injection angle of 17.5^{o}, the same as that used for static actual rating calculation, is taken for the calculation of the dynamic rating.

Fig. 5-5 gives an example of one-year calculated dynamic ratings compared to the "actual" ratings for static rating determination and determined static ratings. These ratings are based on the simulated weather data in high emission scenario in Slough in the 2020s. The hourly "actual" ratings (presented in the blue line) are calculated at constant wind speed of 0.5 m/s over 30 years to determine the pre-fault static ratings (presented in red line) in three seasons at the specified exceedence probability level introduced in the previous section. The dynamic ratings (presented in black line) are calculated with the varying wind speeds and show a significant increase in the current carrying ability compared to the "actual" ratings and static ratings, benefiting from the massive convectional cooling.

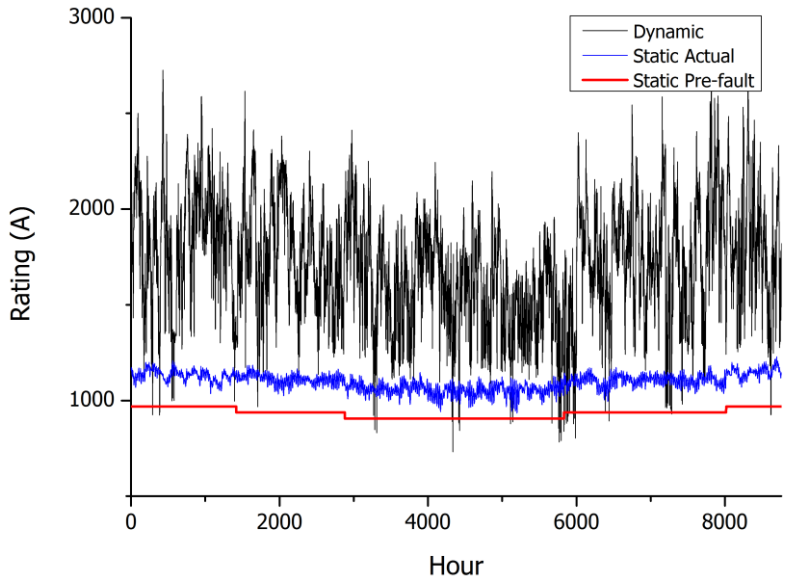

Fig. 5-5: One year of calculated dynamic ratings, actual ratings and static ratings based on simulated weather data in Slough in the 2020s in high emission scenario

5.2 Impacts of Climate Change on Component Ratings

The ratings of power components can be greatly affected by weather conditions as discussed in Chapter 4. To investigate the impacts of climate change, the ratings are assessed based on the simulated weather data. The difference between the rating calculated with future weather and those with baseline weather is used to quantify the impacts.

As introduced in Chapter 2, future climate is simulated in a stochastic approach by running climate models and UCKP09 Weather Generator, according to the high, medium and low emission scenarios. Within each emission scenario, 1,000 variants of different possible future climate projections are generated to give a range of climate change levels to cover the uncertainties in climate modelling. The power system component ratings determined based on these projections are therefore probabilistic.

In this study, the impacts of climate change on both of the rating implementation methods, i.e., static rating and dynamic rating, are assessed in a probabilistic approach. For the static rating, all three types components are examined (in Section5.2.1) whilst

only OHL is investigated in terms of the dynamic rating (in Section 5.2.2). Due to space limitation, assessment results are only shown for the case with the greatest climate change level (i.e., worst case) which is located in Slough in high emission scenario. More results for other locations and emission scenarios can be found in Appendix B.

5.2.1 Impacts of Climate Change on Static Ratings

5.2.1.1 Probabilistic Assessment of Impacts on Static Ratings

The approach to assess the impacts of climate change on power system components' static ratings is illustrated in the flow chart shown in Fig.5-6.

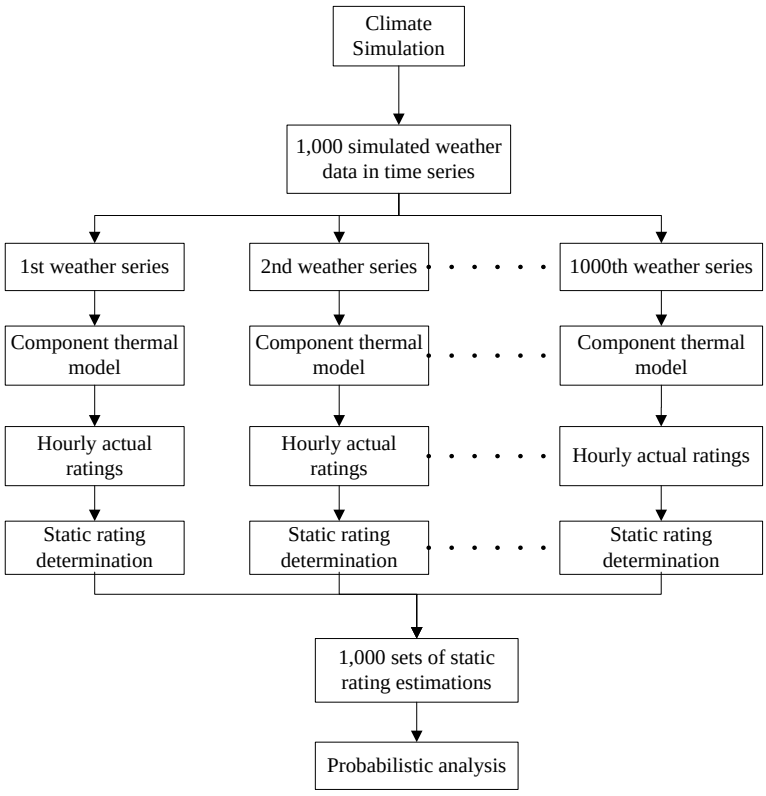

Fig.5-6: Probabilistic assessment of the impacts of climate change on static ratings

Firstly, the future weather data are simulated using the models described in Chapter 2. For the determination of static ratings, air temperature, solar radiation and soil temperature are the three weather variables required. The air temperature and solar

radiation are simulated with UKCP09 Weather Generator (WG). Each run of WG generates a version of 30-year hourly series of air temperature and solar radiation. The soil temperatures are then calculated based on this WG weather series combined with a random time series of re-sampled wind speeds from the wind model. Therefore, the soil temperature series is consistent with the weather series of air temperature and solar radiation from each WG run. These three weather variables are bound into a weather series according to the time. In such a way, 1,000 different versions of weather series are generated from 1,000 runs of WG and soil temperature model. These weather series are independent from each other and present the range of possible climate change levels.

The next step is to determine the static ratings (for the three components) based on the simulated weather series. As these 1000 weather series are independent, each of them is regarded as an individual case. The static rating determination process is carried out as described in Section 5.1.1. The actual hourly ratings are calculated through the component thermal models based on a 30-year hourly weather series. The static ratings are then determined from these actual hourly ratings according to the exceedence probability levels. As a result, 1,000 sets of static rating estimations are determined from the 1,000 simulated weather series. One set of static rating includes:

- Pre-fault and post-fault OHL static ratings over three seasons (summer, spring/autumn and winter)
- Cable static ratings over two seasons (summer and winter)
- Transformer static ratings over three seasons (summer, spring/autumn and winter)

Finally, these 1,000 sets of static ratings are analysed probabilistically. For each static rating type (e.g. summer post-fault rating of OHL), a number of 1,000 ratings of the specified type are extracted from all the sets and regarded as one analysis group. These ratings are sorted from low to high and placed into a cumulative probability distribution curve for probabilistic analysis (an example will be given later in this section in Fig.5-8).

On this distribution curve, the median of the ratings is taken at 50 percentile and is regarded as the central estimation. The full range of static ratings can be taken between the lowest rating and highest rating. Furthermore, six probability levels (as shown in

Table 5-1) are selected to divide the distribution of ratings into three ranges according to the likelihood of occurrence:

Table 5-1: Probability levels to range the ratings calculated from climate projections

Probability Level	Comment
0%	Never to be less than
10%	Very unlikely to be less than
33%	Unlikely to be less than
50%	Average: central estimate
66%	Unlikely to greater than
90%	Very unlikely to greater than
100%	Never to be greater than

The static rating assessment of the post-fault rating of Zebra ACSR OHL under the climate in Slough in the summers of the 2080s is given as an example for demonstration. Fig.5-7 illustrates the post-fault ratings determined by four Weather Series (WS) examples randomly selected from the simulated 1,000. It can be seen that the post-fault ratings determined from four different weather series are different. A total of 1,000 post-fault ratings are determined from the 1,000 weather series and are placed in to a histogram to present their probability distribution, as shown in the bottom half of Fig.5-8.The histogram shows that the ratings are centralized at the average rating of 897 A. The cumulative probability curve of the determined post-fault ratings is shown in the top half of Fig.5-8. The probability levels are applied to this curve and divide the ratings into three ranges. As a result, the likely range of post-fault ratings is between 885 A and 908 A. The conservative estimations of the ratings are from 868 A to 928 A. The full range of ratings are from 789 A to 959 A.

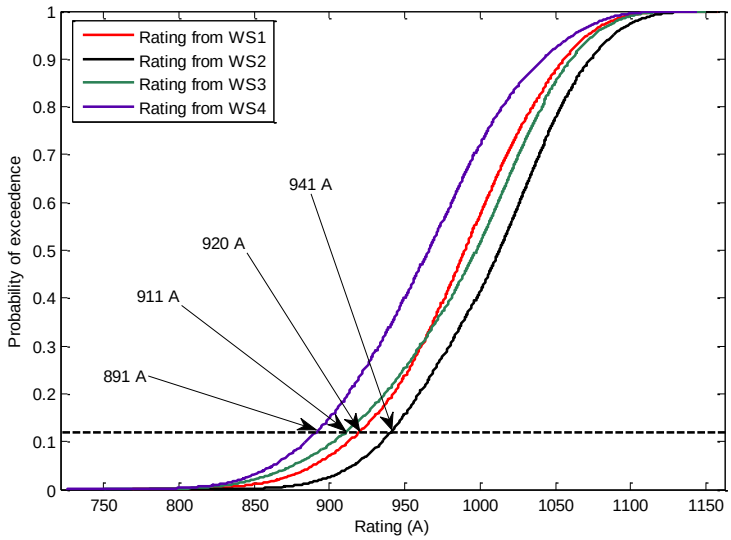

Fig.5-7: Post-fault ratings determined based on four weather series

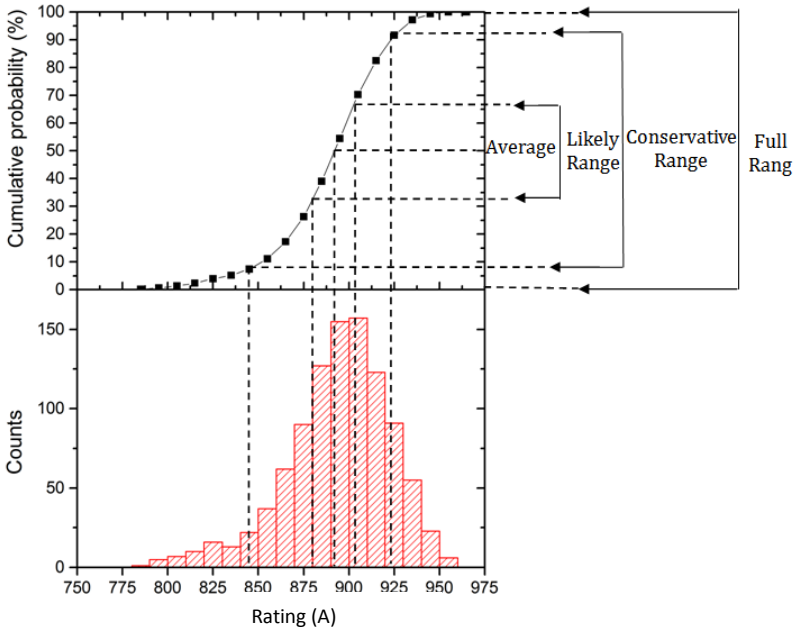

Fig.5-8: Histogram and cumulative probability distribution curve of the post-fault ratings from the 1000 weather series

5.2.1.2 Impacts on Overhead Line Static Ratings

An example of static rating assessment of Zebra ACSR conductor under the climate simulated in the high emission scenarios is demonstrated first. Then a comparison of

average ratings between the different types of the conductors is shown based on the weather in the 2080s only.

a) Impacts on Zebra ACSR Conductor

The projected static ratings are determined in four time periods which are baseline, 2020s, 2050s and 2080s. The impacts of climate change on the ratings are measured as the difference between the ratings in each future period (i.e., 2020s, 2050s and 2080s) and those in the baseline. Using the approach described in Section 5.2.1.1, the determined pre-fault and post-fault static ratings are presented in box plots in Fig.5-9 and Fig.5-10, respectively. In each figure, the ratings are grouped into three seasons, i.e., summer, spring/autumn and winter.

The boxes in the figures present the likelihood of occurrence of the ratings by different percentiles. The midline of the box indicates the average rating at 50 percentile. The top and bottom of the box are ratings at 66 and 33 percentiles, respectively. The upper and lower ends of the whiskers are the maximum and minimum ratings. Hence, the ratings within likely range are shown within the box. The ratings in full range are between the ends of whisker. For the clarity of presentation, the conservative range is not illustrated in box plots but given in the numbers in Table 5-2 and Table 5-3. The boxes plots are also used to show the ratings ranges of other types of components in the following sections. All boxes and whiskers in these plots refer to the description in this paragraph.

Fig.5-9 and Fig.5-10 show that both the pre-fault and post-fault ratings of OHL are expected to decrease as a result of climate change. The de-ratings become more and more serious from the 2020s, through the 2050s, to the 2080s. It should be noted that the ratings determined in a later time period are more disperse as more uncertainties are involved. The detailed values of average and different ranges of pre-fault and post-fault ratings taken from Fig.5-9 are shown in Table 5-2 and Table 5-3.

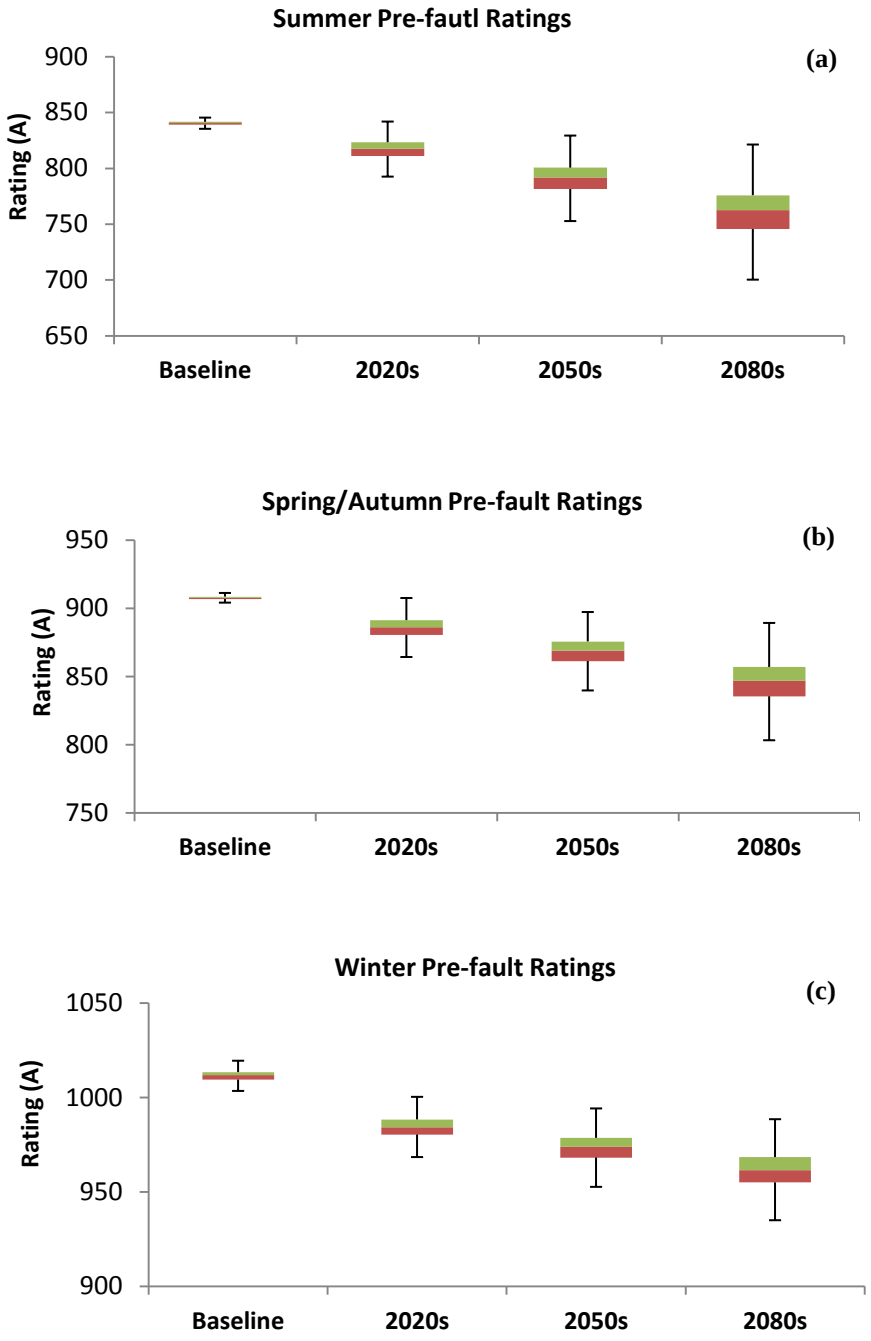

Fig.5-9: Projected pre-fault ratings of Zebra ACSR conductor in Slough in high emission scenario: (a) in Summer; (b) in Spring/August; (c) in Winter

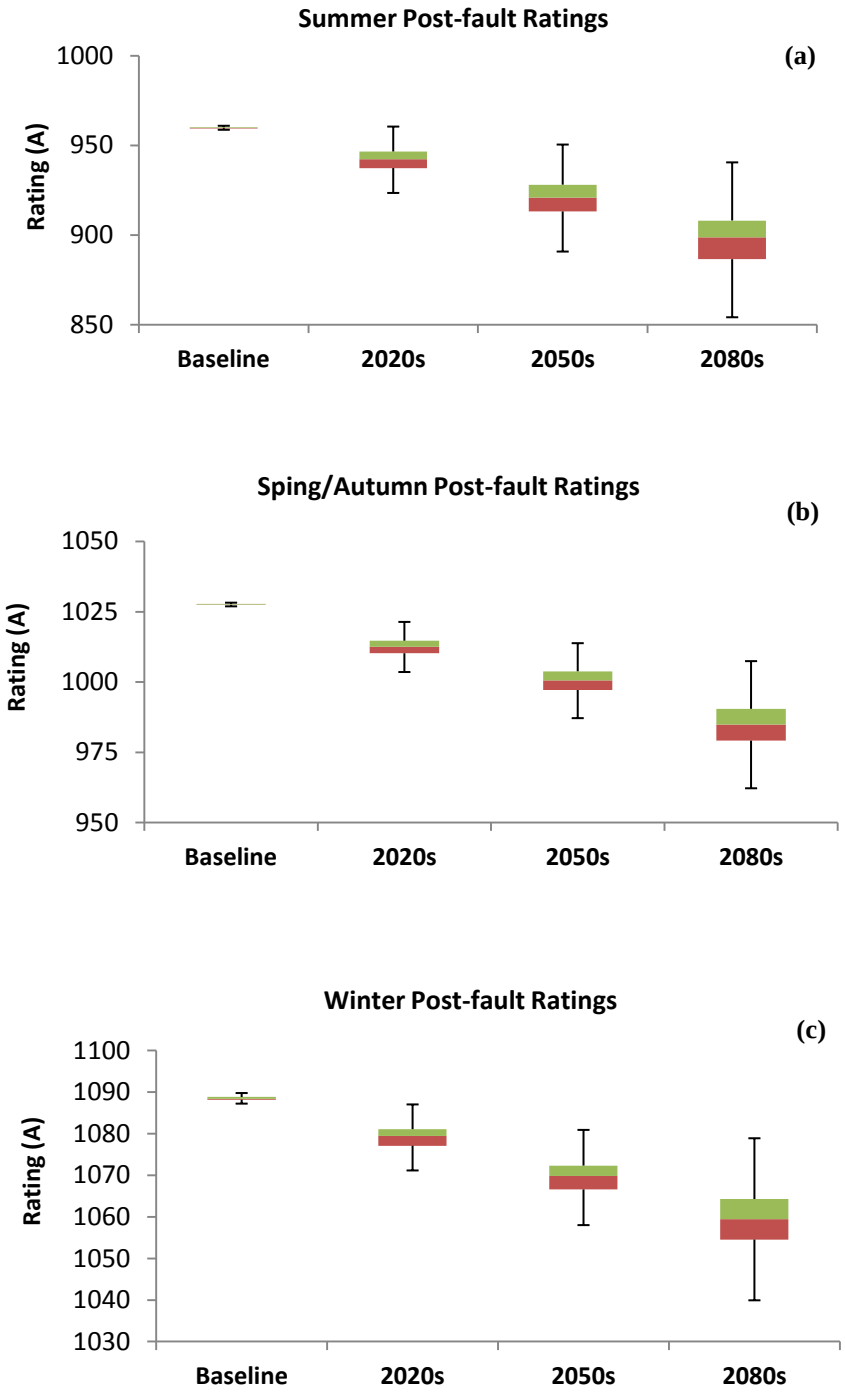

Fig.5-10: Projected post-fault ratings of Zebra ACSR conductor in Slough in high emission scenario: (a) in Summer; (b) in Spring/August; (c) in Winter

Table 5-2: Ranges of the projected pre-fault ratings of Zebra ACSR conductor in Slough in high emission scenario (Unit: A)

Period	Season	Average	Likely Range	Conservative Range	Full Range
2020s	Summer	816	811 to 823	797 to 835	766 to 855
	Spring	886	881 to 891	870 to 902	842 to 920
	Winter	984	953 to 1011	972 to 995	953 to 1011
2050s	Summer	789	781 to 801	755 to 818	698 to 849
	Spring	868	861 to 876	845 to 890	812 to 915
	Winter	973	968 to 979	958 to 987	938 to 1002
2080s	Summer	756	746 to 776	702 to 800	608 to 837
	Spring	845	835 to 857	810 to 877	756 to 906
	Winter	961	955 to 968	941 to 981	914 to 1006

Table 5-3: Ranges of the projected post-fault ratings of Zebra ACSR conductor in Slough in high emission scenario (Unit: A)

Period	Season	Average	Likely Range	Conservative Range	Full Range
2020s	Summer	941	937 to 947	926 to 955	901 to 970
	Spring	1012	1009 to 1016	1005 to 1019	994 to 1029
	Winter	1079	1077 to 1081	1073 to 1086	1063 to 1093
2050s	Summer	919	913 to 928	894 to 941	850 to 962
	Spring	1000	913 to 928	990 to 1010	969 to 1024
	Winter	1069	1067 to 1072	1059 to 1078	1044 to 1089
2080s	Summer	895	887 to 908	858 to 927	789 to 959
	Spring	984	979 to 990	967 to 1000	937 to 1020
	Winter	1059	1055 to 1064	1043 to 1073	1021 to 1090

Taking the existing static ratings calculated based on the baseline weather data as the references, the percentage of the average de-ratings are gained and shown in Fig.5-11. It can be observed that from the 2020s to the 2050s and to the 2080s, the de-ratings of

both the pre-fault and post-fault in different seasons all become greater since the level of climate change gradually increases with time. Furthermore, the summer ratings are challenged by the greatest reductions whilst the winter ratings have the least reductions. The greatest de-ratings are expected to take place in the summer of 2080s with the reductions of 10.05% and 6.79% for pre-fault ratings and post-fault ratings respectively. It can also be observed that at a certain time frame, the de-ratings of post-fault ratings are less than those of pre-fault ratings in each season. This indicates that the climate change has more impact on the pre-fault ratings with the increasing extreme weather conditions in the future.

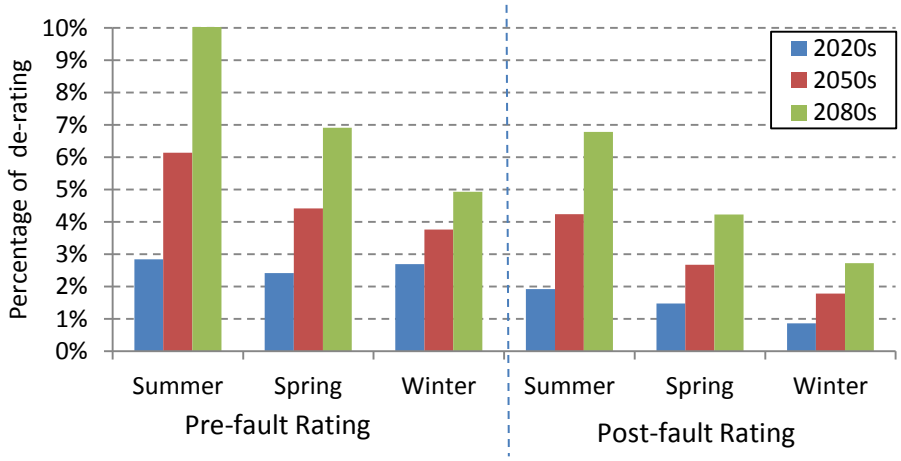

Fig.5-11: Percentage of average de-ratings of Zebra ACSR conductor in High emission scenario

b) Other types of conductors

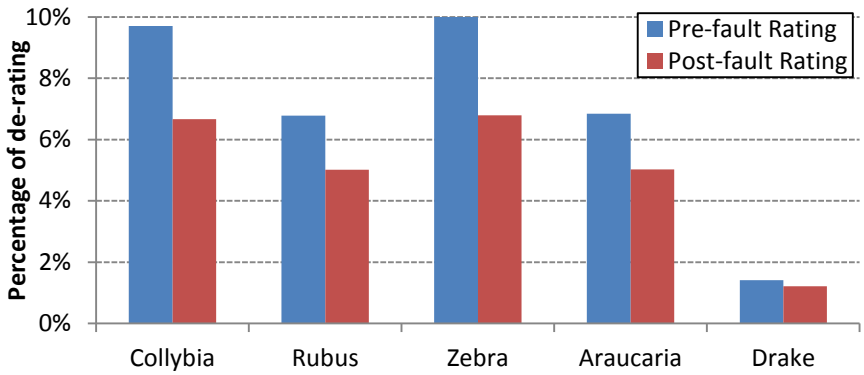

Fig.5-12: Comparison of the percentage of average summer de-ratings between different types of conductors in high emission scenario in the 2080s

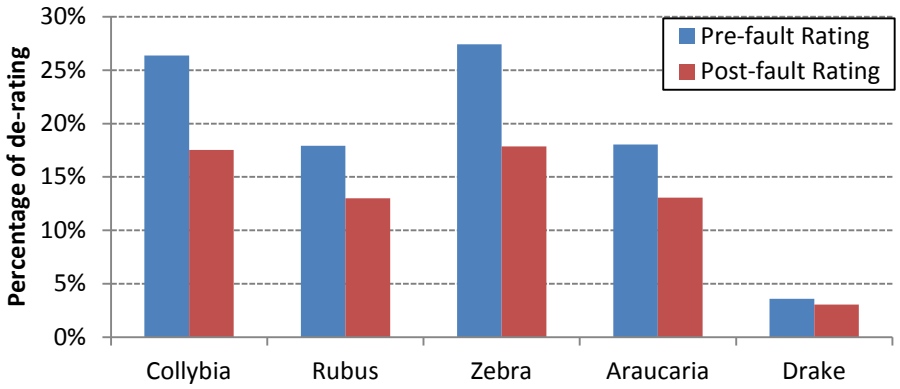

Fig. 5-13: Comparison of the percentage of maximum summer de-ratings between different types of conductors in high emission scenario in the 2080s

Various types of overhead line conductors are selected to compare the impact of climate change on their ratings. The comparison of the percentage of average and maximum summer de-ratings for these conductors is shown in Fig.5-12 and Fig. 5-13, respectively.

It can be seen in Fig.5-12 that the de-rating of an overhead line is dominated by its rated temperature. The Collybia ACAR and Zebra ACSR have the greatest decrease in ratings as they are limited by a low rated temperature at 75 ℃. The percentages of de-ratings of the AAAC conductors with a rated temperature at 90 ℃ are much less than those of ACAR and ACSR conductors. The novel Drake ACCR conductor has the least percentages of de-ratings of 1.41% and 1.21% for pre-fault and post-fault ratings benefiting from its high rated temperature at 240 ℃.

For the conductors with the same rated temperature, the one with a smaller diameter has a slightly higher percentage of de-ratings. For example, although Rubus conductors and Araucaria conductors have a difference of 5.76 mm in diameter, their percentages of reduction in pre-fault ratings are only with a difference of 0.06% (Rubus 6.78% and Araucria 6.84%).

Fig. 5-13 shows that the maximum de-rating of Zebra ACSR conductor can be as high as 27.41% in the summer of 2080s. It clearly indicates that the Drake ACCR conductor performs well against the climate change even in this worst case with a maximum de-

rating of 3.6% only.

5.2.1.3 Impact on Cable Ratings

Within this section, the impacts of climate change on an example XLPE 1600 mm^2 cable are presented. The de-ratings of different types of cables are also provided.

a) XLPE 1600 mm^2 Cable

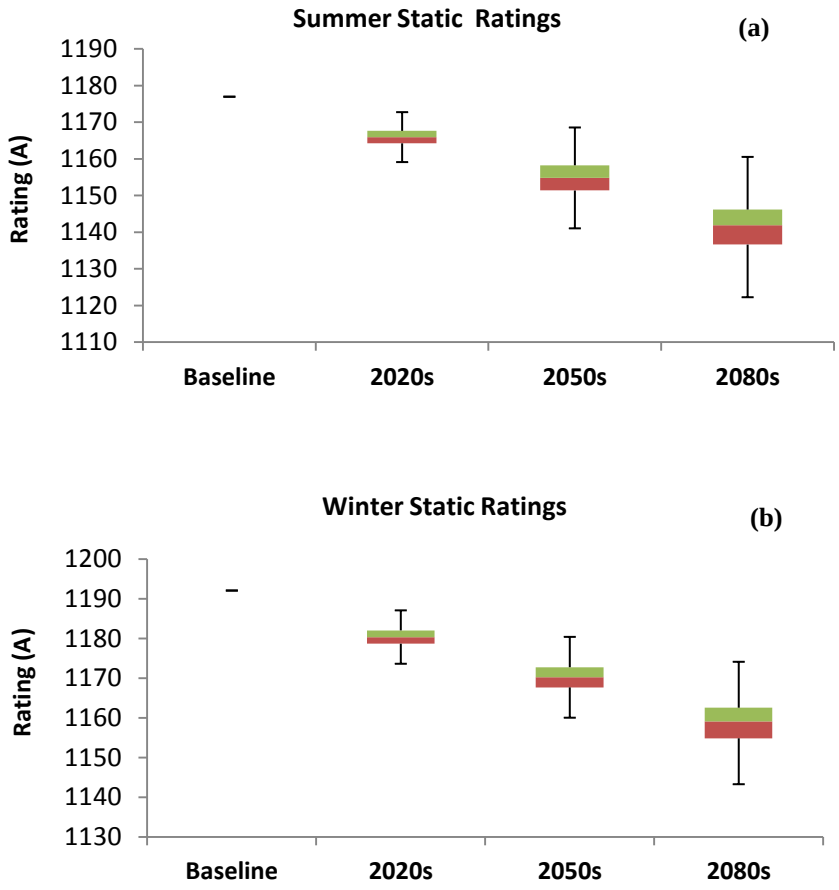

Fig.5-14: Projected static ratings of XLPE 1600 mm^2 cable in Slough in high emission scenario: (a) in Summer; (b) in Winter

An XLPE 1600 mm^2 cable is used as an example to demonstrate the impact of climate change on cable ratings. The soil moisture condition surrounding the cable is assumed to be consistent with that for the soil temperature model, i.e., the soil thermal resistivity

is at 1.2 Km/W. The cables are supposed to be directly buried in the flat formation at the depth of 2 m with spacing of 0.8 m from each other. The sheath loss and armour loss are considered in the calculation.

The ranges of the ratings calculated from the 1000 simulated climate projections with an assumption of high emission scenario are shown in Fig.5-14. The results show that the cable ratings decrease as a result of climate change. More details of the ranges at different levels are presented in Table 5-4.

Table 5-4: Ranges of projected static ratings of XLPE 1600 mm2 cable in Slough in high emission scenario (Unit: A)

Period	Season	Average	Likely Range	Conservative Range	Full Range
2020s	Summer	1166	1164 to 1168	1159 to 1172	1151 to 1179
	Winter	1180	1179 to 1182	1174 to 1185	1166 to 1190
2050s	Summer	1154	1151 to 1158	1144 to 1163	1125 to 1173
	Winter	1170	1168 to 1173	1162 to 1178	1147 to 1186
2080s	Summer	1141	1137 to 1146	1124 to 1155	1097 to 1170
	Winter	1158	1155 to 1163	1145 to 1170	1123 to 1183

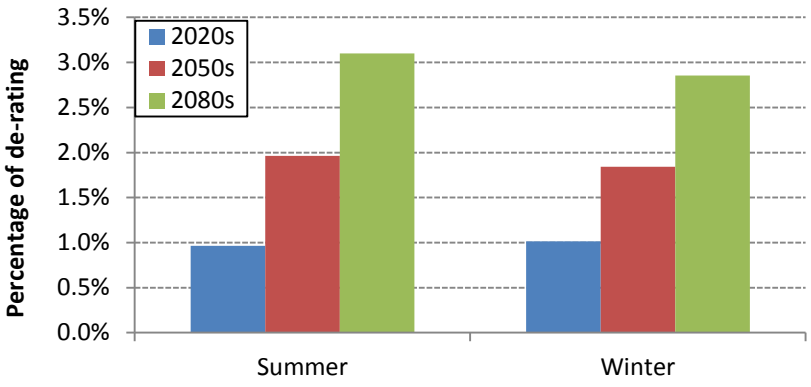

Fig.5-15: Percentage of average de-ratings of XLPE 1600 mm2 cable in High emission scenario

The percentages of de-ratings of XLPE 1600 mm2 cable are obtained by comparing the "future" ratings to existing ratings and are shown in Fig.5-15. It can be seen in the

figure that the maximum de-ratings of the cable occurs in the summers of the 2080s and is only 3.10%. The summer ratings have more reduction than the winter ratings. However, the difference is not significant.

b) Other Types of Cables

The study of both XLPE and Fluid-Filled cable ratings under future climate conditions are carried out. The average percentages of de-ratings in the 2080s of high emission scenario are shown in Fig.5-16. It can be seen that the de-ratings are below 5% for all the types of cable in different sizes. Fluid-filled 2500 mm^2 cable's rating has the most reduction of 4.63%. The XLPE cables are less affected by climate change than the Fluid-filled cables. As all types of the cables are rated at the same temperature of 90 °C, the differences in de-ratings are caused by the design of the insulation system. The fluid-filled cables are designed to use the paper insulation with a higher thermal resistivity than XPLE insulated cables. For the same type of cables, the cable with a larger conductor size has a smaller de-rating. This difference caused by conductor size is significant for Fluid-filled cables but insignificant for XLPE cables.

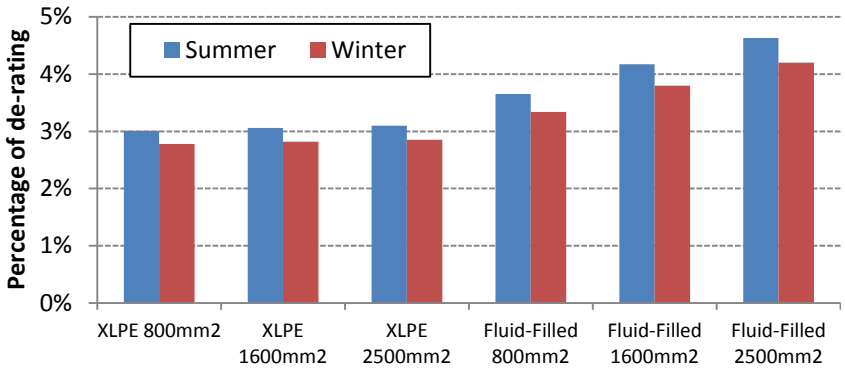

Fig.5-16: Comparison of the percentage of average de-ratings between different types of cables in high emission scenario in the 2080s

The comparison of the maximum de-ratings between different types of cables is presented in Fig. 5-17. In the worst case, the de-ratings of all cables assessed are over 6.5% in the summers of the 2080s. The fluid-filled 2500 mm^2 cable has the greatest

maximum de-rating which can be up to 10.28%.

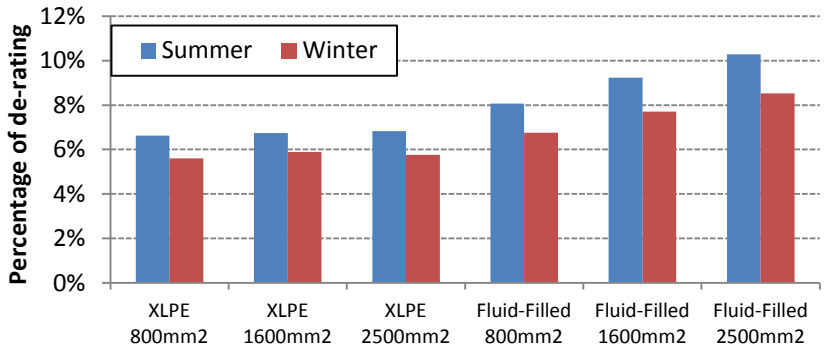

Fig. 5-17: Comparison of the percentage of maximum de-ratings between different types of cables in high emission scenario in the 2080s

5.2.1.4 Impact on Transformer Ratings

This section presents the impacts of climate change on an ONAF transformer as an example, and compares the de-ratings of different types of transformers.

a) ONAF Transformer

The ranges of static ratings of ONAF transformer within high emission scenarios is shown in Fig.5-18. The transformer ratings are presented in the form of load factor which is defined as load current over rated current. The unit of load factor is p.u. The ratings decrease with the climate change in all the rating seasons. Table 5-5 gives the details the ratings in different ranges.

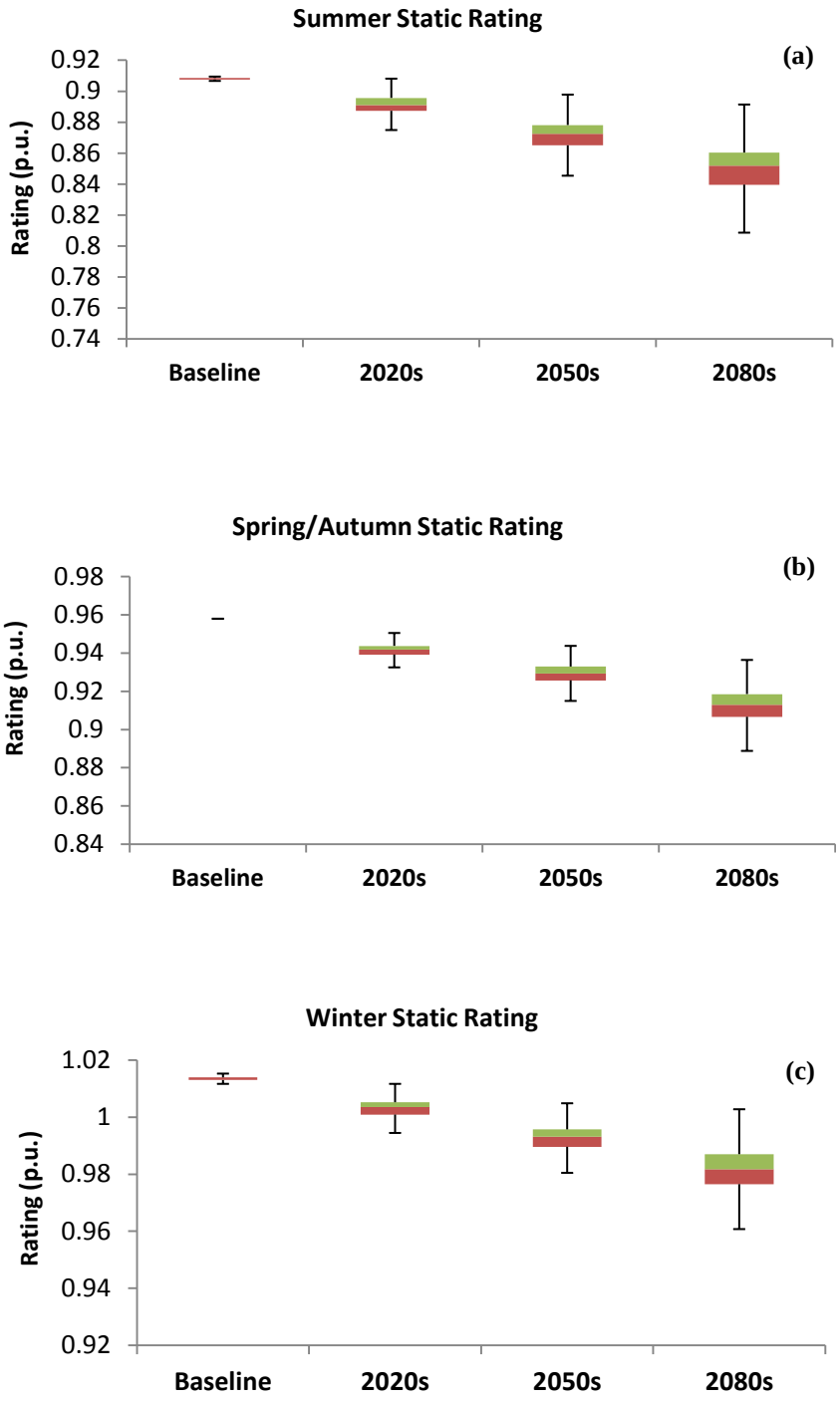

Fig.5-18: Projected ratings of ONAF transformer in Slough in high emission scenario: (a) in Summer; (b) in Spring/August; (c) in Winter

Table 5-5: Ranges of projected static ratings of ONAF transformer in Slough in high emission scenario (Unit: p.u.)

Period	Season	Average	Likely Range	Conservative Range	Full Range
2020s	Summer	0.8905	0.8873 to 0.8956	1 to 0.903	0.8547 to 0.9167
	Spring	0.9414	0.9392 to 0.9437	1 to 0.949	0.923 to 0.9588
	Winter	1.0035	1.0009 to 1.0052	1 to 1.0104	0.9861 to 1.0182
2050s	Summer	0.8704	0.865 to 0.8781	1 to 0.891	0.8108 to 0.9085
	Spring	0.9287	0.9257 to 0.9329	1 to 0.9392	0.8984 to 0.9526
	Winter	0.9923	1 to 1.0018	1 to 1.0018	0.9677 to 1.013
2080s	Summer	0.8478	0.8396 to 0.8603	1 to 0.879	0.7545 to 0.9021
	Spring	0.9119	0.9066 to 0.9185	1 to 0.9293	0.866 to 0.9482
	Winter	0.9810	0.9765 to 0.987	1 to 0.9966	0.9428 to 1.0147

Compared to the ratings calculated with the baseline climate, the percentages of de-ratings of ONAF transformers are gained and shown in Fig.5-19. It shows that the ratings in the 2020s are similar to the baseline ratings with less than 2% of de-ratings. The de-ratings become obvious in the 2050s and reach the maximum in the 2080s with a reduction of 6.64%, 4.78% and 3.22% for summer, spring and winter, respectively.

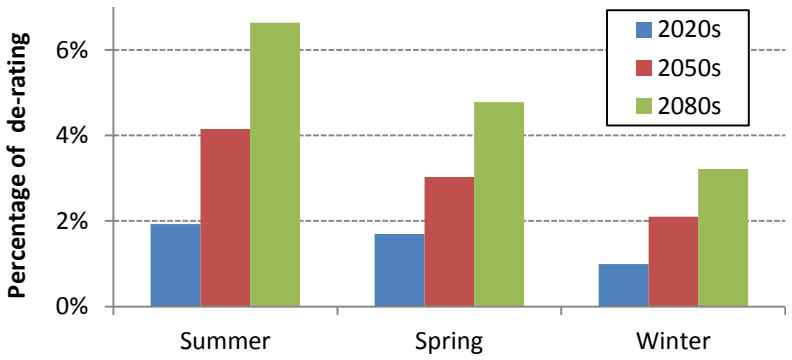

Fig.5-19: Percentage of average de-ratings of ONAF transformer in High emission scenario

b) Other Types of Transformers

The comparisons of de-ratings between various types of transformers in Fig.5-20 and Fig. 5-21 indicate that the de-ratings of the transformers are dominated by the methods of oil cooling. This is proved by the fact that ONAF transformers have the highest level of de-rating whist the OF transformer has the least.

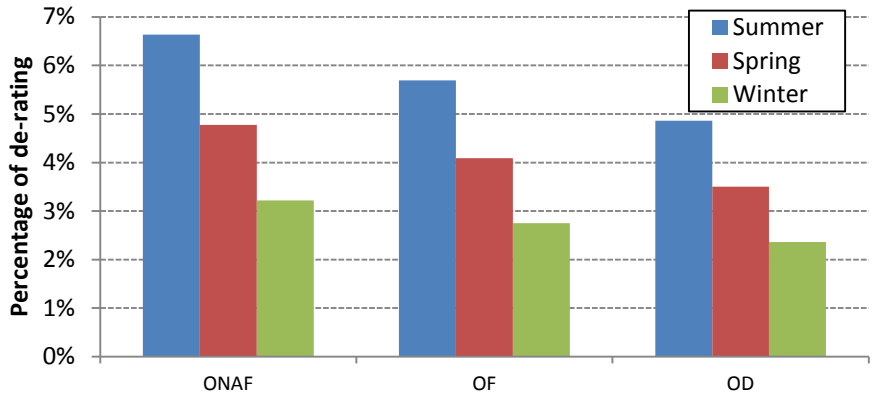

Fig.5-20: Comparison of the percentage of average de-ratings between different types of transformers in high emission scenario in the 2080s

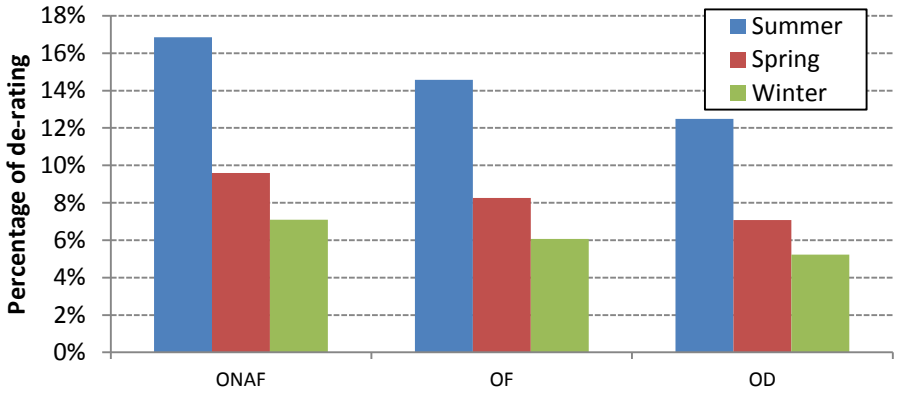

Fig. 5-21: Comparison of the percentage of maximum de-ratings between different types of transformers in high emission scenario in the 2080s

Shown in the two figures, the average and maximum summer de-ratings of ONAF transformers are up to 6.64% and 16.86% by the 2080s. The de-ratings of OF and OD transformers are relatively lower than those of ONAF transformers. For OF transformers, the summer de-ratings are 5.69% on average and 14.57% as maximum. The OD transformer has the lowest de-ratings of 4.86% and 12.48% on average and the

worst case, respectively, in the summer of the 2080s. The de-ratings in other seasons are also presented in the figures.

5.2.2 Impacts of Climate Change on Overhead Line Dynamic Ratings

5.2.2.1 Probabilistic Assessment of Impacts on Dynamic Ratings

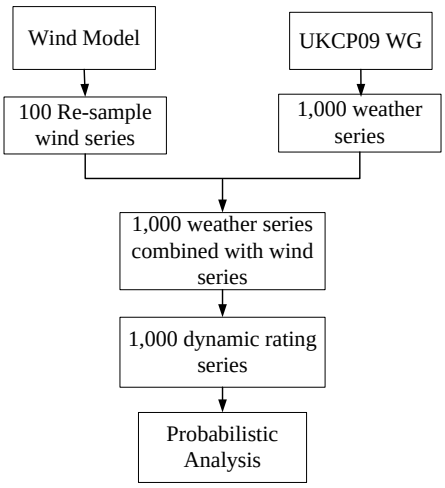

Fig.5-22: Probabilistic assessment of the impacts of climate change on dynamic ratings

The approach to assess the impacts of climate change on dynamic ratings is similar to that on static ratings. It calculates the ratings based on 1,000 weather series and analysis the results probabilistically. In the calculation, wind speed is also considered as a variable in addition to air temperature and solar radiation used for static ratings. Furthermore, dynamic ratings are implemented considering all the calculated hourly ratings based on varying weather conditions, whilst static ratings only care about the extreme weather scenarios and are fixed ratings determined at the certain probability levels on the distribution curve of calculated hourly ratings. Fig.5-22 illustrates the probabilistic approach used in this study to assess the impacts of climate change on the dynamic rating. The air temperature and solar radiation are generated in UKCP09 WG and are presented in the form of hourly weather series. The wind speeds are re-sampled with the wind model. A number of 100 re-sampled wind series are provided. As wind is not correlative to the air temperature and solar radiation, one weather series from the WG is combined with a wind series randomly picked from the 100 series. In such a way,

enough variety in combinations of wind and other weather variables covering all the possible cases are provided. The hourly dynamic ratings are then calculated based on these 1,000 combined weather series at each time point. The final step is to analysis these 1,000 dynamic rating series to investigate the impacts of climate change on them. A Zebra ACSR OHL is taken as an example to demonstrate the approach and present the study results.

Assuming that the Zebra ACSR OHL is located at Slough, the dynamic ratings are calculated based on the weather data within four time periods: baseline (i.e. existing climate), 2020s, 2050s and 2080s. In each of the time periods, a series of 30-year hourly dynamic ratings can be obtained from one weather series. A series of dynamic ratings can form cumulative distribution curves. 1,000 such curves from 1,000 weather series form the shadow area as shown in Fig.5-23. At each percentile, the minimum and maximum values are calculated to give a range of possible ratings.

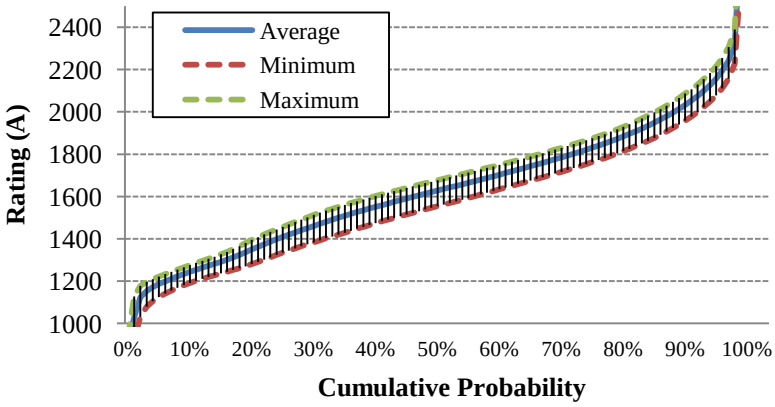

Fig.5-23: Range of the hourly ratings of Zebra ACSR conductor based on 1000 runs of the simulation weather data in the 2080s

5.2.2.1 Impacts on average ratings

Due to the limitation of space, only the ratings at seven percentiles (2%, 5%, 25%, 50%, 75%, 95%, and 98%) are presented as the study results. Table 5-6 shows the average ratings of a zebra ACSR OHL at the seven percentiles. It can be seen that the rating at each percentile keeps decreasing from now to the 2080s as the result of climate change.

Taking the ratings under baseline climate as the references, the percentage of reduction of average ratings are calculated and presented in Table 5-7. The results show that the reductions are only from 1.02% to 1.70% in 2020s. The most severe reductions take place in the 2080s with a range between 2.76% and 5.52%, which is much smaller compared to the reduction of 10% for static rating shown in Section 5.2.1.1. Therefore, an overhead line that operates with dynamic ratings would appear to be more resilient to climate change when compared to that operating with a static rating. This is due to the inclusion of wind speed in the thermal model which provides a significant level of cooling meaning the air temperature is no longer the primary factor in determining the rating.

Table 5-6: Average ratings of zebra ACSR OHL at different percentiles (Unit: A)

	2%	5%	25%	50%	75%	95%	98%
baseline	1090	1223	1456	1687	1887	2189	2307
2020	1071	1207	1437	1665	1864	2166	2283
2050	1052	1191	1420	1644	1844	2147	2263
2080	1029	1171	1398	1620	1821	2126	2243

Table 5-7: Reduction of average ratings of Zebra ACSR OHL at Different Percentiles (Unit: %)

	2%	5%	25%	50%	75%	95%	98%
2020	1.70	1.35	1.26	1.30	1.19	1.04	1.02
2050	3.47	2.61	2.49	2.52	2.27	1.93	1.87
2080	5.52	4.23	3.96	3.94	3.48	2.89	2.76

5.2.2.2 Range of rating reductions

Further study of the 1,000 calculated dynamic rating series can determine the ranges of the rating reductions (the average values given above being the mean scenario). These ranges are bounded with the maximum and minimum ratings provided by the 1000 simulated weather series data. Table 5-8 gives the minimum ratings. The baseline

ratings remain the same as shown in Table 5-6 since these are ratings in the existing climate. The predicted minimum ratings in the 2020s, 2050s and 2080s are calculated based on the worst assumption of unfavourable climate change. The percentage decreases in the minimum ratings are presented in Table 5-9. A significant de-rating of 15.18% can be seen at 2% probability level. This de-rating is very close to the 14% de-rating of the static rating given in [1]. However, the de-ratings are less (from 6.39% to 9.61%) at other percentiles. This reinforces the conclusion that an overhead line operated with the dynamic rating can mitigate the impact of climate change.

Table 5-8: Minimum ratings of zebra ACSR OHL at different percentiles (Unit: A)

	2%	5%	25%	50%	75%	95%	98%
baseline	1090	1223	1456	1687	1887	2189	2307
2020	979	1181	1406	1634	1833	2125	2238
2050	958	1148	1371	1592	1796	2093	2202
2080	924	1105	1324	1546	1753	2049	2156

Table 5-9: Reduction of minimum ratings of Zebra ACSR OHL at Different Percentiles (Unit: %)

	2%	5%	25%	50%	75%	95%	98%
2020	10.13	3.41	3.44	3.12	2.86	2.89	2.96
2050	12.10	6.13	5.83	5.64	4.80	4.36	4.54
2080	15.18	9.61	9.08	8.36	7.10	6.39	6.54

Table 5-10 and Table 5-11 show the maximum ratings and their de-ratings at different percentiles. These results are obtained based on the best assumption of a more favourable climate change, i.e. more favourable weather conditions than those under the baseline climate in some cases. Negative numbers are presented in Table 5-11 and indicate upratings of the overhead line. The de-ratings caused by climate change will start to take place at some percentiles (5%, 50% and 75%) from the 2050s. The most significant decrease in maximum rating is only up to 1.11% at 75% probability level in the 2080s.

Table 5-10: Maximum ratings of zebra ACSR OHL at different percentiles (Unit: A)

	2%	5%	25%	50%	75%	95%	98%
baseline	1090	1223	1456	1687	1887	2189	2307
2020	1141	1226	1464	1693	1893	2205	2322
2050	1135	1221	1459	1685	1881	2191	2314
2080	1128	1210	1444	1670	1866	2184	2307

Table 5-11: Reduction of maximum ratings of Zebra ACSR OHL at Different Percentiles (Unit: %)

	2%	5%	25%	50%	75%	95%	98%
2020	-4.69	-0.24	-0.58	-0.33	-0.31	-0.74	-0.69
2050	-4.13	0.2	-0.21	0.14	0.29	-0.12	-0.32
2080	-3.53	1.09	0.78	1.01	1.11	0.21	-0.02

5.3 Summary

This chapter applied the climate models and simulation tools to the thermal models of power system components to assess the impacts of climate change on the ratings of power system components.

The determination methods of static ratings for all of the three components were then described, whilst the determination method of the dynamic rating was only presented for OHL. To assess the impacts of climate change on the rating of these components, the probabilistic assessment approach was presented. Results were shown for all the three components for static ratings and only OHL for dynamic ratings.

Within the results, the components ratings projected for future periods (i.e., 2020s, 2050s and 2080s) were compared to those in the baseline climate. The differences in between were used to quantify the impacts of climate change.

Chapter 6 Impacts of Climate Change on Power System Reliability

Until now, the impacts of climate change that have been investigated in this thesis are on individual power system components. As identified in Chapter 1, power system reliability may also be affected by climate change due to components de-rating, although no study concerning this issue has been completed in the past. This chapter addresses this gap in research, which presents the *third original contribution* of this thesis.

In this chapter, a general description of the methodology is firstly provided. The uncertain factors that are considered during the assessment, the test network, the Sequential Simulation (SS) approach, and the indices used to represent the power system reliability are all introduced. The reliability of the test network is assessed without and with component failure. Under each condition, case studies are carried out with different combinations of assumptions for rating and load scenarios.

6.1 Methodology

The methodology used in this thesis to assess the impacts of climate change on power system reliability is illustrated in Fig. 6-1. Firstly, the future rating and load scenarios are predetermined according to the climate change level and assumption of future energy demand, respectively. The power component ratings and load profile from these scenarios are then used to reconfigure the test network. The uncertainties involved are the variation of load conditions and failure event of the transmission lines, which are sampled using Sequential Simulation (SS) technique. The reliability evaluation is carried out through the power flow study under the system conditions given by the SS. Finally, the reliability indices are calculated based on the simulation results to indicate the reliability changes in different assumed scenarios.

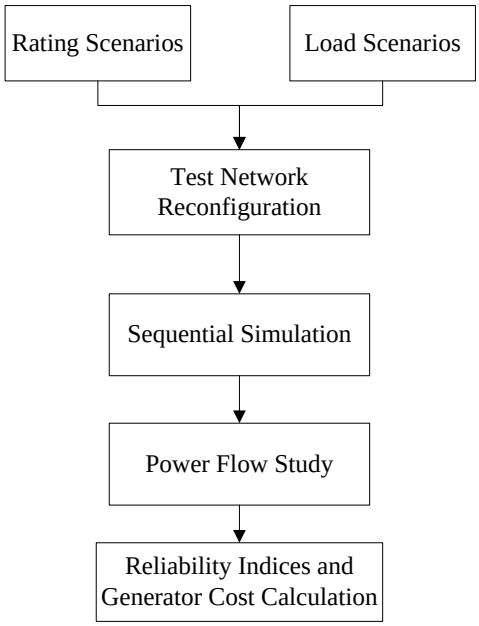

Fig. 6-1: Assessment of impacts of climate change on power system reliability

6.1.1 Future Rating Scenario

A transmission route consists of overhead lines (OHLs), cables and transformers which are connected in series to deliver the electric power. Since the OHLs are expected to have larger percentages of de-ratings than the transformers and the cables, the power

delivery ability of a route, in the context of climate change, is actually limited by de-ratings of OHLs. To simplify the study, only the OHL de-ratings are considered to configure the thermal limits of the test network for the system reliability evaluation. The ratings of other components in the future are assumed to remain the same as the designed ratings.

The future rating scenarios used in this study are based on OHL pre-fault static rating assessment results presented in Chapter 5. The Zebra ACSR conductor is selected to demonstrate the impact of its de-rating on the system reliability because it is expected to have the greatest de-rating among different types of conductors. Compared to the designed ratings based on the baseline climate, the percentages of maximum de-ratings of Zebra ACSR summer pre-fault static ratings at Slough from the 2020s to the 2080s are shown in Fig. 6-2. Although a maximum de-rating of approximately 30% will occur in the 2080s according to assessment results, a higher maximum de-rating of 50% is taken to test the system reliability under an even worse case. Therefore, the de-ratings from 0% to 50% are used to reconfigure the test network, where 0% means no de-rating happens.

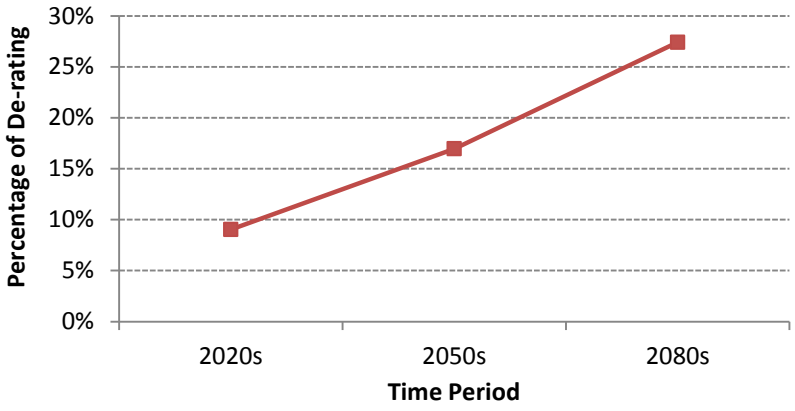

Fig. 6-2: Percentages of maximum reduction of Zebra ACSR summer pre-fault static ratings in Slough from the 2020s to the 2080s

6.1.2 Future Load Scenario

The increasing load is another challenge to the system reliability. In this study, the

future peak load is assumed to be 1.2 times the baseline peak load. This is chosen according to the Gone Green scenario described by *UK future Energy Scenario Report* in which the study results predict peak loads to increase by 1.17 times from 2015 to 2035[83].

6.1.3 Test Network

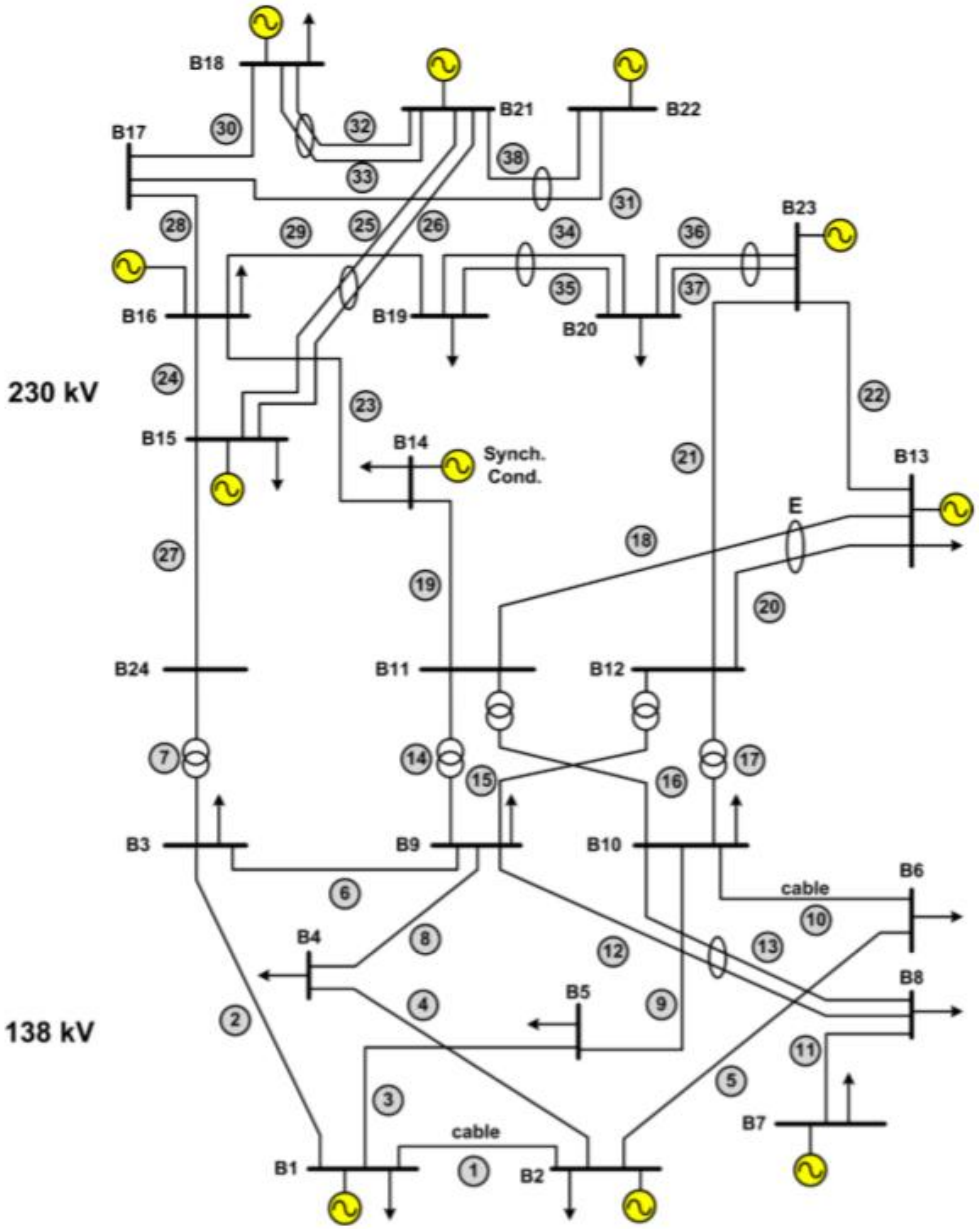

Fig. 6-3: IEEE Reliability Test System 1996 network diagram

The IEEE Reliability Test System (RTS) 1996 is utilized throughout this chapter to demonstrate the impacts of climate change on system reliability. As shown in Fig. 6-3, this system contains 24 buses, 38 branches and 11 generators. All system details including line parameters, standard loading, generator parameters and OPF data are included in Appendix C. A full description of the network can be found in [30].

6.1.4 Sequential Simulation

To reconfigure the test network, two uncertainties are sampled using Sequential Simulation (SS) technique, including load conditions and component failure.

Regarding the load conditions, the chronological annual load is sampled from the load curve and performs reliability assessment at each hourly load [83]. The annual reliability indices are calculated using an equal probability of 1/8760 for each hourly load.

The component failure event is sampled according to the components' random behaviour. The system state is unpredictable as failures can occur at any time and location in the system. SS captures this uncertainty by generating random outages for all system components. The time of a component to failure (*TTF*) and time to repair the failure component (*TTR*) are generated on the basis of a random generated number *U* in the range 0 to 1. In this study, exponential distribution is used to sample *TTF* and *TTR*, as shown below:

$$TTF = -\frac{1}{\lambda} lnU_1 \tag{6.1}$$

$$TTR = -\frac{1}{\mu} lnU_2 \tag{6.2}$$

$$\lambda = \frac{1}{MTTF} \tag{6.3}$$

$$\mu = \frac{1}{MTTR} \tag{6.4}$$

where, λ is the component failure rate (occurrence/year) and μ is the component repair rate (1/hrs). MTTF and MTTR are Mean Time To Failure and Mean Time To Repair, respectively. The operating cycle is created in time series by the sampled *TTF* and *TTR* as illustrated in Fig. 6-4. The component is available in "UP" condition and is unavailable during repair in "DOWN" condition.

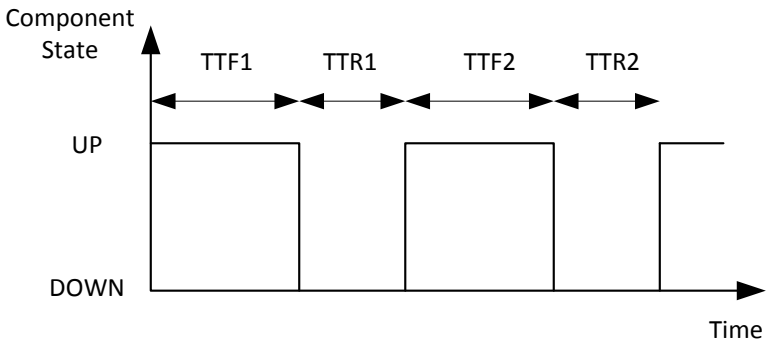

Fig. 6-4: Component operating cycle based on randomly sampled TTF and TTR

6.1.5 Power Flow Study

The power flow study is to gain a specified patter of load and generation by solving for the set of voltages and power flows in a network. The DC optimal power flow study is carried out in this thesis. Thus, the optimization vector x only consists voltage angle, Θ, and generator real power injection, P_g, as described in Equation (6.5).

$$x = \begin{bmatrix} \Theta \\ P_g \end{bmatrix} \tag{6.5}$$

The objective of the optimization is to solve the power flow patterns providing the minimum generator cost as the form below.

$$min \sum_{i=1}^{n_g} f_P^i(P_g^i) \tag{6.6}$$

subject to

$$g_P(\Theta, P_g) = B_{bus}\Theta - P_g = 0 \tag{6.7}$$

$$h_f(\Theta) = B_f\Theta - \mathrm{F_{max}} \leq 0 \tag{6.8}$$

$$h_t(\Theta) = -B_t\Theta - \mathrm{F_{max}} \leq 0 \tag{6.9}$$

$$\Theta_{\mathrm{i}}^{\mathrm{ref}} \leq \Theta_{\mathrm{i}} \leq \Theta_{\mathrm{i}}^{\mathrm{ref}}, \quad i \in \mathrm{I_{ref}} \tag{6.10}$$

$$P_g^{i,min} \leq P_g \leq P_g^{i,max}, \quad i = 1 \dots n_g \tag{6.11}$$

where $n_g$is generator number, $\mathrm{I_{ref}}$ is generator indices, B is susceptance matrix, $\mathrm{F_{max}}$ is the branch flow limit which is affected by the component ratings, t and f denote to *from* and *to* the end, respectively.

The modelling of the IEEE 24-bus RTS has been completed using MATLAB environment (version 8.2.0.701 R2013b) with the network data provided in [30]. The power flow study is performed using Optimal Power Flow (OPF) function in MATPOWR [31].

6.1.6 Reliability Indices and Generator Cost Calculation

Loss-of-Load Duration (LOLD) and Expected Energy Not Supplied (EENS) are two reliability indices used to measures the system's reliability in this thesis. A loss of load is defined as a system failure to match demand due to insufficient available generation capacity or outage of system components. The LOLD is the total duration of loss of load events over a specified period. The EENS is the expected energy that will not be supplied during the loss of load event.

The LOLD is calculated as shown in (6.5).

$$LOLD = \frac{1}{N}\left(\frac{1}{8760}\sum_{i=1}^{N} LLD_i\right) \tag{6.5}$$

The EENS is calculated as shown in (6.6), respectively.

$$EENS = \frac{1}{N}\sum_{i=1}^{N} ENS_i \tag{6.6}$$

The cost for an individual generator is calculated with a polynomial function as described in (6.7). The calculation of total generator cost is given in (6.8).

$$Cost = c_2 p^2 + c_1 p + c_0 \tag{6.7}$$

$$Cost_{total} = \frac{1}{N}\sum_{i=1}^{N}\sum_{j=1}^{M} Cost_{i,j} \tag{6.8}$$

The definitions for all the symbols above are as follows:

ENS_i	Energy not supplied in sampling year i
N	Number of sampling year.
LLD_i	Loss of load duration in sampling year i
M	Number of generators in the system
p	Generator output
c_1, c_2, c_3	Generator cost coefficient

6.2 Reliability Assessment without Component Failure

In this part of the study, it is assumed that all the components are fully reliable. Therefore, no component failure and repair time are considered. The assessment approach is firstly described. The reliability assessment results from four case studies are then presented.

6.2.1 Assessment Approach

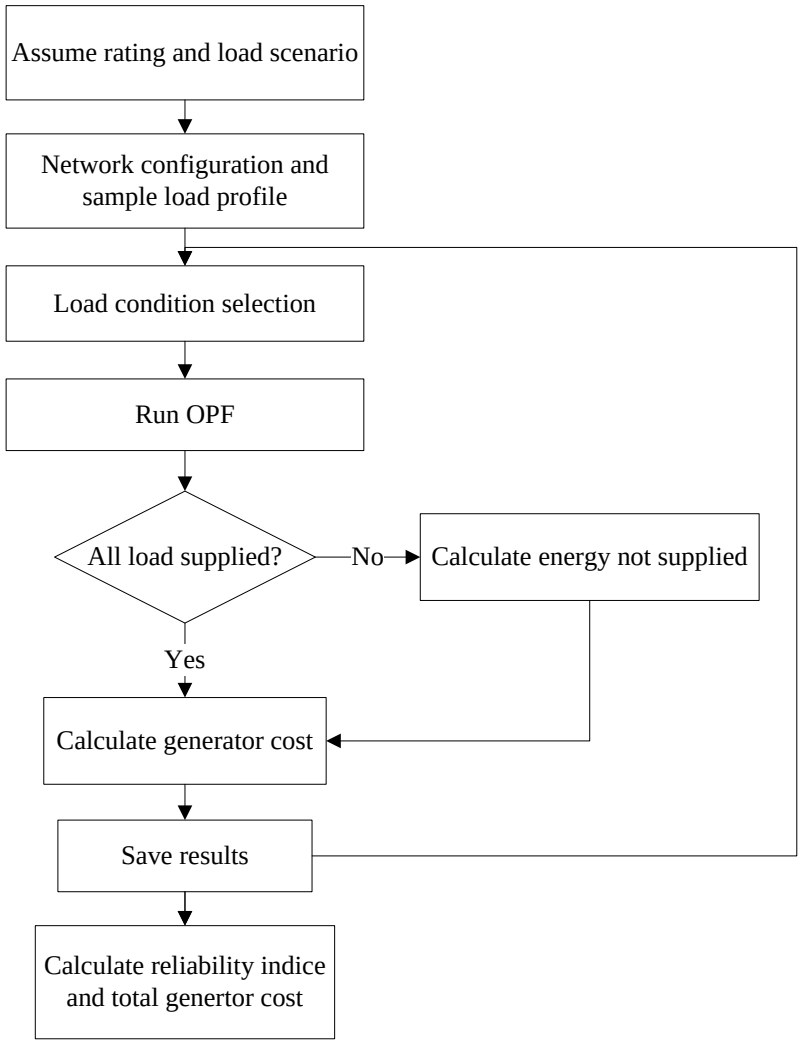

Fig. 6-5: Assessment approach of impacts of climate change on power system reliability without component failure

To assess the reliability of the test network with no component failure, the first step is to predetermine the rating and load scenarios according to the climate change level and assumptions of energy demand, respectively. The power component ratings are then used to reconfigure the test network. One year of an hourly load profile, containing 8760 load conditions, is sampled from the load curve in the assumed energy scenario. For each load condition, the OPF constrained by the thermal limit of the transmission lines and the generator costs is carried out. According to the OPF results, if the expected load is not met as a result of thermal constraints, the energy not supplied is calculated

and a loss of load event is counted. Whether the expected load is matched or not, the generator costs are calculated and saved. To assess the system performance under all the load conditions throughout a year, the OPF study is repeated 8760 times. Finally, the reliability indices, including Loss of Load Frequency (LOLD), Expected Energy Not Supplied (EENS) and total generator costs, are calculated based on the results. This whole process is summarized in Fig. 6-5.

6.2.2 Case Studies

Four case studies are conducted based on different ratings and load scenarios to investigate the impacts of climate change on power system reliability. In the first three cases, the system is operated with static ratings only. In the fourth case, a study of application of dynamic ratings is carried out.

The baseline load presents the existing load scenario sampled from the load profile suggested by the IEEE RTS. The future load profile is assumed to increase. However, it should be noted that the change in load is not correlated to the change in climate in this study.

The baseline ratings designed according to the existing climate are taken as the static ratings. The de-ratings of power system components at different levels of climate change are considered as future rating scenarios. As discussed in Section 6.1.1, in this study, the impacts of climate change on power system reliability are determined by the OHL de-rating which thermally constrains the power delivery ability on a transmission branch.

6.2.2.1 Case 1: Baseline Load and Baseline Rating

In this case, the reliability of the test network is evaluated with the baseline load and baseline rating scenario, as a benchmark. The ratings of transmission lines remain the same as designed and the baseline load profile is used. The total system load in each hour is sorted from the largest to the smallest and presented in the load curve illustrated

in Fig. 6-6. The load condition is sampled from this curve in each iteration of the OPF study. The load at each bus is then calculated according to its proportion of the total load as suggested in [30].

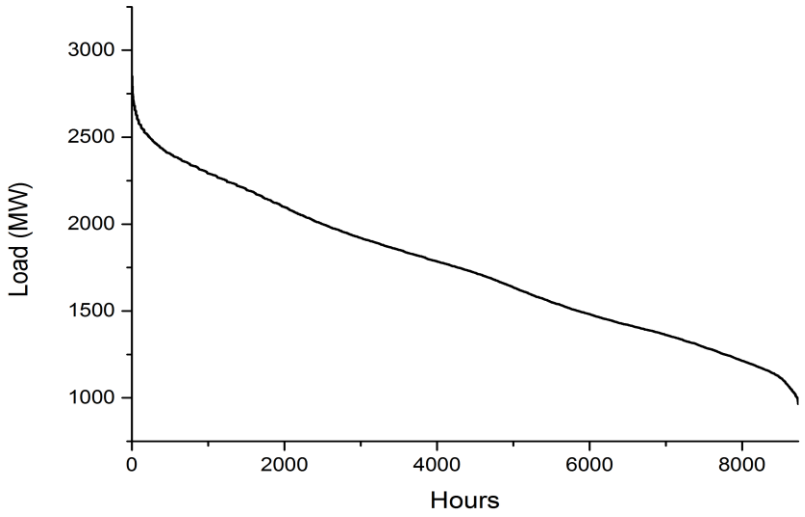

Fig. 6-6: Load curve in baseline load scenario

The study result shows the system is perfectly reliable since no loss-of-load event occurs throughout all the load conditions. The total generator cost is 191.55 M$ in this case.

6.2.2.2 Case 2: Baseline Load and Future Rating

This case considers that the system is stressed by the de-ratings caused by climate change but the load remains as baseline.

The results show that no loss-of-load took place under any of the load conditions, i.e. the demand is always fully supplied, even when a 50% of de-rating scenario is applied, and therefore EENS is 0 MWh. Fig. 6-7 shows the total generator cost according to the increase in the percentage of de-rating. When the de-rating goes from 0 to 20%, the generator cost remains around 192.55 M$. However, it increases significantly to 245.60 M$ when the de-rating goes up to 50%. This proves that the system remains fully reliable with de-rating up to 50% by paying an increasing generator cost.

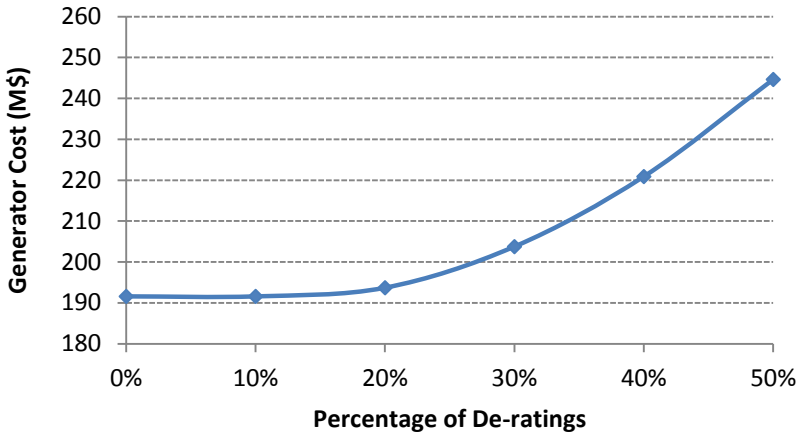

Fig. 6-7: Total generator cost in case 2: baseline load and future rating

6.2.2.3 Case 3: Future Load and Future Rating

In this case study, the future load is assumed to increase 1.2 times that of the baseline load. The future load curve is shown in the red line while the baseline load curve is shown in the black line in Fig. 6-8.

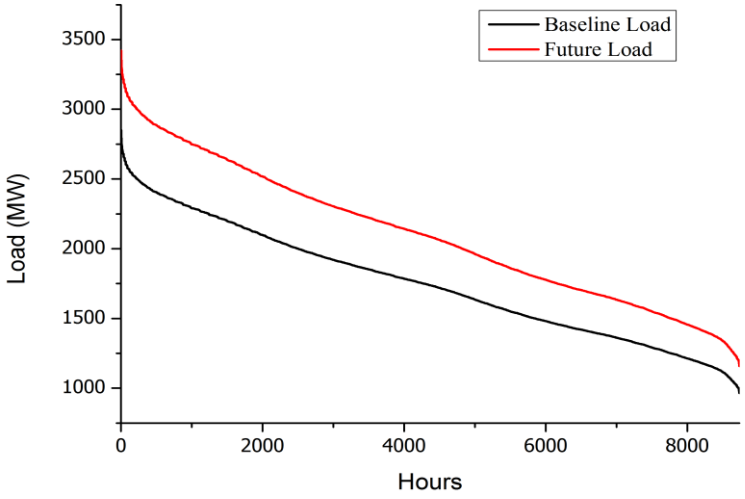

Fig. 6-8: Load curves in future and baseline load scenarios

The results in this case indicate that the system reliability is reduced as the result of the combination of increasing load and decreasing ratings. The LOLD increases with decreasing ratings as shown in Fig. 6-9. It reaches 4.11% when a de-rating of 50% is

assumed. As shown in Fig. 6-10, the EENS also increases as a result of loss-of-load event and can be up to 7546 MWh in the worst situation. Moreover, as can be seen from the two figures, the increase in both LOLF and EENS is minor when the de-rating is less than 30%, and becomes significant when the de-rating is over 40%.

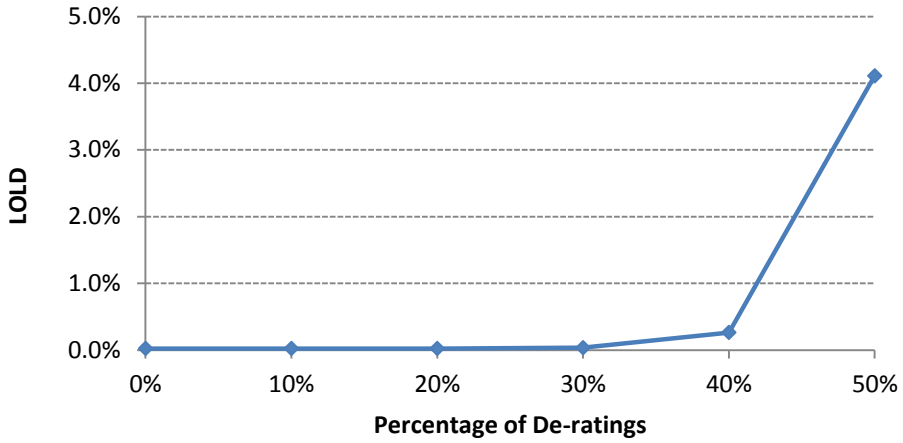

Fig. 6-9: LOLD in case 3: future load and future rating

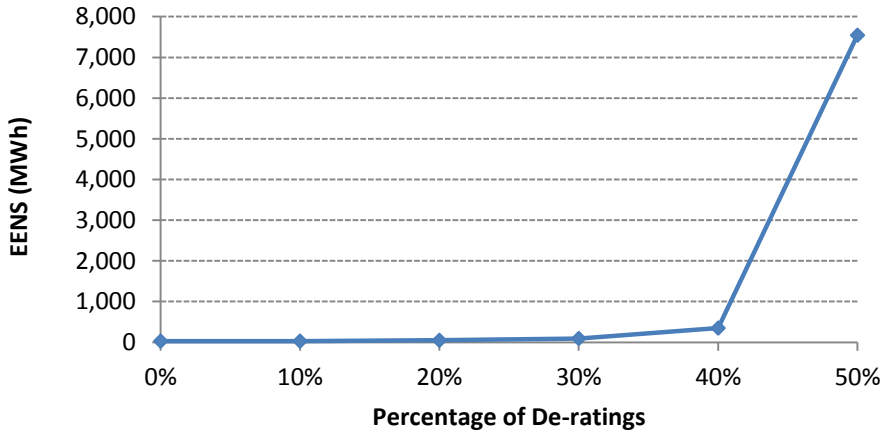

Fig. 6-10: EENS in case 3: future load and future rating

Furthermore, Fig. 6-11 indicates that the thermal limits on the transmission lines will result in more total generator cost. The increase in cost becomes significant when the de-rating is over 20%. According to the previous results of LOLD and EENS, the system still maintains good reliability when the de-rating is below 30%. This indicates

the system can still remain reliable but more constraints cost is expected when the de-rating is between 20% and 30%.

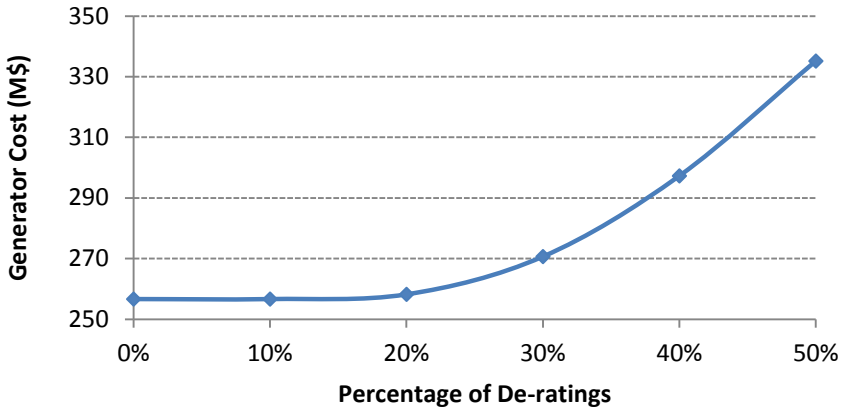

Fig. 6-11: Total generator cost in case 3: future load and future rating

6.2.2.4 Case 4: Application of Dynamic Ratings

In Case 4, the impact of climate change on the system reliability is revaluated assuming that the OHL dynamic rating is applied. The study is carried out based on the worst case with a future load increase 1.2 times that of the baseline load and a de-rating of 50%. The Zebra ACSR conductor is assumed as the type of the selected line operated with dynamic rating. The hourly dynamic rating is calculated based on the air temperature and solar radiation at Slough in the 2080s simulated from UKCP09 WG and the wind speeds re-sampled with a wind model.

a) Application of Dynamic Rating on One Line

The first attempt is to operate only one of the transmission lines in the test network with dynamic rating. To select this line, the full load hours of all the lines are counted based on the power flow study result on the system operated with static ratings only. As shown in Fig. 6-12, line 22 has the largest full load time of 5729 hours. It is therefore selected to be operated with the dynamic rating.

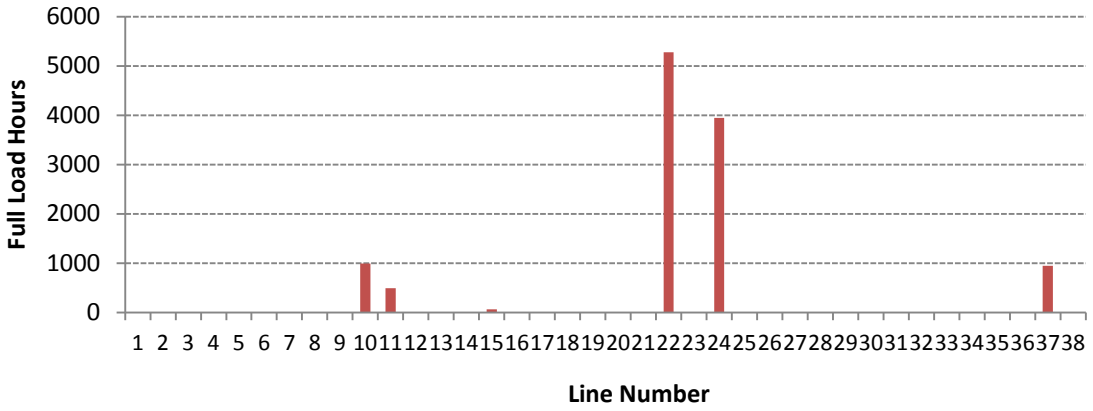

Fig. 6-12: Full load hours of each transmission line when the whole system is operated with static ratings

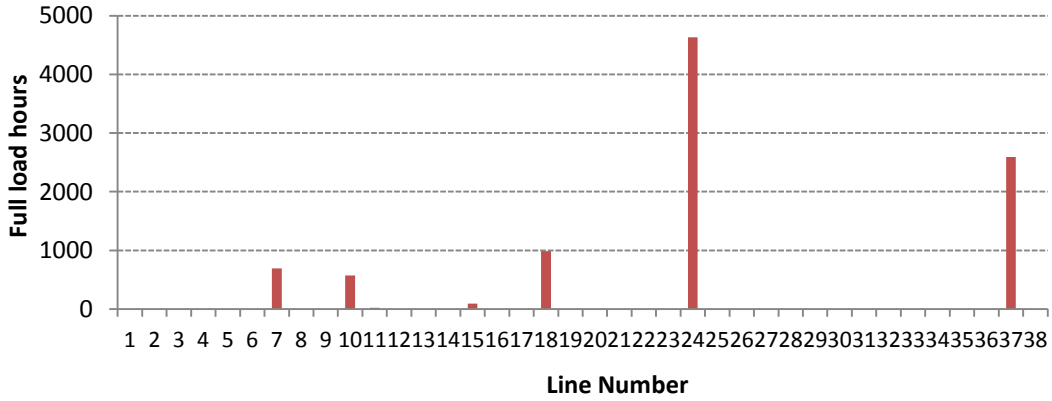

Fig. 6-13: Full load hours of each transmission line when Line 22 is operated with dynamic ratings

The system reliability is then evaluated assuming that Line 22 is operated with the dynamic rating; the other 37 lines are operated with the static rating, and the load is 1.2 times that of the baseline load. Fig. 6-13 shows that Line 22 is never constrained when it is at dynamic ratings. The resulting indices show that the LOLF decreases from 4.11% when all lines are at static ratings, to 3.08% when Line 22 is at dynamic rating. The EENS decreases from 7546 MWh to 3035 MWh. Moreover, the generator cost is 335 M$ with the dynamic rating application which is lower than 300 M$ with systems operated at static ratings only. Even when only one line is operated at dynamic ratings, the study results indicate huge benefit in terms of not only the enhancement in system

reliability but also in the reduction in generator cost. Hence, the application of dynamic ratings can mitigate impacts of component de-ratings caused by climate change.

b) Application of Dynamic Rating on Three Lines

Furthermore, an application of dynamic ratings on three lines is investigated. Based on the analysis on the full load hours of the system operated with dynamic rating on Line 22, as shown in Fig. 6-13, Line 24 and Line 37 are another two lines which are frequently thermally constrained (by 4634 hours and 2591 hours, respectively).

For the system with dynamic rating implemented on the three lines, the reliability assessment results, including the LOLD, EENS and total generator cost, are presented inFig. 6-14, Fig. 6-15 and Fig. 6-16, respectively. For the purpose of comparison, the indices obtained from the system with only static ratings and the system with dynamic ratings on Line 22 are also included in these figures.

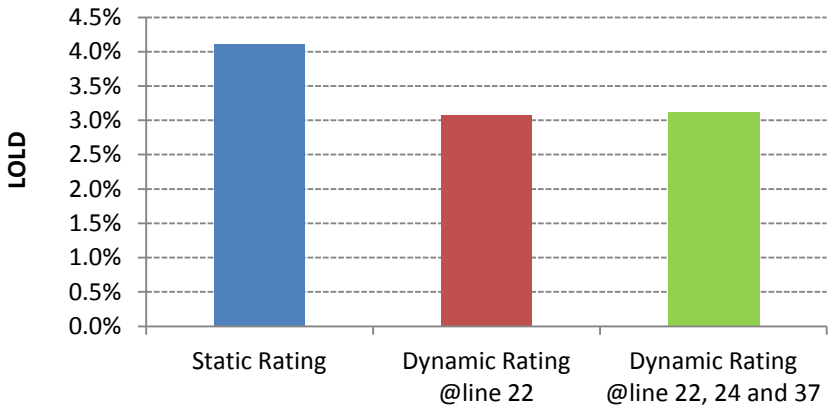

Fig. 6-14: Comparison of LOLD of the system operated with static ratings and dynamic ratings

Looking first at Fig. 6-14, the LOLF is 3.11% for the system with three lines operated at dynamic ratings, which is close to 3.08% for the system with only one line operated at dynamic rating. Fig. 6-15 shows that EENS decreases slightly from 3035MWh to 2883MWh when the number of lines with dynamic ratings changes from one to three. Both of these figures demonstrate that although the system reliability can be

significantly improved when dynamic rating is implemented (compared to the situation in which only static rating is used), increasing the number of lines operated with dynamic rating from one to three can only further enhance the system reliability very slightly. Finally, it can be seen from Fig. 6-16 that the generator cost is decreased from 300 M$ to 275 M$ when three transmission lines are operated using the dynamic rating.

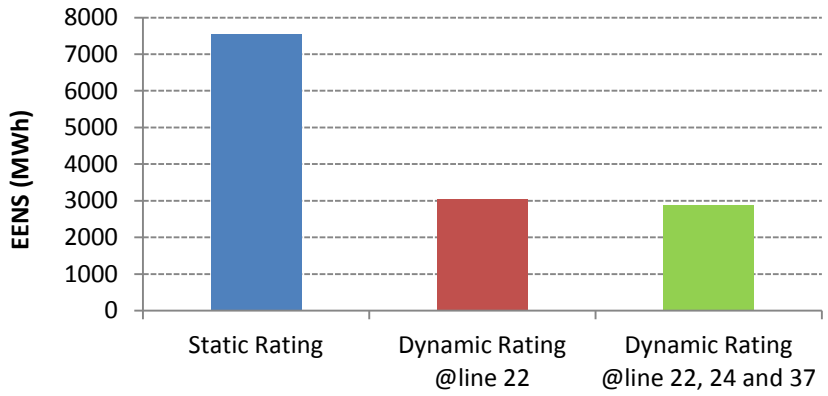

Fig. 6-15: Comparison of EENS of the system operated with static ratings and dynamic ratings

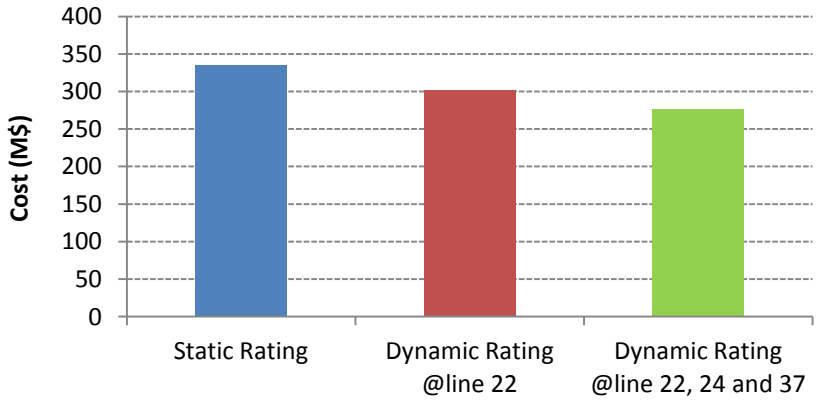

Fig. 6-16: Comparison of generator cost of the system operated with static ratings and dynamic ratings

6.3 Reliability Assessment with Component Failure

The system reliability in this section is evaluated assuming the component failure follows N-1 criterion, which means only one component may be unavailable at one time.

The approach to assessing the system reliability is described in section 6.3.1. The case study results are presented in Section 6.3.2. As the assessment involving component failure is extremely time-consuming in terms of computation, the application of dynamic ratings is not included in this section.

6.3.1 Assessment Approach

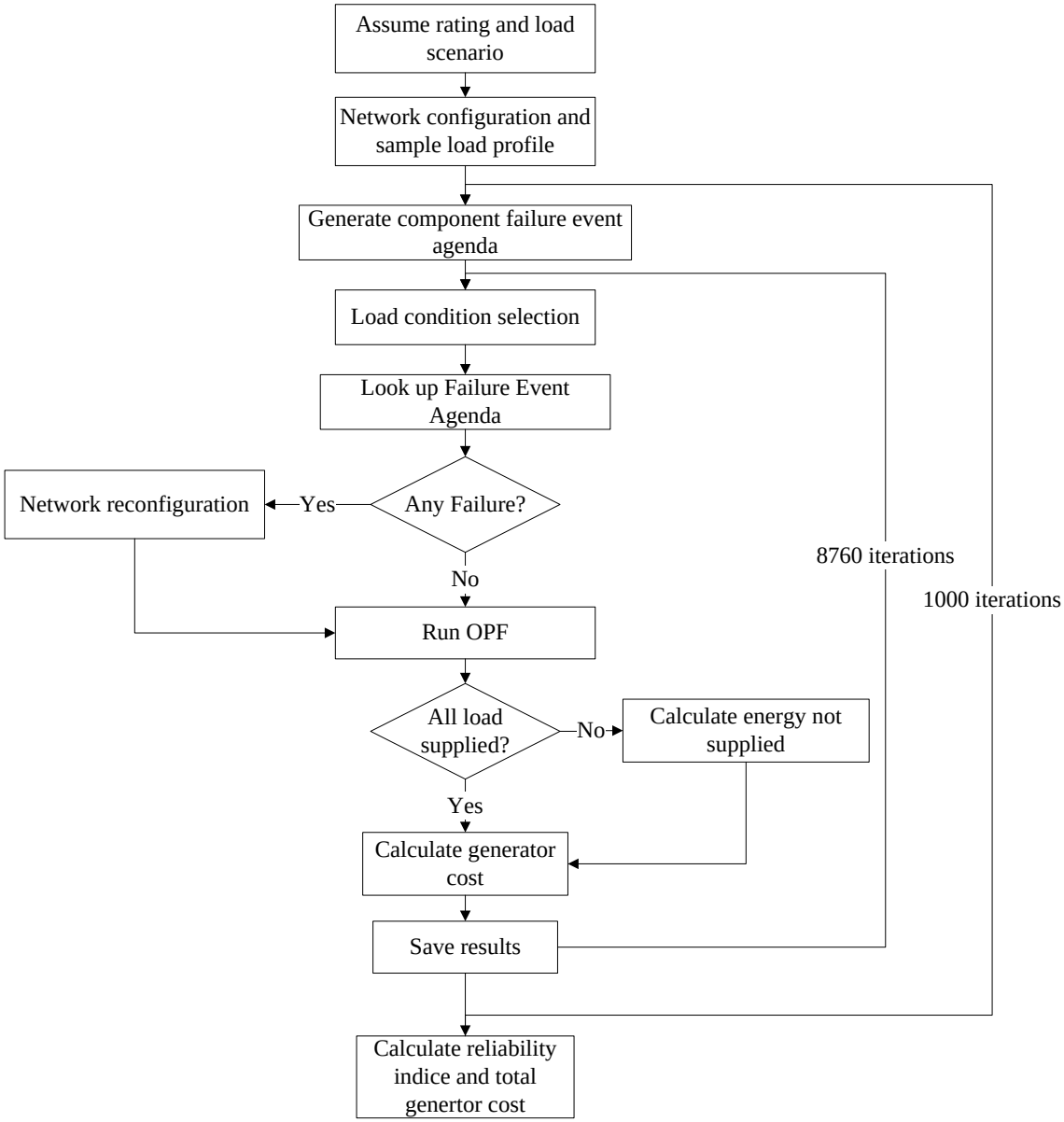

Fig. 6-17: Assessment approach of impacts of climate change on power system reliability with component failure

The assessment approach to evaluate the system reliability with component failures is illustrated in Fig. 6-17. The OHL de-ratings and load increase are the uncertain factors that cause the change in system reliability. The same rating scenario and load scenario are assumed as those in Section 6.2, and are used to configure the network and generate the load profile. The component failure event is then sampled using SS techniques and placed in an agenda in an hourly time series. A different failure event is generated in each iteration. At each selected hourly load condition, the failure event agenda is firstly checked. If no component fails in the hour, the OPF is immediately processed. Otherwise the network is reconfigured by disabling the failed lines. The OPF is then carried out on the reconfigured network. Based on the OPF results, the energy expected not supplied and generator cost are calculated and saved. This is repeated until all the 8760 load conditions with failure event agenda are computed. Furthermore, the assessment is repeated with new sampled failure event agendas 1000 times. Then the final assessment result is calculated as the average of all the 1000 results.

6.3.2 Case Studies

Two cases studies are carried out under the assumption of the OHL de-ratings along with baseline and future load scenarios, respectively.

6.3.2.1 Case 5: Baseline Load and Future Rating

As shown in the blue lines in Fig. 6-18 and Fig. 6-19, no loss-of-load event is expected to take place without the consideration of component failure. Considering component failure, the system can still be reliable when the de-rating is less than 30%. However, when the de-rating is over 30%, the values of LOLD and EENS dramatically increase, as shown in the red lines in the figures. This indicates that the climate change can influence the system reliability by decreasing component ratings even in the baseline load scenario. Fig. 6-20 shows that the generator costs of no component failure system and N-1 system are almost the same at each de-rating percentage (and both go up when the de-rating increases), and therefore the component failure will not change the generator cost.

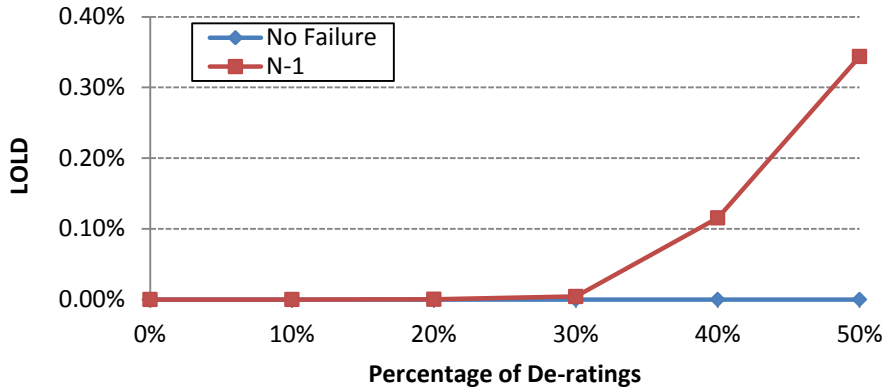

Fig. 6-18: LOLD in case 5: baseline load and future rating

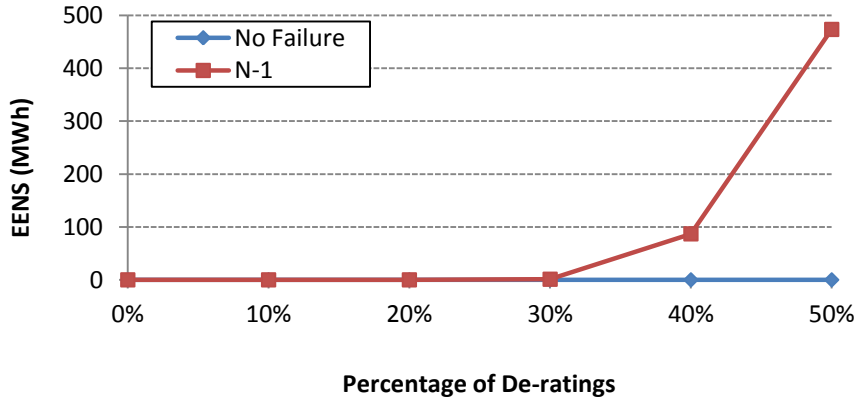

Fig. 6-19: EENS in case 5: baseline load and future rating

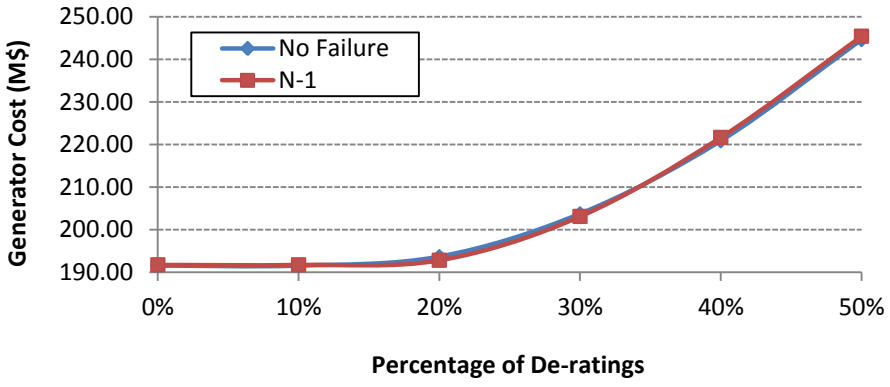

Fig. 6-20: Generator cost in case 5: baseline load and future rating

6.3.2.2 Case 6: Future Load and Future Rating

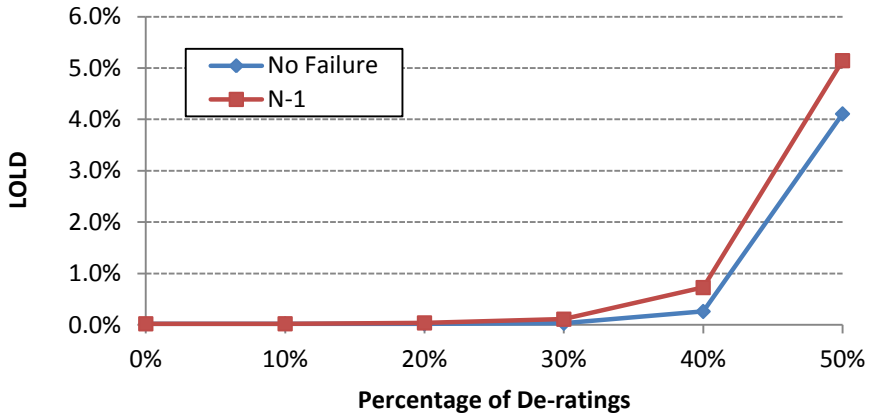

Fig. 6-21: LOLD in case 6: baseline load and future rating

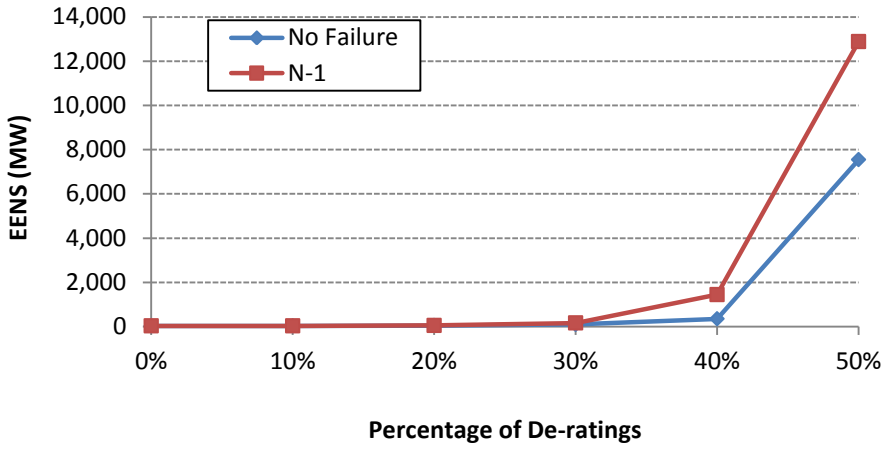

Fig. 6-22: EENS in case 6: baseline load and future rating

Case 6 assesses the reliability of the test system with component failure in a future load scenario. Fig. 6-10 and Fig. 6-11 indicate that the component failure can increase the impact of climate change on system reliability. Without component failure, the LOLF (blue line) are 0.03%, 0.26% and 4.11% at de-ratings of 30%, 40% and 50%, respectively. Considering component failure in N-1 criterion, it (red line) increases to 0.11%, 0.73%, 5.14%, respectively. The EENS is also expected to be greater with component failure. At de-ratings of 50%, it can be as high as 12883 MWh, about 1.7 times as that without failure. Fig. 6-23 again demonstrates only slight increases in

generator cost, indicating that the cost is primarily influenced by component ratings rather than component failure.

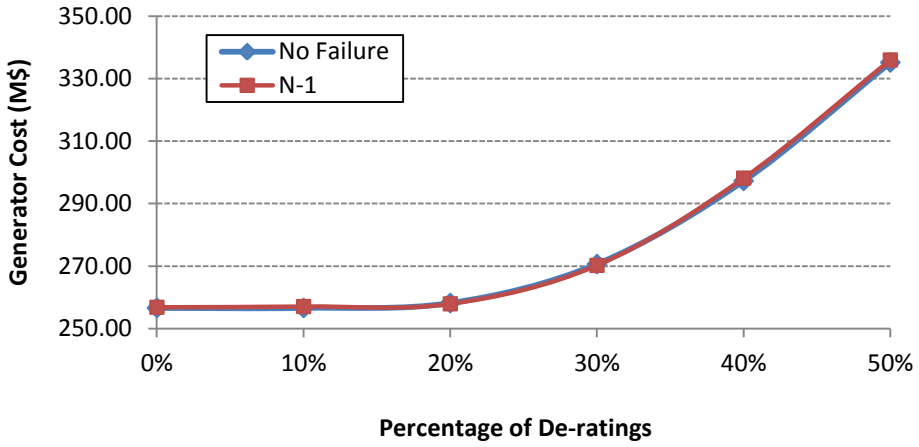

Fig. 6-23: Generator cost in case 6: baseline load and future rating

6.4 Summary

In this chapter, the impacts of climate change on power system reliability are investigated considering the components de-rating. The IEEE 24-bus Reliability Test System is used as the test network. The overhead line de-ratings subjected to different climate change levels are taken as the input rating scenario to configure the network, together with the component failure event sampled using Sequential Monte Carlo Simulation technique. Then the power flow study is carried out under the selected load condition over a year and provides the results for reliability indices calculation.

The reliability of the network is first assessed with no component failure considered. Three cases under the combinations of different load and rating scenarios were studied assuming the network is operated with only static ratings. One case regarding the application of dynamic ratings is also presented.

Furthermore, component failure is also taken into consideration for the reliability assessment of the test network. Two cases were carried out using only static ratings. No application of dynamic ratings was studied in this situation.

Chapter 7 Impacts of Climate Change on Transformer Ageing

This chapter investigates the impacts of climate change on transformer ageing, which is the fourth contribution of the thesis. Although there are four major factors that influence a transformer's ageing rate, including temperature, moisture content, oxygen content and acid content [12, 30, 31], only the factor of temperature is considered for the assessment of impacts of climate change.

The calculation of transformer ageing is given in this chapter. Then the methodology to assess the impacts of the climate change on transformer ageing is described. Finally, the results and discussions are presented.

7.1 Transformer Ageing Calculation

The most vulnerable part of a transformer is the windings. Since it is the hot-spot, the

winding insulation system is subject to the greatest deterioration among different parts of the transformer. Therefore, the ageing of a transformer refers to the ageing of the winding insulation. The relative ageing rate, V, is introduced to quantify the age of a transformer. It is defined as the ratio of the expected life loss at a given temperature over the life loss at rated condition.

The relative ageing rate V is calculated by (7.1) for non-thermally upgraded paper and by (7.2) for thermally upgraded paper, where θ_h is the hot-spot temperature in ℃.

$$V = 2^{(\theta_h - 98)/6} \tag{7.1}$$

$$V = e^{\left(\frac{15000}{110+273} - \frac{15000}{\theta_h+273}\right)} \tag{7.2}$$

Table 7-1: Relative ageing rates at different hot-spot temperatures

θ_h(℃)	Non-upgraded paper insulation V	Upgraded paper insulation V
80	0.125	0.036
86	0.25	0.073
92	0.5	0.145
98	1.0	0.282
104	2.0	0.536
110	4.0	1.0
116	8.0	1.83
122	16.0	3.29
128	32	5.8
134	64.0	10.1
140	128.0	17.2

The relative ageing rates calculated at the hot-spot temperatures from 80 ℃ to 140 ℃ with the two different types of insulation are listed in Table 7-1. The rated temperature of transformers with upgraded insulation is 110 ℃, which is higher than

that of transformers with non-upgraded paper (i.e., 98 ℃). The table shows that the ageing rate is exponentially influenced by the hot-spot temperature. When the hot-spot temperature is above the rated value, the relative ageing rate of non-upgraded insulation is doubled for every 6 ℃ rise. 140 ℃ is the limitation for both types of transformer. If the hot-spot temperature exceeds 140 ℃, the accelerated ageing of the paper dielectric takes place and bubbling may happen if the oil becomes over saturated with gases.

Given the relative ageing rate V, the loss of life L over a certain period of time equals:

$$L = \int_{t_1}^{t_2} V dt \ \ or \ L \approx \sum_{n=1}^{N} V_n \times t_n \tag{7.3}$$

where V_n is the relative ageing rate during interval n, t_n is the nth time interval, n is the number of each time interval, N is the total number of intervals during the period considered.

7.2 Hot-spot Temperature Calculation

As previously described, the calculation of the ageing rate requires the "real-time" hot-spot temperature. As the transformer has a significant thermal capacity, there is a delay between the variation of its insulation temperature and the variation of its load. Hence, the steady-state thermal model cannot be used to calculate the change in the insulation temperature. The dynamic thermal model provided by IEC Std 60076 [29] is used to calculate the hot-spot temperature in this study. The model can be described by the differential equations below:

$$\frac{dT_o}{dt} = \frac{1}{k_{11}\tau_o} T_o + \frac{1}{k_{11}\tau_o} T_a + \frac{1}{k_{11}\tau_o} T_{o,r} \left(\frac{1+K^2R}{1+R}\right)^2 \tag{7.4}$$

$$\frac{dT_{hs1}}{dt} = \frac{1}{k_{22}\tau_w} T_{hs1} + \frac{1}{k_{22}\tau_w} k_{21} K^y T_{o,r} \tag{7.5}$$

$$\frac{dT_{hs2}}{dt} = -\frac{k_{22}}{\tau_o} T_{hs2} + \frac{k_{22}}{\tau_o} (k_{21} - 1) K^y T_{o,r} \tag{7.6}$$

where K is the load factor (load current/rated current), subscript r refers to rated values. Other factors used within the formula, e.g., x, y k_{11}, k_{21}, and k_{22} have been determined empirically and can be found in [29].

An example of the one-day hot-spot temperature output from the dynamic model is presented in Fig. 7-1 . Given the hourly transformer load in p.u., the hot-spot temperature is calculated and updated with a time step of 3 minutes. It can be seen from the figure that the delay exists between the variations of hot-spot temperature and variation of load. There is a delay of 4 hours in the hot-spot temperature peak of the after the load peak of the day.

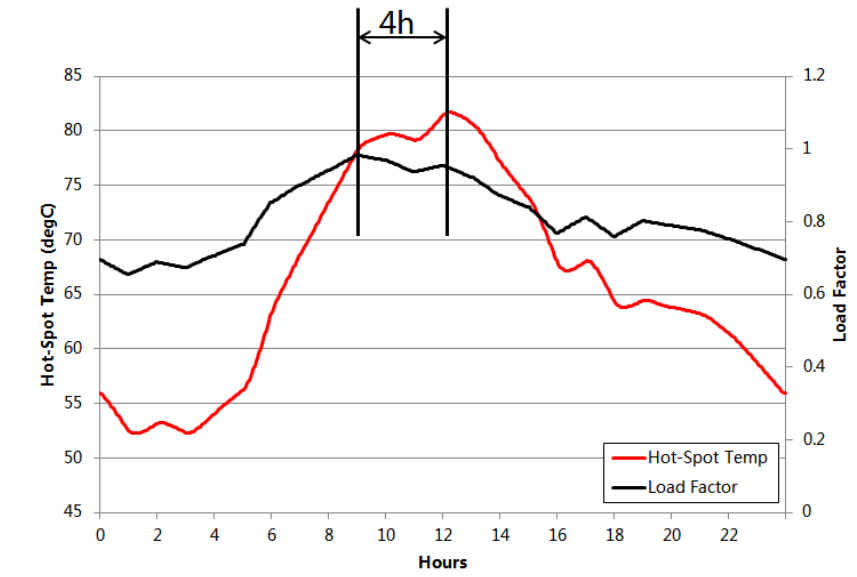

Fig. 7-1: Hot-spot temperatures calculated based on one-day load profile

7.3 Assessment Methodology

The methodology to assess the impacts of climate change on transformer ageing is illustrated in Fig. 7-2. First of all, a one-year hourly load profile is replicated for 30 times to form a 30-year hourly load profile to match the size of a weather data series. A 30-year hourly weather data series is randomly generated from UKCP09 Weather Generator (WG). The weather is simulated in two scenarios: baseline and future climate. The baseline weather series presents the existing climate without any modification on

the standard WG configuration. The future weather series in the 2080s is simulated in the same way as that for baseline weather but assumes a high emission scenario. The hot-spot temperatures are then calculated through the dynamic transformer thermal model based on the load and weather conditions. According to the hot-spot temperatures, the relative ageing rate can be calculated at each hour. The loss of life over this 30-year period is then obtained based on ageing rates and are averaged into loss of life per year for further analysis. The above process is repeated 500 times to model the uncertainties of the climate change and gives a distribution of the loss of life. The impacts of climate change are measured as the difference between the loss of life from baseline weather and future weather.

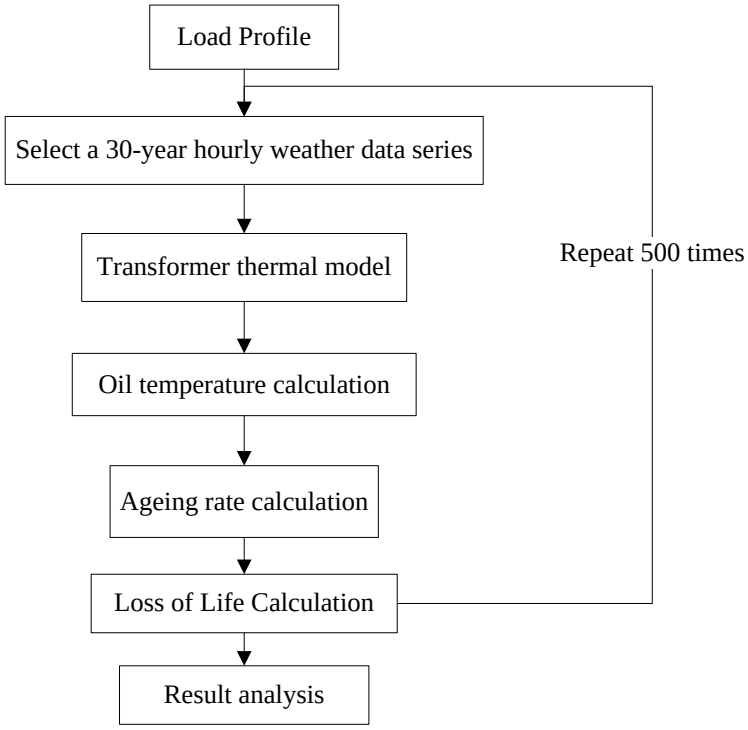

Fig. 7-2: Illustration of methodology to assess the impacts of climate change on transformer ageing

7.4 Results

In this section, the study of impacts of climate change is carried out on an ONAN power transformer with non-thermal upgraded paper insulation as an example. The one-year baseline load is shown in Fig.7-3 with an average load factor of 0.825 p.u. In this profile,

the load factor at hour number 1 refers to that in the first hour of Jan 1st.This load profile is chosen to be relatively higher than the usual power system transformer load for better demonstration as it contains more over load hours. The future load profile is modified by increasing the baseline line load profile to 1.2 times, as shown in Fig. 7-4. Both baseline and future weather data are simulated by the UKCP09 WG. Only air temperatures are taken for the calculations in this study. The baseline weather is simulated to present the existing climate whilst the future weather data is simulated assuming it is in Slough in the 2080s in high emission scenario.

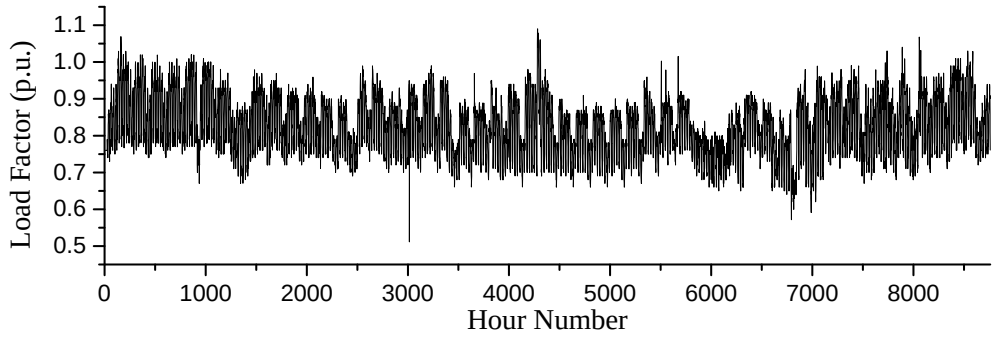

Fig.7-3: One-year of baseline load profile

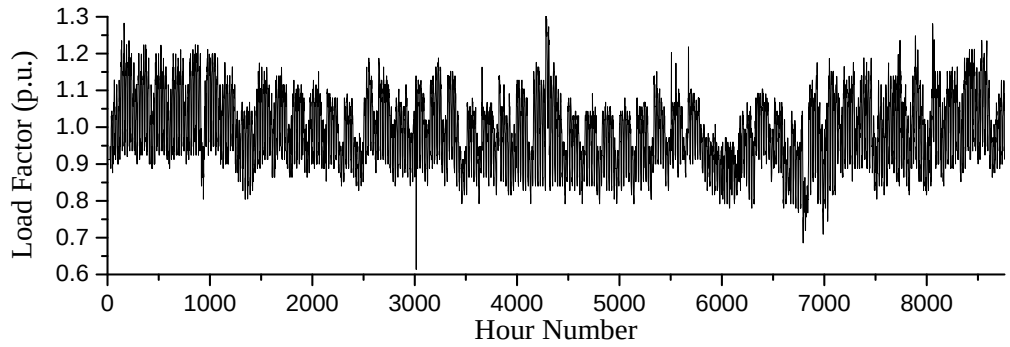

Fig. 7-4: One-year of future load profile

7.4.1 Example of Loss of Life Calculation

An example of life loss of the transformer over 30 years calculated based on one-year simulated future weather data is presented in Fig. 7-5. As shown in the figure, the transformer life loss fluctuates in different years. Since the same baseline load profile is used to calculate the hot-spot temperatures in each year, the fluctuation is caused by the difference in air temperatures. This indicates that the change in air temperatures can

influence the ageing process of transformers. The average expected life loss per year is 0.1799 year. This is much lower than 1 as the hot spot temperature rarely exceeds the rated temperature. In Fig. 7-6, the operating time in which the hot-spot temperature is over 98℃ is shown for 30 years.

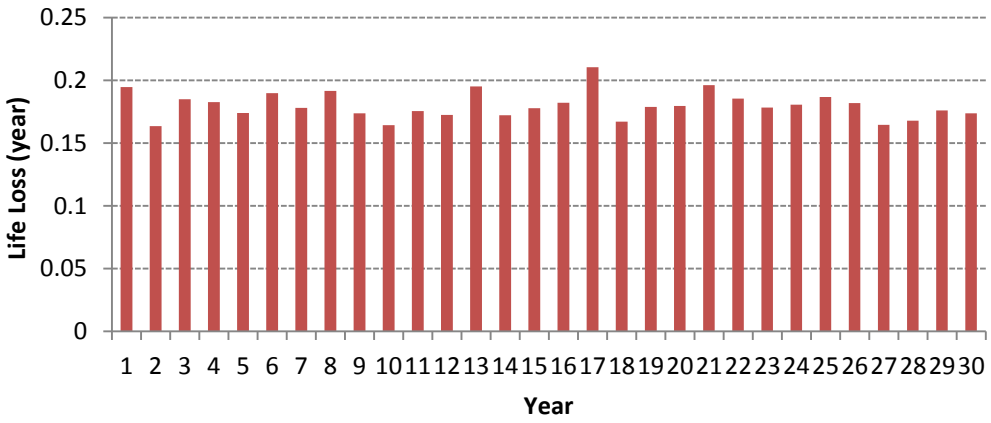

Fig. 7-5: Example of life loss over 30 years calculated based on simulated future weather data and baseline load

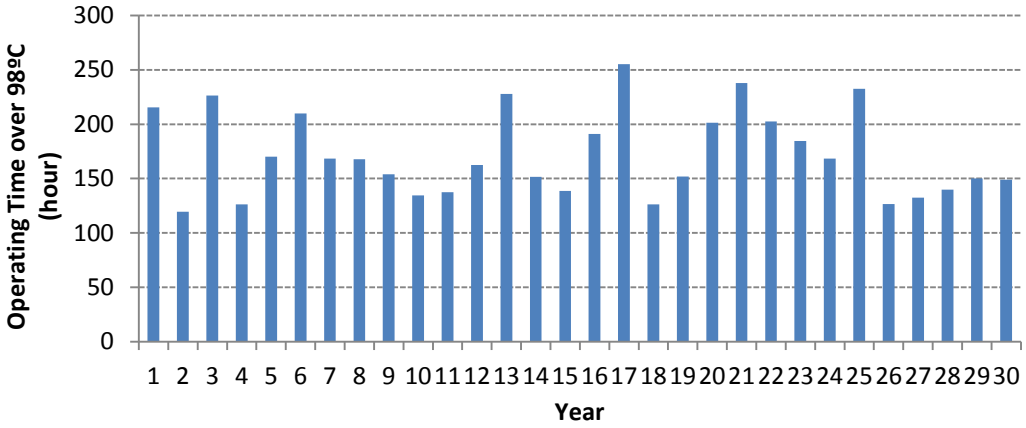

Fig. 7-6: Example of operating time in which hot-spot temperature is over rated 98℃ over 30 years calculated based on simulated future weather data and baseline load

7.4.2 Case Studies

The studies are implemented in four cases based on the different combinations of load scenarios and climate scenarios as follows:

- Case 1: Baseline load and baseline climate
- Case 2: Baseline load and future climate
- Case 3: Future load and baseline climate
- Case 4: Future load and future climate

A yearly expected life loss is calculated as an average of total expected life loss based on a 30-year weather series. In each of the four cases, 500 yearly expected life loss are generated based on different weather series. They are placed in the histograms to show their probability distribution in Fig. 7-7, Fig. 7-8, Fig. 7-9 and Fig. 7-10. The average expected life loss and hot-spot operating hours over rated temperature are given in Table 7-2.

Fig. 7-7 and Fig. 7-8 present the histograms of yearly expected life loss calculated in case 1 and case 2, respectively. It can be seen that expected life loss per year ranges from 0.0773 to 0.0788 year under baseline climate. For the transformer with the same load profile but a year under the future climate, it is between 0.0976 and 0.2605. This shows that the air temperature rises as a result of climate change, can increase the life loss of a transformer. As listed in Table 7-2, the average life loss per year under future climate is 0.1453 year, which is about twice of that under baseline climate. The hot-spot operating hours over rated temperature increases from 15.59 hours under baseline climate to 95.82 hours under future climate.

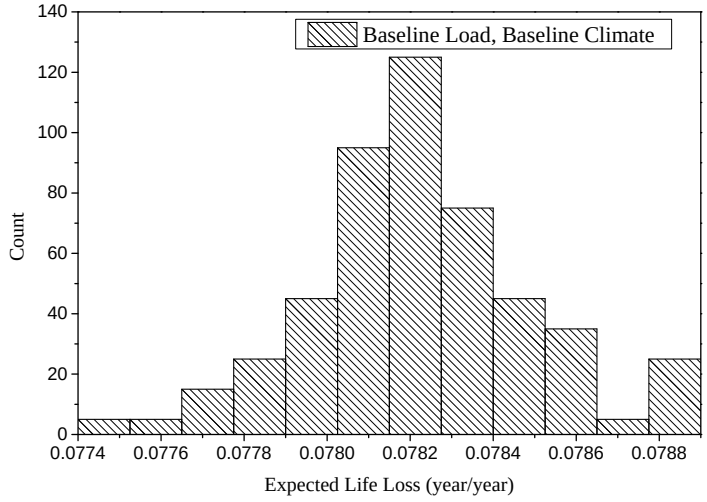

Fig. 7-7: Case 1: Yearly expected life loss assuming baseline load and baseline climate

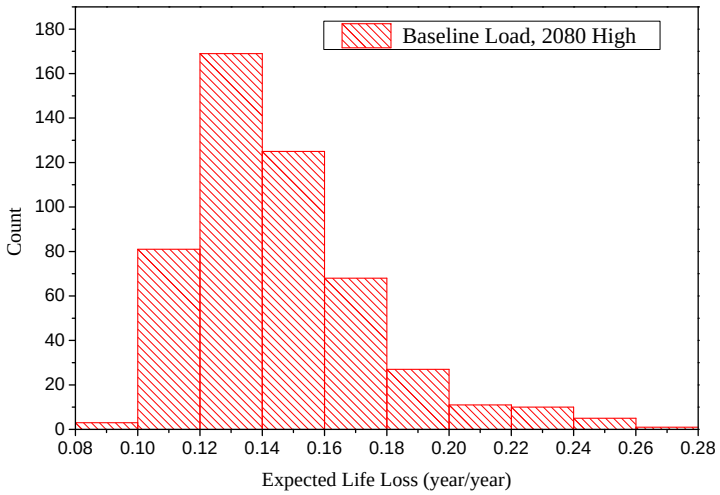

Fig. 7-8: Case 2: Yearly expected life loss assuming baseline load and future climate

Table 7-2: Average expected life loss and hot-spot temperature over rated temperature per year

	Case 1	Case 2	Case 3	Case 4
Life Loss (year/year)	0.0782	0.1453	0.6825	1.1024
Hours of hot-spot over rated temperature (℃)	15.59	95.82	1748.63	2580.23

The histograms of yearly expected life loss in case 3 and 4 are shown in Fig. 7-9 and Fig. 7-10 considers a future load profile which is 1.2 times that of baseline load. It is obvious that the increasing load can significantly increase the life loss. Looking first at Fig. 7-9, the yearly expected life loss is from 0.6749 year to 0.6900 year, which is much higher than that with baseline load (Fig. 7-7). As shown in Table 7-2, in this case, the hot-spot temperature has much more time to exceed the rated temperature than that with baseline load. Considering the climate change, the air temperature can aggravate transformer ageing. The yearly average expected life loss is 1.1024 year under future climate, which is much higher than that of 0.6825 under baseline climate. In the worst case, the yearly expected life loss can be as high as 2.2240 year as shown in Fig. 7-10. As the result of a combination of load increase and climate change, the hot-spot temperature is over the rated temperature for an average of 2580 hours which is about 25% of the year, as shown in Table 7-2.

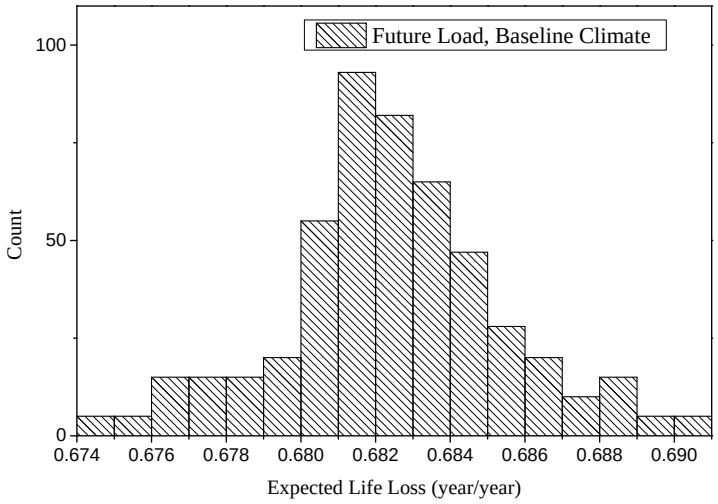

Fig. 7-9: Case 3: Yearly expected life loss assuming future load and baseline climate

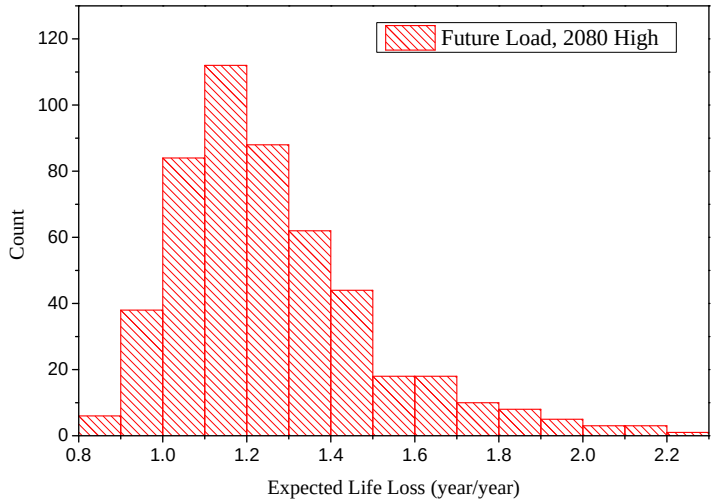

Fig. 7-10: Case 4: Yearly expected life loss assuming future load and future climate

A simple numerical example is given for better understanding of the impact of air temperature rises and load profile change on transformer aging. Compared to the yearly life loss in Case 1, the life loss is about 1.86, 8.73 and 14.10 times of that in Case 2, Case 3 and Case 4, respectively. This means that a transformer designed with an service expectancy of 60 years considering existing load and climate can actually serve for 32.30, 6.87 and 4.26 years in Case 2, Case 3 and Case 4, respectively. Comparing that

in Case 1 and Case 2, the air temperature rise halves the transformer life. In case 4, the transformer life decreases significantly to only 1/14 of that designed, due to a combination of air temperature rises and load increases.

7.5 Summary

In summary, this chapter presented the impacts of climate change associated with loading effect on transformer ageing. The transformer ageing and hot-spot calculation were first described. Given the load profile and weather data in different scenarios, the life loss was assessed based on hot-spot temperature through the dynamic transformer thermal model. The case studies result indicated that as the air temperature rises, as a result of climate change, the faster the life loss of a transformer.

Chapter 8 Conclusions and Future Work

8.1 Conclusions

This thesis presents a comprehensive assessment of the impact of climate change on power system operational performance. The assessment is based on the simulated weather data from UKCP09 Weather Generator and other developed climate models, and covers the impacts on component ratings, system reliability and transformer ageing.

The assessment results are both important and relevant to power system operators and policy makers. The identification and quantification of the impacts of climate change can help them to have a better understanding of the system performance against climate change and to contribute to the reinforcement and design of the future power system.

The majority of the future climate data, including air temperature and solar radiation, is simulated from the UKCP09 Weather Generator. With the wind model developed in this

thesis and the constants of soil properties assumed, the future soil temperature changes are simulated through a modified physical soil temperature model. All the simulated data is provided in synthetic hourly time series and reflects a range of possible future climate projections from extensive runs of models based on different assumptions.

8.1.1 Impacts on Component Ratings

The impacts of climate change on power system component ratings are assessed in a probabilistic approach which provides the likelihood of the impacts happening. Generally, it can be concluded from the results that the rating reduction is expected to take place for all the three components (i.e., OHL, cable and transformer) as a result of climate change and is expected to become more severe from the 2020s, though the 2050s to the 2080s.

The results of OHL indicate that the conductors which operate at different rated temperatures perform differently against climate change. The conductor with a lower rated temperature is more sensitive to the climate change. For instance, the ACSR Zebra conductor rated at 75℃ has an average 10.05% de-rating in the summers of the 2080s, whilst that of ACCR drake conductor rated at 240℃ is only 1.41%. For the OHL conductors operated at the same rated temperature, the one with a smaller conductor diameter has a higher percentage of de-rating. Among the assessed OHL conductors, the ACSR Zebra has the most de-ratings. Its pre-fault average de-ratings are 10.05%, 6.91% and 4.93% in summer, spring and winter, respectively, by the 2080s. The numbers for post-fault de-ratings are 6.79%, 4.23% and 2.72%, respectively. It can be concluded that higher de-ratings are expected in the summer than in the spring and winter. Also, the de-rating of the post-fault rating is less than that of the pre-fault rating. It should be pointed out that the maximum summer de-rating of ACSR Zebra can be up to 27.4% by the 2080s in the worst scenario. Moreover, the studies show that the OHL that operates at the dynamic rating is less affected by climate change. The maximum dynamic rating at 50% percentile is only 8.36%, which is much less than that of the pre-fault static rating of 27.4%.

According to the simulation results of soil temperature model developed in this thesis, the soil temperature will increase from 12.57℃ to 16.33℃ at average in Slough by the 2080s in high emission scenario. Cable ratings are calculated based on this model's outputs. The results show that the fluid-filled cable is expected to have a greater rating decrease than the XLPE cable in the same conductor size. For example, the average summer de-rating of fluid-filled 2500 mm^2 cable is 4.63% in the 2080s, greater than that of XLPE 2500 mm^2 which is 3.10%. For the same types of conductor, the one with a bigger conductor size is more sensitive to climate change. The reduction in the summer rating of a fluid-filled 1600 mm^2 cable is 3.65% less than that of a 2500 mm^2 cable of 4.63%. The rating reduction of a fluid-filled 2500 mm^2 cable is the greatest among the examined cables. In the 2080s, its average de-ratings are 4.63% and 4.20% in summer and winter, respectively, whilst the maximum de-ratings are 10.28% and 8.53%. It can be observed again that the de-rating in summer is greater than that in winter.

The study of the impacts of climate change on transformer ratings shows that ONAF transformers have the greatest rating decrease of 6.64%, 4.78% and 3.22% on average in summer, spring and winter, respectively, in the 2080s, among different types of transformers. In the worst case, the maximum de-ratings of ONAF transformers can be up to 16.86%, 9.59% and 7.09% in three seasons in the 2080s. It can be seen that the de-ratings in summer are expected to be greater than those in spring and winter. The OF and OD transformers have lower rating reductions which are no more than 14.57% and 12.48%, respectively, in the summers of the 2080s.

The OHL conductors, which have the highest percentages of de-ratings, are shown as the most sensitive components to climate change among the three components. OHL is therefore considered as the most vulnerable component to climate change. Importantly, the high-temperature conductor and dynamic rating are demonstrated to be able to mitigate the impacts of climate change, and can be used to reinforce the OHL routes.

8.1.2 Impacts on System Reliability

The impacts of climate change on system reliability are also investigated on the test network in this thesis. The study is first carried out ignoring the component failure. The results show that the de-ratings of OHLs will diminish the system's reliability and increase the constraint cost. The test network presents good reliability when the baseline load profile is applied even with the occurrence of OHL de-ratings. However, the generator cost is increased to maintain the reliability. Considering an increased future load scenario, the LOLD and EENS start to occur when the de-rating is over 30%. It can be observed that the LOLD and EENS increase dramatically and non-linearly. The study also proves that the system reliability can be boosted by the application of the dynamic rating on critical OHL routes. In the case where the static de-rating is 50% and the future load scenario is applied, LOLD and EENS drop to 3.11% and 2883MWh, respectively, when three lines are at dynamic ratings, compared to those of 4.11% and 7,546 MWh when the system is operated with static ratings only. The generator cost increased from 275.62 M$ to 335.12 M$.

Considering the component failure, the reliability of the test network is further constrained. The LOLD and EENS are increased from 4.11% and 7,546 MWh, respectively, to 5.14% and 12,833MWh, respectively.

8.1.3 Impacts on Transformer Ageing

The final study of this thesis looked into the impacts of climate change on transformer ageing. The expected life loss per year of the ONAF transformer is 0.1453 year under the climate in the 2080s, about two times that of under baseline climate. Increasing the load profile to 1.2 times of the baseline, the life loss in the 2080s can be as high as 1.1024 year. This revealed that the climate change will increase the transformer ageing rate. According to the case studies, the air temperature rises can half the transformer life expectancy. Combined with an increasing load profile, the transformer life expectancy can be only as 1/14 as designed.

8.2 Future Work

The work presented within this thesis has fulfilled all of the research aims which were initially defined. Nevertheless, there are a number of areas where this research could be extended.

- The benefits of dynamic ratings implemented on OHLs to mitigate the impacts of climate change have been shown in the studies into both rating and system reliability. It would be valuable to extend the research of dynamic ratings to cables and transformers. This will reveal whether the use of dynamic rating can also mitigate the impacts on these two types of components and further improve the system reliability

- In this thesis, the system reliability assessment assumes the same level of OHL de-ratings across the whole test network (i.e., the OHL de-ratings in Slough is used). However, a large power system may cover a couple of locations at which the climate change levels are different. For example, Slough is expected to have greater temperature rise than Edinburgh. The rating reductions at these locations are therefore different. It would be desirable to include these differences in the study for a more practical reliability assessment.

- The study has shown that transformer ageing can be affected by air temperature rise as a result of climate change. The same as transformer, ageing is also one of the major concerns in cable design and implementation. Therefore, an assessment on the impacts of climate change on cable ageing will be of interest.

- Finally, the load condition acts as an important role in the assessments of both system reliability and component ageing. In the foreseen future, load profile is expected to change as a result of penetration of renewable energy, increasing demand and future system operation techniques. In this thesis, the future load profile is simply projected as a certain times of the existing load profile and can be

improved by taking the above factors into consideration.

References

[1] T. F. Stocker, *et al.*, "Climate Change 2013: The Physical Science Basis. Contribution of Working Group I to the Fifth Assessment Report of the Intergovernmental Panel on Climate Change," IPCC, Cambridge, United Kingdom and New York, NY, USA, 2013.

[2] J. B. Smith and D. A. Tirpak, *The potential effects of global climate change on the United States* vol. 1: Office of Policy, Planning and Evaluation, US Environmental Protection Agency, 1989.

[3] D. J. Griggs and M. Noguer, "Climate change 2001: the scientific basis. Contribution of working group I to the third assessment report of the intergovernmental panel on climate change," *Weather,* vol. 57, pp. 267-269, 2002.

[4] K. McGuffie and A. Henderson-Sellers, *The Climate Modelling Primer*: John Wiley & Sons, 2014.

[5] N. Nakicenovic and R. Swart, "Special report on emissions scenarios," *Special Report on Emissions Scenarios, Edited by Nebojsa Nakicenovic and Robert Swart, pp. 612. ISBN 0521804930. Cambridge, UK: Cambridge University Press, July 2000.*, vol. 1, 2000.

[6] J. T. Houghton, *Climate change 1995: The science of climate change: contribution of working group I to the second assessment report of the Intergovernmental Panel on Climate Change* vol. 2: Cambridge University Press, 1996.

[7] J. J. McCarthy, *Climate change 2001: impacts, adaptation, and vulnerability: contribution of Working Group II to the third assessment report of the Intergovernmental Panel on Climate Change*: Cambridge University Press, 2001.

[8] S. Solomon, *et al.*, *Climate Change 2007 - The Physical Science Basis: Working Group I Contribution to the Fourth Assessment Report of the IPCC*: Cambridge University Press, 2007.

[9] *SP Energy Networks, Climate adaptation Report* [Online], avaliable: http://archive.defra.gov.uk/environment/climate/documents/adapt-reports/04distribute-trans/sp-energy-networks.pdf, 2011.

[10] *National Grid, Climate Change Adaptation Report* [Online], avaliable: http://archive.defra.gov.uk/environment/climate/documents/adapt-reports/04distribute-trans/national-grid-electricity.pdf, 2010.

[11] J. Murphy, *et al.*, "UKCP09 Climate change projections," *Met Office Hadley Centre, Exeter*, 2009.

[12] "Electricity Networks Climate Change Adaptation Report, 2011, [Online]" Avaliable: http://archive.defra.gov.uk/environment/climate/documents/adapt-reports/04distribute-trans/ena-networks.pdf, Energy Networks Association.

[13] D. S. Kirschen, *et al.*, "Computing the value of security," *Generation, Transmission and Distribution, IEE Proceedings-*, vol. 150, pp. 673-678, 2003.

[14] M. A. Rios, *et al.*, "Value of security: modeling time-dependent phenomena and weather conditions," *Power Systems, IEEE Transactions on,* vol. 17, pp. 543-548, 2002.

[15] D. Chinh, *et al.*, "Electrical aging of extruded dielectric cables: review of existing theories and data," *Dielectrics and Electrical Insulation, IEEE Transactions on,* vol. 3, pp. 237-247, 1996.

[16] L. E. Lundgaard, *et al.*, "Aging of oil-impregnated paper in power transformers," *Power Delivery, IEEE Transactions on,* vol. 19, pp. 230-239, 2004.

[17] T. J. Overbye and T. A. Leader, "Engineering resilient cyber-physical systems," in *Power and Energy Society General Meeting, 2012 IEEE,* 2012, pp. 1-1.

[18] M. Chaudry, *et al.*, "Building a resilient UK energy system," 2011.

[19] M. Panteli and P. Mancarella, "The Grid: Stronger, Bigger, Smarter?: Presenting a Conceptual Framework of Power System Resilience," *Power and Energy Magazine, IEEE,* vol. 13, pp. 58-66, 2015.

[20] M. Panteli and P. Mancarella, "Influence of extreme weather and climate change on the resilience of power systems: Impacts and possible mitigation strategies," *Electric Power Systems Research,* vol. 127, pp. 259-270, 2015.

[21] J. C. Lam, "Climatic and economic influences on residential electricity consumption," *Energy Conversion and Management,* vol. 39, pp. 623-629, 1998.

[22] M. J. Scott, *et al.*, "Effects of climate change on commercial building energy demand," *Energy sources,* vol. 16, pp. 317-332, 1994.

[23] C. Cartalis, *et al.*, "Modifications in energy demand in urban areas as a result of climate changes: an assessment for the southeast Mediterranean region," *Energy Conversion and Management,* vol. 42, pp. 1647-1656, 2001.

[24] C. C. Mitigation, "IPCC special report on renewable energy sources and climate change mitigation," 2011.

[25] P. B. Breslow and D. J. Sailor, "Vulnerability of wind power resources to climate change in the continental United States," *Renewable Energy,* vol. 27, pp. 585-598, 2002.

[26] S. Pryor and R. Barthelmie, "Climate change impacts on wind energy: A review," *Renewable and sustainable energy reviews,* vol. 14, pp. 430-437, 2010.

[27] R. Sims, "Renewable energy: a response to climate change," *Solar energy,* vol. 76, pp. 9-17, 2004.

[28] B. Schaefli, *et al.*, "Climate change and hydropower production in the Swiss Alps: quantification of potential impacts and related modelling uncertainties," *Hydrology and Earth System Sciences Discussions,* vol. 11, pp. 1191-1205, 2007.

[29] "Power transformers. Loading guide for oil-immersed power transformers," in *BS IEC 60076-7:2005*, ed, 2005.

[30] P. Wong, *et al.*, "The IEEE Reliability Test System-1996. A report prepared by the Reliability Test System Task Force of the Application of Probability Methods Subcommittee," *Power Systems, IEEE Transactions on,* vol. 14, pp. 1010-1020, 1999.

[31] R. D. Zimmerman, *et al.*, "MATPOWER: Steady-state operations, planning, and analysis tools for power systems research and education," *Power Systems, IEEE Transactions on,* vol. 26, pp. 12-19, 2011.

[32] NERC, "Understanding the grid: reliability terminology [Online]. Available: www.nerc.com/page.php," North American Electric Reliability Corporation.

[33] R. Billinton and R. N. Allan, "Power-system reliability in perspective," *Electronics & Power,* vol. 30, pp. 231-236, 1984.

[34] R. Allan, *Reliability evaluation of power systems*: Springer Science & Business Media, 2013.

[35] R. Billinton, *Power system reliability evaluation*: Taylor & Francis, 1970.

[36] W. Li, *Reliability assessment of electric power systems using Monte Carlo methods*: Springer Science & Business Media, 2013.

[37] ENA, *Electricity Networks Climate Change Adaptation Report Issue 1* [Online], avaliable: http://archive.defra.gov.uk/environment/climate/documents/adapt-reports/04distribute-trans/ ena-networks.pdf, 2001.

[38] Rademaekers, Koen, et al. "Investment needs for future adaptation measures in EU nuclear power plants and other electricity generation technologies due to effects of climate change," 2011.

[39] *Northern Power Grid, Climate Apatation Report* [Online], avaliable: http://archive.defra.gov.uk/environment/climate/documents/adapt-reports/04distribute-trans/northern-grid.pdf, 2011.

[40] *SSE Power Distribution, Climate Apatation Report* [Online], avaliable: http://archive.defra.gov.uk/environment/climate/documents/adapt-reports/04distribute-trans/sse-power-distribution.pdf, 2011.

[41] *UK Power Networks, Climate Apatation Report* [Online], avaliable: http://archive.defra.gov.uk/environment/climate/documents/adapt-reports/04distribute-trans/uk-power-networks.pdf, 2010.

[42] *Western Power Distribution, Climate Apatation Report* [Online], avaliable: http://archive.defra.gov.uk/environment/climate/documents/adapt-reports/04distribute-trans/western-power.pdf, 2011.

[43] L. C. Cradden and G. P. Harrison, "Adapting overhead lines to climate change: Are dynamic ratings the answer?," *Energy Policy,* vol. 63, pp. 197-206, 2013.

[44] A. Shiri, *et al.*, "Investigation of the ambient temperature effects on transformer's insulation life," *Electrical Engineering,* vol. 93, pp. 193-197, 2011.

[45] J. W. Stahlhut, *et al.*, "A Preliminary Assessment of the Impact of Ambient Temperature Rise on Distribution Transformer Loss of Life," *Power Delivery, IEEE Transactions on,* vol. 23, pp. 2000-2007, 2008.

[46] B. R. Sathyanarayana, *et al.*, "Distribution transformer life assessment with ambient temperature rise projections," *Electric Power Components and Systems,* vol. 37, pp. 1005-1013, 2009.

[47] "IEEE guide for loading mineral-oilimmersed transformers," *IEEE Std C,* vol. 57, pp. 1-112, 1995.

[48] S. Brown, *et al.*, "Interpretation for use of surface windspeed projections from the 11-member Met Office Regional Climate Model ensemble," *UKCP09 Tech. Note,* 2009.

[49] "IEEE Standard for Calculating the Current-Temperature of Bare Overhead Conductors," *IEEE Std 738-2006 (Revision of IEEE Std 738-1993),* pp. c1-59, 2007.

[50] IEC, "Electric Cables–Calculation of the current rating BS IEC 60287-1-1: 2006," *British Standards Institution*.

[51] "TGN(T)67 Current Ratings for Cables," National Grid,1996.

[52] L. A. Ramdas, "Some new instruments and experimental techniques developed in the Agricultural Meteorogy Section at Poona," *J. Sci. Ind. Res.*, vol. 7, pp. 16-29, 1948.

[53] G. Jenkins, *et al.*, "UK Climate Projections: Briefing report," Met Office Hadley Centre, Exeter2009.

[54] C. Gordon, *et al.*, "The simulation of SST, sea ice extents and ocean heat transports in a version of the Hadley Centre coupled model without flux adjustments," *Climate dynamics*, vol. 16, pp. 147-168, 2000.

[55] V. Pope, *et al.*, "The impact of new physical parametrizations in the Hadley Centre climate model: HadAM3," *Climate dynamics*, vol. 16, pp. 123-146, 2000.

[56] M. Collins, *et al.*, "The internal climate variability of HadCM3, a version of the Hadley Centre coupled model without flux adjustments," *Climate dynamics*, vol. 17, pp. 61-81, 2001.

[57] T. S. von Deimling, *et al.*, "Climate sensitivity estimated from ensemble simulations of glacial climate," *Climate dynamics*, vol. 27, pp. 149-163, 2006.

[58] P. Jones, *et al.*, "UK Climate Projections science report: Projections of future daily climate for the UK from the Weather Generator," *University of Newcastle, UK*, 2009.

[59] C. W. Richardson, "Stochastic simulation of daily precipitation, temperature, and solar radiation," *Water Resources Research*, vol. 17, pp. 182-190, 1981.

[60] N. Nakicenovic and R. Swart, "IPCC Special Report on Emission Scenarios," IPCC, Cambridge2000.

[61] "Met Office Integrated Data Archive System (MIDAS) Land and Marine Surface Stations Data (1853-current). NCAS British Atmospheric Data Centre," 2012.

[62] *UK Meteorological Office. MIDAS Land Surface Stations data (1853-current), NCAS British Atmospheric Data Centre, 2006*.

[63] P. L. Lewin, *et al.*, "Method for rating power cables buried in surface troughs," *Generation, Transmission and Distribution, IEE Proceedings-*, vol. 146, pp. 360-364, 1999.

[64] "Hadley Centre for Climate Prediction and Research: Met Office Hadley Centre Regional Climate Model (HadRM3-PPE) Data," 2008.

[65] "IEEE Guide for Soil Thermal Resistivity Measurements," *IEEE Std 442-1981*, pp. 1-16, 1981.

[66] "IEEE Standard for Calculating the Current-Temperature of Bare Overhead Conductors," in *IEEE Std 738-2006 (Revision of IEEE Std 738-1993)*, ed, 2007, pp. c1-59.

[67] "Overhead line electrical conductors – calculation methods for stranded bare conductors," in *IEC 61597*, ed, 1995.

[68] CIGRE, "22.12: Thermal behaviour of overhead conductors Section 1 and 2: Mathematical model for evaluation of conductor temperature in the steady state and the application thereof," *Electra*, 1992.

[69] G. F. Moore and B. Cables, *Electric cables handbook*: Blackwell, 1997.

[70] N. P. Schmidt, "Comparison between IEEE and CIGRE ampacity standards," *Power Delivery, IEEE Transactions on*, vol. 14, pp. 1555-1559, 1999.

[71] IEC, "IEC 60287-1," *Calculation of current rating part*, vol. 1, p. 100.

[72] G. J. Anders, *Rating of electric power cables: ampacity computations for transmission, distribution, and industrial applications*: IEEE, 1997.

[73] IEC, "60287-2-1 (2006) Electric cables—Calculation of the current rating—Part 2-1: Thermal resistance—calculation of thermal resistance—general," *IEC, Geneva*.

[74] IEC, "60853-2,“Calculation of the Cyclic and Emergency Current Ratings of Cables," *Part*, vol. 2, pp. 853-2.

[75] W. A. Fessler, *et al.*, "A refined mathematical model for prediction of bubble evolution in transformers," *Power Delivery, IEEE Transactions on*, vol. 4, pp. 391-404, 1989.

[76] G. Swift, *et al.*, "A fundamental approach to transformer thermal modeling. I. Theory and equivalent circuit," *Power Delivery, IEEE Transactions on*, vol. 16, pp. 171-175, 2001.

[77] IEC, "IEC 60076-7: 2005 Loading Guide for Oil-Immersed Power Transformers," *International Electrotechnical Commission, Geneva, Switzerland*, 2005.

[78] "IEEE Guide for Loading Mineral-Oil-Immersed Transformers," *IEEE Std C57.91-1995*, pp. 1-112, 2012.

[79] "Electric cables. Calculation of the current rating. Current rating equations (100% load factor) and calculation of losses. General," in *BS IEC 60287-1-1:2006*, ed, 2006.

[80] "TGN(T)26 Current Ratings for Overhead Lines."

[81] H. C. Zhao, *et al.*, "Probabilistic cable rating based on cable thermal environment studying," in *Power System Technology, 2000. Proceedings. PowerCon 2000. International Conference on*, 2000, pp. 1071-1076 vol.2.

[82] "TGN(T)29 Transformer Loading Guidance Guide Issue 1," National Grid Ltd.March 1994.

[83] R. Smith, "UK Future Energy Scenarios," National Grid2014.

Appendix A UKCP09 Weather Generator Variants

In this appendix, the ID numbers of the 1000 variants of UKCP09 Weather Generator used in this thesis are listed in Table A-1.

Table A-1: UKCP09 Weather Generator variants used in this thesis

26	50	60	61	62	82	82	83	86	90
91	93	109	110	135	136	139	145	145	168
175	198	203	205	209	228	233	242	249	286
289	294	310	315	331	334	344	348	349	350
356	368	371	373	403	440	441	445	454	463
493	537	539	549	549	561	562	574	581	583
627	645	660	663	668	673	673	680	698	706
714	716	716	724	731	738	740	742	745	751
754	757	771	774	783	789	792	800	806	809
824	830	836	853	874	880	881	889	889	890
895	907	909	911	927	931	932	940	940	957
975	985	988	1004	1022	1030	1033	1040	1042	1045
1048	1057	1070	1071	1073	1107	1151	1162	1162	1162
1199	1200	1211	1211	1213	1228	1244	1244	1248	1250
1256	1269	1270	1273	1287	1289	1292	1299	1306	1337
1340	1355	1367	1381	1394	1397	1417	1424	1439	1442

1457	1469	1476	1484	1499	1511	1524	1532	1542	1554
1554	1562	1571	1577	1579	1602	1603	1611	1612	1613
1618	1624	1639	1658	1664	1677	1694	1701	1720	1769
1773	1776	1801	1816	1879	1890	1902	1926	1930	1934
1951	1983	1987	1992	1997	2001	2013	2019	2047	2053
2056	2119	2129	2143	2144	2148	2149	2151	2157	2170
2170	2190	2194	2205	2211	2239	2252	2270	2272	2276
2284	2288	2293	2298	2301	2306	2309	2332	2336	2349
2353	2363	2373	2414	2414	2422	2431	2433	2438	2450
2458	2461	2466	2470	2480	2481	2484	2494	2520	2524
2529	2529	2535	2541	2547	2547	2551	2552	2556	2559
2574	2590	2593	2596	2598	2617	2628	2628	2649	2650
2662	2725	2735	2736	2740	2740	2741	2770	2772	2774
2787	2790	2794	2804	2804	2805	2814	2818	2838	2846
2869	2869	2873	2875	2880	2890	2925	2959	2966	2967
2975	2978	2996	3002	3002	3003	3011	3031	3035	3040
3041	3041	3060	3070	3081	3098	3099	3111	3121	3128
3129	3137	3150	3151	3158	3163	3169	3196	3211	3217
3225	3233	3234	3260	3261	3273	3273	3278	3278	3278
3281	3319	3327	3328	3349	3363	3364	3376	3386	3396
3396	3406	3452	3460	3461	3472	3482	3485	3493	3493
3493	3501	3506	3508	3536	3552	3594	3598	3603	3620
3621	3626	3644	3654	3665	3672	3698	3715	3715	3727
3729	3731	3731	3734	3740	3742	3747	3749	3751	3761
3779	3787	3797	3814	3815	3822	3823	3832	3846	3848
3857	3888	3892	3915	3917	3932	3938	3950	3977	3983
3986	3989	4021	4040	4045	4055	4077	4080	4108	4113
4140	4150	4162	4167	4173	4192	4193	4206	4209	4218
4226	4241	4272	4281	4291	4298	4312	4320	4338	4339
4345	4352	4384	4393	4407	4413	4422	4455	4456	4457
4461	4464	4486	4489	4492	4496	4498	4514	4540	4548
4548	4549	4561	4564	4584	4607	4626	4629	4631	4667
4682	4682	4690	4694	4697	4705	4705	4706	4709	4713
4730	4780	4794	4812	4822	4829	4839	4843	4849	4874
4892	4902	4949	4966	4967	4970	4986	4992	5014	5019
5033	5035	5036	5042	5045	5047	5049	5049	5065	5080
5081	5081	5090	5091	5097	5105	5110	5119	5124	5136
5160	5162	5178	5213	5224	5227	5228	5240	5245	5246
5247	5284	5316	5316	5329	5342	5345	5364	5405	5419
5430	5432	5475	5482	5493	5509	5510	5534	5535	5556
5572	5580	5582	5584	5591	5627	5636	5637	5638	5642
5659	5660	5670	5675	5699	5729	5733	5745	5749	5754
5766	5769	5795	5808	5817	5824	5855	5866	5888	5889
5902	5910	5919	5920	5923	5934	5935	5945	5946	5950
5955	5956	5971	5995	5999	6037	6038	6049	6053	6057
6068	6069	6091	6111	6116	6126	6130	6144	6145	6150
6153	6157	6165	6171	6172	6173	6193	6197	6204	6223
6232	6233	6236	6240	6260	6272	6279	6287	6289	6305

6320	6326	6339	6343	6351	6354	6356	6357	6357	6359
6360	6376	6404	6407	6412	6422	6441	6447	6455	6463
6473	6486	6503	6511	6526	6540	6541	6557	6579	6580
6583	6586	6599	6602	6610	6611	6636	6639	6649	6652
6662	6679	6684	6689	6693	6707	6724	6726	6733	6761
6762	6770	6773	6789	6809	6829	6830	6845	6870	6872
6878	6891	6892	6906	6911	6914	6941	6950	6960	6999
7018	7022	7037	7060	7063	7071	7086	7092	7104	7130
7132	7134	7135	7151	7176	7195	7195	7196	7229	7235
7237	7238	7255	7257	7258	7280	7285	7297	7314	7336
7343	7346	7356	7356	7360	7363	7363	7376	7380	7380
7387	7392	7404	7409	7444	7448	7471	7474	7489	7492
7501	7501	7503	7548	7550	7563	7578	7580	7582	7585
7586	7591	7605	7611	7614	7625	7629	7648	7651	7676
7684	7689	7694	7711	7720	7732	7742	7759	7760	7767
7778	7781	7791	7799	7809	7817	7818	7823	7830	7832
7843	7852	7854	7858	7865	7870	7879	7889	7902	7921
7928	7964	7966	7968	7997	8001	8013	8023	8036	8040
8070	8076	8077	8077	8097	8102	8111	8114	8135	8146
8150	8157	8170	8178	8199	8201	8206	8237	8243	8256
8272	8280	8282	8294	8322	8348	8363	8366	8366	8421
8440	8445	8458	8458	8472	8475	8491	8503	8507	8507
8511	8517	8519	8521	8523	8525	8544	8549	8552	8567
8591	8595	8602	8603	8603	8631	8632	8642	8650	8651
8656	8667	8670	8689	8727	8759	8765	8766	8787	8790
8805	8830	8836	8854	8911	8924	8927	8936	8936	8937
9017	9025	9034	9043	9058	9079	9092	9111	9122	9127
9130	9130	9134	9136	9187	9228	9231	9233	9245	9250
9256	9292	9309	9312	9317	9318	9336	9340	9341	9353
9358	9393	9402	9407	9408	9409	9420	9424	9434	9436
9440	9452	9455	9458	9460	9462	9469	9476	9488	9495
9499	9505	9519	9524	9541	9546	9550	9554	9559	9564
9569	9571	9598	9598	9622	9634	9643	9662	9695	9695
9711	9716	9733	9744	9745	9763	9763	9763	9766	9770
9791	9805	9816	9817	9826	9852	9867	9871	9875	9880
9889	9914	9925	9935	9948	9950	9952	9965	9971	9985

Appendix B Projected Component Ratings

B.1 Projected Overhead Line Ratings

The projected static ratings of ACSR Zebra OHL are:

Table B-1: Ranges of projected static ratings of ACSR Zebra OHL in high emission scenario (Unit: A.)

Period	Season	Average	Likely Range	Conservative Range	Full Range
2020s	Summer	941	937 to 947	926 to 955	901 to 970
	Spring	1012	1009 to 1016	1005 to 1019	994 to 1029
	Winter	1079	1077 to 1081	1073 to 1086	1063 to 1093
2050s	Summer	919	913 to 928	894 to 941	850 to 962
	Spring	1000	913 to 928	990 to 1010	969 to 1024
	Winter	1069	1067 to 1072	1059 to 1078	1044 to 1089
2080s	Summer	895	887 to 908	858 to 927	789 to 959
	Spring	984	979 to 990	967 to 1000	937 to 1020
	Winter	1059	1055 to 1064	1043 to 1073	1021 to 1090

Table B-2: Ranges of projected static ratings of ACSR Zebra OHL in medium emission scenario (Unit: A)

Period	Season	Average	Likely Range	Conservative Range	Full Range
2020s	Summer	973	970 to 978	960 to 985	940 to 999
	Spring	1022	1020 to 1025	1014 to 1030	1004 to 1039
	Winter	1080	1079 to 1083	1074 to 1087	1067 to 1094
2050s	Summer	958	952 to 965	937 to 975	900 to 992
	Spring	1012	1008 to 1015	1001 to 1022	986 to 1034
	Winter	1073	1071 to 1076	1063 to 1083	1052 to 1092
2080s	Summer	944	937 to 955	915 to 968	863 to 987
	Spring	1002	998 to 1008	988 to 1015	964 to 1030
	Winter	1066	1062 to 1071	1053 to 1079	1037 to 1091

Table B-3: Ranges of projected static ratings of ACSR Zebra OHL in low emission scenario (Unit: A.)

Period	Season	Average	Likely Range	Conservative Range	Full Range
2020s	Summer	972	969 to 977	961 to 983	944 to 993
	Spring	1022	1020 to 1025	1015 to 1029	1005 to 1036
	Winter	1081	1079 to 1083	1075 to 1086	1068 to 1094
2050s	Summer	963	958 to 970	943 to 980	910 to 997
	Spring	1016	1014 to 1020	1006 to 1025	991 to 1035
	Winter	1076	1073 to 1079	1067 to 1084	1055 to 1092
2080s	Summer	956	950 to 964	934 to 977	889 to 995
	Spring	1010	1006 to 1014	997 to 1021	977 to 1033
	Winter	1070	1067 to 1073	1059 to 1080	1045 to 1089

The projected static ratings of AAAC Araucaria OHL are:

Table B-4: Ranges of projected static ratings of AAAC Araucaria OHL in high emission scenario (Unit: A.)

Period	Season	Average	Likely Range	Conservative Range	Full Range
2020s	Summer	1504	1499 to 1511	1486 to 1521	1455 to 1538
	Spring	1588	1585 to 1591	1578 to 1596	1566 to 1608
	Winter	1671	1668 to 1673	1663 to 1679	1651 to 1688
2050s	Summer	1477	1469 to 1487	1447 to 1505	1395 to 1530
	Spring	1572	1569 to 1577	1559 to 1585	1535 to 1602
	Winter	1658	1655 to 1662	1646 to 1669	1630 to 1682
2080s	Summer	1447	1437 to 1464	1403 to 1488	1321 to 1525
	Spring	1553	1546 to 1561	1531 to 1572	1495 to 1597
	Winter	1645	1640 to 1652	1625 to 1663	1601 to 1683

Table B-5: Ranges of projected static ratings of AAAC Araucaria OHL in medium emission scenario (Unit: A)

Period	Season	Average	Likely Range	Conservative Range	Full Range
2020s	Summer	1503	1498 to 1510	1486 to 1520	1457 to 1540
	Spring	1587	1584 to 1590	1579 to 1596	1565 to 1610
	Winter	1671	1669 to 1673	1663 to 1678	1654 to 1688

2050s	Summer	1482	1475 to 1492	1454 to 1506	1407 to 1532
	Spring	1575	1571 to 1578	1562 to 1587	1540 to 1601
	Winter	1662	1659 to 1666	1650 to 1674	1636 to 1686
2080s	Summer	1464	1456 to 1478	1428 to 1495	1363 to 1527
	Spring	1562	1557 to 1568	1545 to 1579	1514 to 1598
	Winter	1653	1649 to 1659	1637 to 1669	1619 to 1685

Table B-6: Ranges of projected static ratings of AAAC Araucaria OHL in low emission scenario (Unit: A.)

Period	Season	Average	Likely Range	Conservative Range	Full Range
2020s	Summer	1502	1497 to 1508	1486 to 1517	1464 to 1533
	Spring	1587	1585 to 1590	1579 to 1595	1566 to 1604
	Winter	1671	1669 to 1674	1664 to 1678	1656 to 1688
2050s	Summer	1489	1482 to 1499	1463 to 1513	1419 to 1542
	Spring	1580	1576 to 1585	1567 to 1591	1548 to 1603
	Winter	1665	1662 to 1669	1654 to 1676	1639 to 1685
2080s	Summer	1481	1473 to 1492	1450 to 1509	1392 to 1534
	Spring	1571	1567 to 1576	1556 to 1586	1530 to 1601
	Winter	1658	1654 to 1662	1644 to 1670	1627 to 1682

The projected static ratings of AAAC Rubus OHL are:

Table B-7: Ranges of projected static ratings of AAAC Rubus OHL in high emission scenario (Unit: A.)

Period	Season	Average	Likely Range	Conservative Range	Full Range
2020s	Summer	1210	1206 to 1215	1195 to 1223	1170 to 1236
	Spring	1276	1274 to 1278	1268 to 1283	1258 to 1293
	Winter	1342	1340 to 1344	1336 to 1349	1326 to 1356
2050s	Summer	1188	1182 to 1197	1164 to 1210	1123 to 1230
	Spring	1264	1261 to 1267	1253 to 1274	1234 to 1287
	Winter	1332	1329 to 1335	1322 to 1341	1309 to 1351
2080s	Summer	1165	1156 to 1178	1129 to 1197	1064 to 1226
	Spring	1248	1243 to 1254	1230 to 1263	1202 to 1284
	Winter	1322	1317 to 1327	1306 to 1336	1286 to 1352

Table B-8: Ranges of projected static ratings of AAAC Rubus OHL in medium emission scenario (Unit: A)

Period	Season	Average	Likely Range	Conservative Range	Full Range
2020s	Summer	1209	1205 to 1214	1195 to 1222	1172 to 1238
	Spring	1276	1273 to 1278	1268 to 1283	1257 to 1294
	Winter	1342	1340 to 1344	1336 to 1348	1329 to 1357
2050s	Summer	1192	1186 to 1200	1170 to 1211	1132 to 1232
	Spring	1265	1262 to 1268	1255 to 1275	1238 to 1287
	Winter	1335	1332 to 1338	1326 to 1344	1314 to 1354
2080s	Summer	1178	1171 to 1189	1149 to 1203	1096 to 1228
	Spring	1256	1252 to 1260	1242 to 1269	1217 to 1284

	Winter	1328	1324 to 1332	1315 to 1340	1300 to 1354

Table B-9: Ranges of projected static ratings of AAAC Rubus OHL in low emission scenario (Unit: A.)

Period	Season	Average	Likely Range	Conservative Range	Full Range
2020s	Summer	1208	1205 to 1213	1195 to 1220	1177 to 1233
	Spring	1275	1273 to 1278	1269 to 1282	1258 to 1289
	Winter	1342	1340 to 1344	1336 to 1348	1330 to 1356
2050s	Summer	1198	1192 to 1206	1177 to 1217	1142 to 1240
	Spring	1270	1267 to 1273	1259 to 1279	1244 to 1288
	Winter	1338	1335 to 1341	1329 to 1347	1317 to 1354
2080s	Summer	1191	1185 to 1200	1166 to 1213	1120 to 1234
	Spring	1263	1259 to 1267	1250 to 1274	1229 to 1287
	Winter	1332	1328 to 1335	1321 to 1341	1307 to 1351

The projected static ratings of ACAC Collybia OHL are:

Table B-10: Ranges of projected static ratings of ACAC Collybia OHL in high emission scenario (Unit: A.)

Period	Season	Average	Likely Range	Conservative Range	Full Range
2020s	Summer	1032	1027 to 1038	1016 to 1048	987 to 1062
	Spring	1107	1104 to 1109	1098 to 1115	1087 to 1125
	Winter	1180	1178 to 1183	1174 to 1187	1162 to 1195
2050s	Summer	1008	1001 to 1017	980 to 1033	932 to 1055
	Spring	1093	1089 to 1097	1081 to 1104	1059 to 1119
	Winter	1169	1166 to 1173	1158 to 1179	1143 to 1190
2080s	Summer	980	971 to 996	939 to 1018	862 to 1050
	Spring	1075	1069 to 1082	1055 to 1093	1022 to 1115
	Winter	1158	1153 to 1164	1140 to 1174	1118 to 1191

Table B-11: Ranges of projected static ratings of ACAC Collybia OHL in medium emission scenario (Unit: A)

Period	Season	Average	Likely Range	Conservative Range	Full Range
2020s	Summer	1031	1027 to 1037	1016 to 1046	989 to 1065
	Spring	1106	1104 to 1109	1098 to 1114	1086 to 1127
	Winter	1180	1178 to 1183	1174 to 1187	1165 to 1196
2050s	Summer	1012	1006 to 1021	987 to 1034	943 to 1057
	Spring	1095	1091 to 1098	1083 to 1106	1064 to 1119
	Winter	1173	1170 to 1176	1162 to 1183	1150 to 1194
2080s	Summer	996	988 to 1009	962 to 1024	901 to 1052
	Spring	1084	1079 to 1089	1068 to 1099	1040 to 1116
	Winter	1165	1160 to 1170	1150 to 1178	1133 to 1193

Table B-112: Ranges of projected static ratings of ACAC Collybia OHL in low emission scenario (Unit: A.)

Period	Season	Average	Likely Range	Conservative Range	Full Range
2020s	Summer	1030	1026 to 1036	1016 to 1044	995 to 1058
	Spring	1106	1104 to 1109	1098 to 1113	1087 to 1121
	Winter	1180	1179 to 1183	1174 to 1187	1167 to 1196
2050s	Summer	1019	1012 to 1028	994 to 1041	954 to 1066
	Spring	1100	1096 to 1104	1088 to 1110	1071 to 1120
	Winter	1175	1173 to 1179	1166 to 1185	1152 to 1193
2080s	Summer	1011	1004 to 1021	983 to 1036	929 to 1060
	Spring	1092	1088 to 1097	1078 to 1105	1054 to 1119
	Winter	1169	1165 to 1173	1156 to 1180	1141 to 1190

The projected static ratings of ACCR Drake OHL are:

Table B-13: Ranges of projected static ratings of ACCR Drake OHL in high emission scenario (Unit: A.)

Period	Season	Average	Likely Range	Conservative Range	Full Range
2020s	Summer	1816	1814 to 1817	1810 to 1820	1801 to 1825
	Spring	1840	1839 to 1840	1837 to 1842	1833 to 1846
	Winter	1865	1864 to 1866	1862 to 1867	1859 to 1870
2050s	Summer	1808	1806 to 1811	1799 to 1816	1785 to 1823
	Spring	1835	1834 to 1836	1831 to 1839	1824 to 1844
	Winter	1861	1860 to 1862	1857 to 1864	1852 to 1868
2080s	Summer	1800	1797 to 1804	1787 to 1811	1765 to 1821
	Spring	1829	1827 to 1831	1823 to 1835	1812 to 1842
	Winter	1857	1855 to 1859	1851 to 1862	1843 to 1869

Table B-14: Ranges of projected static ratings of ACCR Drake OHL in medium emission scenario (Unit: A)

Period	Season	Average	Likely Range	Conservative Range	Full Range
2020s	Summer	1815	1814 to 1817	1810 to 1820	1802 to 1826
	Spring	1839	1838 to 1840	1837 to 1842	1833 to 1846
	Winter	1865	1864 to 1866	1862 to 1867	1860 to 1870
2050s	Summer	1809	1807 to 1812	1801 to 1816	1788 to 1823
	Spring	1836	1834 to 1837	1832 to 1839	1825 to 1844
	Winter	1862	1861 to 1863	1858 to 1866	1854 to 1869
2080s	Summer	1804	1802 to 1808	1794 to 1813	1776 to 1822
	Spring	1832	1830 to 1834	1827 to 1837	1818 to 1843
	Winter	1859	1858 to 1861	1854 to 1864	1849 to 1869

Table B-15: Ranges of projected static ratings of ACCR Drake OHL in low emission scenario (Unit: A.)

Period	Season	Average	Likely Range	Conservative Range	Full Range
2020s	Summer	1815	1814 to 1817	1810 to 1819	1804 to 1824
	Spring	1839	1839 to 1840	1837 to 1842	1833 to 1844

	Winter	1865	1864 to 1866	1863 to 1867	1860 to 1870
2050s	Summer	1811	1809 to 1814	1804 to 1818	1792 to 1826
	Spring	1837	1836 to 1839	1833 to 1841	1828 to 1844
	Winter	1863	1862 to 1864	1860 to 1866	1855 to 1869
2080s	Summer	1809	1807 to 1812	1800 to 1817	1784 to 1824
	Spring	1835	1833 to 1836	1830 to 1839	1822 to 1844
	Winter	1861	1859 to 1862	1856 to 1865	1851 to 1868

B.2 Projected Cable Ratings

The projected static ratings of XLPE 2500 mm^2 cable are:

Table B-16: Ranges of projected static ratings of XLPE 2500 mm^2 cable in high emission scenario (Unit: A.)

Period	Season	Average	Likely Range	Conservative Range	Full Range
2020s	Summer	1259	1256 to 1262	1250 to 1266	1237 to 1276
	Winter	1282	1281 to 1284	1276 to 1289	1265 to 1296
2050s	Summer	1244	1240 to 1249	1230 to 1257	1206 to 1269
	Winter	1271	1267 to 1274	1261 to 1280	1242 to 1291
2080s	Summer	1227	1222 to 1235	1208 to 1245	1171 to 1266
	Winter	1256	1252 to 1262	1241 to 1270	1215 to 1287

Table B-17: Ranges of projected static ratings of XLPE 2500 mm^2 cable in medium emission scenario (Unit: A)

Period	Season	Average	Likely Range	Conservative Range	Full Range
2020s	Summer	1258	1256 to 1262	1250 to 1266	1238 to 1276
	Winter	1282	1280 to 1284	1276 to 1289	1267 to 1296
2050s	Summer	1247	1243 to 1251	1234 to 1259	1215 to 1269
	Winter	1272	1270 to 1276	1263 to 1281	1248 to 1291
2080s	Summer	1237	1233 to 1243	1220 to 1252	1191 to 1263
	Winter	1264	1261 to 1268	1251 to 1275	1229 to 1285

Table B-18: Ranges of projected static ratings XLPE 2500 mm^2 cable in low emission scenario (Unit: A)

Period	Season	Average	Likely Range	Conservative Range	Full Range
2020s	Summer	1272	1271 to 1272	1271 to 1273	1270 to 1274
	Spring	1296	1296 to 1296	1296 to 1296	1296 to 1297
2050s	Winter	1251	1247 to 1256	1238 to 1263	1218 to 1272
	Summer	1276	1274 to 1280	1266 to 1285	1252 to 1292
2080s	Spring	1245	1241 to 1250	1232 to 1259	1206 to 1272
	Winter	1271	1268 to 1275	1260 to 1281	1241 to 1292

The projected static ratings of XLPE 1600 mm^2 cable are:

Table B-19: Ranges of projected static ratings of XLPE 1600 mm^2 cable in high emission scenario (Unit: A)

Period	Season	Average	Likely Range	Conservative Range	Full Range
2020s	Summer	1163	1161 to 1165	1156 to 1169	1148 to 1175
	Spring	1177	1175 to 1179	1171 to 1182	1163 to 1187
2050s	Winter	1151	1149 to 1155	1141 to 1160	1123 to 1170
	Summer	1167	1165 to 1170	1159 to 1175	1144 to 1183
2080s	Spring	1138	1134 to 1143	1122 to 1152	1095 to 1167
	Winter	1155	1152 to 1160	1143 to 1167	1121 to 1180

Table B-20: Ranges of projected static ratings of XLPE 1600 mm^2 cable in medium emission scenario (Unit: A.)

Period	Season	Average	Likely Range	Conservative Range	Full Range
2020s	Summer	1163	1160 to 1165	1156 to 1169	1148 to 1175
	Spring	1177	1175 to 1179	1171 to 1182	1165 to 1187
2050s	Winter	1154	1151 to 1157	1144 to 1162	1130 to 1170
	Summer	1169	1166 to 1171	1160 to 1176	1149 to 1183
2080s	Spring	1145	1142 to 1150	1131 to 1157	1111 to 1167
	Winter	1161	1159 to 1165	1150 to 1170	1132 to 1180

Table B-21: Ranges of projected static ratings XLPE 1600 mm^2 cable in low emission scenario (Unit: A.)

Period	Season	Average	Likely Range	Conservative Range	Full Range
2020s	Summer	1162	1160 to 1165	1157 to 1167	1148 to 1172
	Spring	1176	1175 to 1178	1171 to 1181	1164 to 1186
2050s	Winter	1157	1154 to 1160	1147 to 1165	1133 to 1171
	Summer	1172	1170 to 1175	1164 to 1179	1153 to 1184
2080s	Spring	1152	1149 to 1156	1142 to 1163	1123 to 1172
	Winter	1167	1165 to 1170	1158 to 1176	1143 to 1184

The projected static ratings of XLPE 800 mm^2 cable are:

Table B-22: Ranges of projected static ratings of XLPE 800 mm^2 cable in high emission scenario (Unit: A.)

Period	Season	Average	Likely Range	Conservative Range	Full Range
2020s	Summer	934	933 to 936	929 to 939	922 to 944
	Spring	945	944 to 947	941 to 949	934 to 953
2050s	Winter	925	923 to 928	917 to 932	903 to 940
	Summer	938	936 to 940	931 to 944	920 to 950
2080s	Spring	915	911 to 919	902 to 926	880 to 938
	Winter	928	926 to 932	918 to 938	901 to 947

Table B-23: Ranges of projected static ratings of XLPE 800 mm^2 cable in medium emission scenario (Unit: A)

Period	Season	Average	Likely Range	Conservative Range	Full Range
2020s	Summer	934	932 to 936	929 to 939	922 to 944
	Spring	945	944 to 947	941 to 949	936 to 953
2050s	Winter	927	925 to 930	920 to 934	908 to 940
	Summer	939	937 to 941	932 to 945	924 to 950
2080s	Spring	920	918 to 924	909 to 930	893 to 938
	Winter	933	931 to 936	924 to 940	910 to 947

Table B-24: Ranges of projected static ratings XLPE 800 mm^2 cable in low emission scenario (Unit: A.)

Period	Season	Average	Likely Range	Conservative Range	Full Range
2020s	Summer	934	932 to 936	930 to 938	922 to 942
	Spring	945	944 to 946	941 to 949	935 to 953
2050s	Winter	930	928 to 932	922 to 936	911 to 941
	Summer	941	940 to 944	935 to 947	926 to 951
2080s	Spring	926	924 to 929	918 to 934	903 to 942
	Winter	938	936 to 940	930 to 945	919 to 951

The projected static ratings of fluid-filled 2500 mm^2 cable are:

Table B-25: Ranges of projected static ratings of fluid-filled 2500 mm^2 cable in high emission scenario (Unit: A.)

Period	Season	Average	Likely Range	Conservative Range	Full Range
2020s	Summer	927	925 to 929	919 to 934	909 to 942
	Spring	944	942 to 946	938 to 950	927 to 956
2050s	Winter	913	910 to 918	901 to 924	879 to 936
	Summer	932	929 to 936	922 to 941	905 to 951
2080s	Spring	897	892 to 904	878 to 914	844 to 932
	Winter	918	914 to 923	903 to 932	876 to 947

Table B-26: Ranges of projected static ratings of fluid-filled 2500 mm^2 cable in medium emission scenario (Unit: A.)

Period	Season	Average	Likely Range	Conservative Range	Full Range
2020s	Summer	927	924 to 930	919 to 934	909 to 941
	Spring	944	941 to 946	938 to 950	929 to 956
2050s	Winter	916	913 to 920	905 to 926	887 to 936
	Summer	934	931 to 938	924 to 943	911 to 951
2080s	Spring	906	902 to 912	889 to 920	864 to 932
	Winter	926	922 to 930	912 to 937	890 to 947

Table B-27: Ranges of projected static ratings fluid-filled 2500 mm^2 cable in low emission scenario (Unit: A.)

Period	Season	Average	Likely Range	Conservative Range	Full Range
2020s	Summer	927	924 to 929	920 to 932	909 to 939
	Spring	944	942 to 945	938 to 949	928 to 955
2050s	Winter	920	917 to 924	908 to 930	891 to 938

	Summer	938	936 to 941	928 to 946	915 to 952
2080s	Spring	914	911 to 919	902 to 927	879 to 939
	Winter	933	930 to 937	921 to 943	904 to 952

The projected static ratings of fluid-filled 1600 mm^2 cable are:

Table B-28: Ranges of projected static ratings of fluid-filled 1600 mm^2 cable in high emission scenario (Unit: A.)

Period	Season	Average	Likely Range	Conservative Range	Full Range
2020s	Summer	889	887 to 891	882 to 895	873 to 902
	Spring	903	902 to 905	897 to 909	889 to 914
2050s	Winter	877	874 to 881	866 to 886	847 to 896
	Summer	893	891 to 896	884 to 901	869 to 909
2080s	Spring	863	859 to 868	846 to 877	817 to 893
	Winter	881	877 to 885	868 to 893	845 to 906

Table B-29: Ranges of projected static ratings of fluid-filled 1600 mm^2 cable in medium emission scenario (Unit: A.)

Period	Season	Average	Likely Range	Conservative Range	Full Range
2020s	Summer	889	886 to 891	882 to 895	873 to 901
	Spring	903	901 to 905	897 to 909	891 to 914
2050s	Winter	879	876 to 883	869 to 888	854 to 896
	Summer	895	892 to 897	886 to 903	875 to 909
2080s	Spring	871	867 to 876	856 to 883	834 to 893
	Winter	887	884 to 891	876 to 897	857 to 906

Table B-30: Ranges of projected static ratings fluid-filled 1600 mm^2 cable in low emission scenario (Unit: A.)

Period	Season	Average	Likely Range	Conservative Range	Full Range
2020s	Summer	888	886 to 891	883 to 893	873 to 898
	Spring	903	902 to 904	897 to 908	890 to 913
2050s	Winter	882	880 to 886	872 to 891	858 to 897
	Summer	898	896 to 901	890 to 905	878 to 910
2080s	Spring	878	875 to 882	867 to 889	847 to 898
	Winter	893	891 to 897	884 to 903	868 to 910

Projected static ratings of fluid-filled 800 mm^2 cable:

Table B-31: Ranges of projected static ratings of fluid-filled 800 mm^2 cable in high emission scenario (Unit: A.)

Period	Season	Average	Likely Range	Conservative Range	Full Range
2020s	Summer	770	769 to 772	765 to 775	759 to 780
	Spring	781	780 to 783	777 to 786	771 to 790
2050s	Winter	761	759 to 765	753 to 769	739 to 776
	Summer	774	772 to 776	767 to 780	756 to 786
2080s	Spring	751	748 to 755	738 to 762	716 to 774

	Winter	764	762 to 768	754 to 774	737 to 784

Table B-32: Ranges of projected static ratings of fluid-filled 800 mm^2 cable in medium emission scenario (Unit: A.)

Period	Season	Average	Likely Range	Conservative Range	Full Range
2020s	Summer	770	769 to 773	765 to 775	759 to 780
	Spring	781	780 to 783	777 to 786	772 to 790
2050s	Winter	763	761 to 766	756 to 770	744 to 776
	Summer	775	773 to 777	769 to 781	760 to 786
2080s	Spring	757	754 to 761	746 to 766	729 to 774
	Winter	769	767 to 773	761 to 776	746 to 784

Table B-33: Ranges of projected static ratings fluid-filled 800 mm^2 cable in low emission scenario (Unit: A.)

Period	Season	Average	Likely Range	Conservative Range	Full Range
2020s	Summer	770	769 to 772	766 to 774	759 to 778
	Spring	781	780 to 782	777 to 785	771 to 789
2050s	Winter	766	764 to 769	758 to 773	747 to 777
	Summer	777	776 to 780	771 to 783	763 to 787
2080s	Spring	762	760 to 765	754 to 771	739 to 778
	Winter	774	773 to 776	767 to 781	755 to 787

B.3 Projected Transformer Ratings

The projected static ratings of ONAF transformer are:

Table B-34: Ranges of projected static ratings of ONAF transformer in high emission scenario (Unit: p.u.)

Period	Season	Average	Likely Range	Conservative Range	Full Range
2020s	Summer	0.8905	0.8873 to 0.8956	1 to 0.903	0.8547 to 0.9167
	Spring	0.9414	0.9392 to 0.9437	1 to 0.949	0.923 to 0.9588
	Winter	1.0035	1.0009 to 1.0052	1 to 1.0104	0.9861 to 1.0182
2050s	Summer	0.8704	0.865 to 0.8781	1 to 0.891	0.8108 to 0.9085
	Spring	0.9287	0.9257 to 0.9329	1 to 0.9392	0.8984 to 0.9526
	Winter	0.9923	1 to 1.0018	1 to 1.0018	0.9677 to 1.013
2080s	Summer	0.8478	0.8396 to 0.8603	1 to 0.879	0.7545 to 0.9021
	Spring	0.9119	0.9066 to 0.9185	1 to 0.9293	0.866 to 0.9482
	Winter	0.9810	0.9765 to 0.987	1 to 0.9966	0.9428 to 1.0147

Table B-35: Ranges of projected static ratings of ONAF transformer in medium emission scenario (Unit: p.u.)

Period	Season	Average	Likely Range	Conservative Range	Full Range

2020s	Summer	0.8902	0.8864 to 0.8947	0.8772 to 0.9021	0.8566 to 0.9167
	Spring	0.94118	0.9383 to 0.9437	0.9329 to 0.949	0.9221 to 0.9588
	Winter	1.0037	1.0018 to 1.0061	0.9966 to 1.0104	0.9887 to 1.019
2050s	Summer	0.8744	0.8688 to 0.8818	0.8538 to 0.892	0.8166 to 0.9094
	Spring	0.93042	0.9266 to 0.9338	0.9194 to 0.941	0.903 to 0.9535
	Winter	0.99592	0.9931 to 0.9992	0.9852 to 1.0061	0.973 to 1.0165
2080s	Summer	0.86062	0.8538 to 0.8716	0.8319 to 0.8846	0.7814 to 0.9039
	Spring	0.92013	0.9157 to 0.9257	0.9057 to 0.9338	0.8809 to 0.949
	Winter	0.98808	0.9835 to 0.9931	0.9738 to 1.0018	0.957 to 1.0156

Table B-36: Ranges of projected static ratings of ONAF transformer in low emission scenario (Unit: p.u.)

Period	Season	Average	Likely Range	Conservative Range	Full Range
2020s	Summer	0.88934	0.8855 to 0.8938	0.8772 to 0.9002	0.8603 to 0.9103
	Spring	0.94111	0.9392 to 0.9437	0.9338 to 0.9482	0.923 to 0.9562
	Winter	1.0038	1.0018 to 1.0061	0.9974 to 1.0096	0.9896 to 1.019
2050s	Summer	0.87951	0.8744 to 0.8864	0.8594 to 0.8975	0.8262 to 0.9148
	Spring	0.93503	0.932 to 0.9392	0.9239 to 0.9446	0.9085 to 0.9544
	Winter	0.9987	0.9957 to 1.0018	0.9887 to 1.0078	0.9756 to 1.0165
2080s	Summer	0.87307	0.8669 to 0.8809	0.85 to 0.8938	0.8059 to 0.9121
	Spring	0.92798	0.9239 to 0.932	0.9148 to 0.9401	0.8938 to 0.9526
	Winter	0.99194	0.9887 to 0.9957	0.98 to 1.0027	0.965 to 1.013

Projected static ratings of OF transformer:

Table B-37: Ranges of projected static ratings of OF transformer in high emission scenario (Unit: p.u.)

Period	Season	Average	Likely Range	Conservative Range	Full Range
2020s	Summer	0.91405	0.9113 to 0.9185	0.9015 to 0.9249	0.8826 to 0.9369
	Spring	0.95837	0.9565 to 0.9604	0.951 to 0.965	0.9424 to 0.9735
	Winter	1.012	1.0098 to 1.0135	1.006 to 1.0179	0.997 to 1.0246
2050s	Summer	0.89637	0.8917 to 0.9032	0.8768 to 0.9145	0.8438 to 0.9297
	Spring	0.94731	0.9448 to 0.951	0.9369 to 0.9565	0.9209 to 0.9681
	Winter	1.0024	1.0001 to 1.0053	0.9933 to 1.0105	0.9811 to 1.0202
2080s	Summer	0.87648	0.8693 to 0.8876	0.8438 to 0.904	0.7936 to 0.9241
	Spring	0.93273	0.9281 to 0.9385	0.9169 to 0.9479	0.8925 to 0.9642
	Winter	0.99259	0.9887 to 0.9978	0.9773 to 1.006	0.9596 to 1.0216

Table B-38: Ranges of projected static ratings of OF transformer in medium emission scenario (Unit: p.u.)

Period	Season	Average	Likely Range	Conservative Range	Full Range
2020s	Summer	0.91376	0.9105 to 0.9177	0.9023 to 0.9241	0.8843 to 0.9369

	Spring	0.95819	0.9557 to 0.9604	0.951 to 0.965	0.9416 to 0.9735
	Winter	1.0122	1.0105 to 1.0142	1.006 to 1.0179	0.9993 to 1.0253
2050s	Summer	0.8999	0.895 to 0.9064	0.8818 to 0.9153	0.8489 to 0.9305
	Spring	0.94885	0.9455 to 0.9518	0.9392 to 0.958	0.9249 to 0.9689
	Winter	1.0055	1.003 to 1.0083	0.9963 to 1.0142	0.9857 to 1.0231
2080s	Summer	0.88778	0.8818 to 0.8974	0.8625 to 0.9088	0.8177 to 0.9257
	Spring	0.93989	0.9361 to 0.9448	0.9273 to 0.9518	0.9056 to 0.965
	Winter	0.99873	0.9948 to 1.003	0.9865 to 1.0105	0.972 to 1.0224

Table B-39: Ranges of projected static ratings of OF transformer in low emission scenario (Unit: p.u.)

Period	Season	Average	Likely Range	Conservative Range	Full Range
2020s	Summer	0.91301	0.9097 to 0.9169	0.9023 to 0.9225	0.8876 to 0.9313
	Spring	0.95813	0.9565 to 0.9604	0.9518 to 0.9642	0.9424 to 0.9712
	Winter	1.0122	1.0105 to 1.0142	1.0068 to 1.0172	1.0001 to 1.0253
2050s	Summer	0.90438	0.8999 to 0.9105	0.8867 to 0.9201	0.8574 to 0.9353
	Spring	0.95286	0.9502 to 0.9565	0.9432 to 0.9611	0.9297 to 0.9696
	Winter	1.0079	1.0053 to 1.0105	0.9993 to 1.0157	0.988 to 1.0231
2080s	Summer	0.89873	0.8933 to 0.9056	0.8784 to 0.9169	0.8395 to 0.9329
	Spring	0.94673	0.9432 to 0.9502	0.9353 to 0.9573	0.9169 to 0.9681
	Winter	1.002	0.9993 to 1.0053	0.9918 to 1.0113	0.9788 to 1.0202

Projected static ratings of OD transformer:

Table B-40: Ranges of projected static ratings of OD transformer in high emission scenario (Unit: p.u.)

Period	Season	Average	Likely Range	Conservative Range	Full Range
2020s	Summer	0.91381	0.9114 to 0.9176	0.9031 to 0.9231	0.887 to 0.9332
	Spring	0.95146	0.9499 to 0.9532	0.9452 to 0.9571	0.9379 to 0.9643
	Winter	0.99692	0.995 to 0.9982	0.9919 to 1.0019	0.9842 to 1.0076
2050s	Summer	0.89874	0.8948 to 0.9045	0.882 to 0.9142	0.8539 to 0.9271
	Spring	0.94207	0.9399 to 0.9452	0.9332 to 0.9499	0.9197 to 0.9597
	Winter	0.98876	0.9868 to 0.9912	0.981 to 0.9956	0.9708 to 1.0038
2080s	Summer	0.88177	0.8756 to 0.8912	0.8539 to 0.9052	0.8109 to 0.9224
	Spring	0.92968	0.9258 to 0.9345	0.9162 to 0.9426	0.8955 to 0.9564
	Winter	0.98047	0.9772 to 0.9849	0.9675 to 0.9919	0.9525 to 1.0051

Table B-41: Ranges of projected static ratings of OD transformer in medium emission scenario (Unit: p.u.)

Period	Season	Average	Likely Range	Conservative Range	Full Range
2020s	Summer	0.91356	0.9107 to 0.9169	0.9038 to 0.9224	0.8884 to 0.9332
	Spring	0.95131	0.9492 to 0.9532	0.9452 to 0.9571	0.9372 to 0.9643

	Winter	0.99704	0.9956 to 0.9988	0.9919 to 1.0019	0.9862 to 1.0082
2050s	Summer	0.90175	0.8976 to 0.9073	0.8863 to 0.9149	0.8583 to 0.9278
	Spring	0.94338	0.9406 to 0.9459	0.9352 to 0.9512	0.9231 to 0.9604
	Winter	0.99138	0.9893 to 0.9938	0.9836 to 0.9988	0.9746 to 1.0063
2080s	Summer	0.89141	0.8863 to 0.8997	0.8699 to 0.9094	0.8315 to 0.9237
	Spring	0.93577	0.9325 to 0.9399	0.9251 to 0.9459	0.9066 to 0.9571
	Winter	0.98567	0.9823 to 0.9893	0.9753 to 0.9956	0.963 to 1.0057

Table B-42: Ranges of projected static ratings of OD transformer in low emission scenario (Unit: p.u.)

Period	Season	Average	Likely Range	Conservative Range	Full Range
2020s	Summer	0.91292	0.9101 to 0.9162	0.9038 to 0.921	0.8912 to 0.9285
	Spring	0.95126	0.9499 to 0.9532	0.9459 to 0.9564	0.9379 to 0.9623
	Winter	0.9971	0.9956 to 0.9988	0.9925 to 1.0013	0.9868 to 1.0082
2050s	Summer	0.90557	0.9017 to 0.9107	0.8905 to 0.919	0.8655 to 0.9319
	Spring	0.94678	0.9446 to 0.9499	0.9386 to 0.9538	0.9271 to 0.961
	Winter	0.99341	0.9912 to 0.9956	0.9862 to 1.0001	0.9766 to 1.0063
2080s	Summer	0.90075	0.8962 to 0.9066	0.8835 to 0.9162	0.8502 to 0.9298
	Spring	0.94157	0.9386 to 0.9446	0.9319 to 0.9505	0.9162 to 0.9597
	Winter	0.98848	0.9862 to 0.9912	0.9798 to 0.9963	0.9688 to 1.0038

Appendix C Test Network Data

This appendix provides the data required in order to perform the reliability assessment on the 24-bus IEEE Reliability Test Network used in Chapter 6. Full network details are adopted from [30].

Table C-1: Bus data

Bus #	Generation				Demand	
	Pmax (MW)	Pmin (MW)	Qmax (MVar)	Qmax (MVar)	P (MW)	Q (MVar)
1	192	62.4	80	-50	108	22
2	192	62.4	80	-50	97	20
3	-	-	-	-	180	37
4	-	-	-	-	74	15
5	-	-	-	-	71	14
6	-	-	-	-	136	28
7	300	75	180	0	125	25
8	-	-	-	-	171	35
9	-	-	-	-	175	36
10	-	-	-	-	195	40
11	-	-	-	-	-	-
12	-	-	-	-	-	-
13	591	207	240	0	265	54
14	0	0	200	-50	194	39
15	215	66.3	110	-50	317	64
16	155	54.3	80	-50	100	20

17	-	-	-	-	-	-
18	400	100	200	-50	-	-
19	-	-	-	-	181	37
20	-	-	-	-	128	26
21	400	100	200	-50	-	-
22	300	60	96	-60	-	-
23	660	248.6	310	-125	-	-
24	-	-	-	-	-	-

Table C-2: Branch data

Branch	From	To	R (p.u.)	X (p.u.)	B (p.u.)	CON	LTE	STE	Tr (p.u.)
1	1	2	0.003	0.14	0.461	175	193	200	0
2	1	3	0.055	0.211	0.057	175	208	220	0
3	1	5	0.022	0.085	0.023	175	208	220	0
4	2	4	0.033	0.127	0.034	175	208	220	0
5	2	6	0.05	0.192	0.052	175	208	220	0
6	3	9	0.031	0.119	0.032	175	208	220	0
7	3	24	0.002	0.084	0	400	510	600	1.015
8	4	9	0.027	0.104	0.028	175	208	220	0
9	5	10	0.023	0.088	0.024	175	208	220	0
10	6	10	0.014	0.061	2.459	175	193	200	0
11	7	8	0.016	0.061	0.017	175	208	220	0
12	8	9	0.043	0.165	0.045	175	208	220	0
13	8	10	0.043	0.165	0.045	175	208	220	0
14	9	11	0.0002	0.084	0	400	510	600	1.03
15	9	12	0.0002	0.084	0	400	510	600	1.03
16	10	11	0.0002	0.084	0	400	510	600	1.015
17	10	12	0.0002	0.084	0	400	510	600	1.015
18	11	13	0.006	0.048	0.1	500	600	625	0
19	11	14	0.005	0.042	0.088	500	600	625	0
20	12	13	0.006	0.048	0.1	500	600	625	0
22	12	23	0.012	0.097	0.203	500	600	625	0
23	13	23	0.011	0.087	0.182	500	600	625	0
24	15	16	0.002	0.017	0.036	500	600	625	0
25	15	21	0.006	0.049	0.103	500	600	625	0
26	15	21	0.006	0.049	0.103	500	600	625	0
27	15	24	0.007	0.052	0.109	500	600	625	0
28	16	17	0.003	0.026	0.055	500	600	625	0
29	16	19	0.003	0.023	0.049	500	600	625	0
30	17	18	0.002	0.014	0.03	500	600	625	0
31	17	22	0.014	0.105	0.221	500	600	625	0
32	18	21	0.003	0.026	0.055	500	600	625	0
33	18	21	0.003	0.026	0.055	500	600	625	0
34	19	20	0.005	0.04	0.083	500	600	625	0

35	19	20	0.005	0.04	0.083	500	600	625	0
36	20	23	0.003	0.022	0.046	500	600	625	0
37	20	23	0.003	0.022	0.046	500	600	625	0
38	21	22	0.009	0.068	0.142	500	600	625	0

CON = Continuous rating

LTE = Long-time emergency rating (24 hour)

STE = Short-time emergency rating (15 min)

Tr = Transformer off-nominal ration

Table C-3: Branch reliability data

Branch #	From Bus	To Bus	Permanent		Transient
			λp	Duration	λt
1	1	2	0.24	16	0.0
2	1	3	0.51	10	2.9
3	1	5	0.33	10	1.2
4	2	4	0.39	10	1.7
5	2	6	0.48	10	2.6
6	3	9	0.38	10	1.6
7	3	24	0.02	768	0.0
8	4	9	0.36	10	1.4
9	5	10	0.34	10	1.2
10	6	10	0.33	35	0.0
11	7	8	0.30	10	0.8
12	8	9	0.44	10	2.3
13	8	10	0.44	10	2.3
14	9	11	0.02	768	0.0
15	9	12	0.02	768	0.0
16	10	11	0.02	768	0.0
17	10	12	0.02	768	0.0
18	11	13	0.40	11	0.8
19	11	14	0.39	11	0.7
20	12	13	0.40	11	0.8
22	12	23	0.52	11	1.6
23	13	23	0.49	11	1.5
24	15	16	0.33	11	0.3
25	15	21	0.41	11	0.8
26	15	21	0.41	11	0.8
27	15	24	0.41	11	0.9
28	16	17	0.35	11	0.4
29	16	19	0.34	11	0.4
30	17	18	0.32	11	0.2
31	17	22	0.54	11	1.8
32	18	21	0.35	11	0.4
33	18	21	0.35	11	0.4

34	19	20	0.38	11	0.7
35	19	20	0.38	11	0.7
36	20	23	0.34	11	0.4
37	20	23	0.34	11	0.4
38	21	22	0.45	11	1.2

λ_p = Permanent Outage Rate (outages/year)

Duration = Permanent Outage Duration (hours)

λ_t = Transient Outage Rate (outages/year)

Table C-4: Generator cost data

Start-up Cost ($)	Shutdown Cost ($)	N	C3 ($/hr)	C2 ($/hr)	C1 ($/hr)
1500	0	3	0	130	400.6849
1500	0	3	0	130	400.6849
1500	0	3	0.014142	16.0811	212.3076
1500	0	3	0.014142	16.0811	212.3076
1500	0	3	0	130	400.6849
1500	0	3	0	130	400.6849
1500	0	3	0.014142	16.0811	212.3076
1500	0	3	0.014142	16.0811	212.3076
1500	0	3	0.052672	43.6615	781.521
1500	0	3	0.052672	43.6615	781.521
1500	0	3	0.052672	43.6615	781.521
1500	0	3	0.00717	48.5804	832.7575
1500	0	3	0.00717	48.5804	832.7575
1500	0	3	0.00717	48.5804	832.7575
1500	0	3	0	0	0
1500	0	3	0.328412	56.564	86.3852
1500	0	3	0.328412	56.564	86.3852
1500	0	3	0.328412	56.564	86.3852
1500	0	3	0.328412	56.564	86.3852
1500	0	3	0.328412	56.564	86.3852
1500	0	3	0.008342	12.3883	382.2391
1500	0	3	0.008342	12.3883	382.2391
1500	0	3	0.000213	4.4231	395.3749
1500	0	3	0.000213	4.4231	395.3749
1500	0	3	0	0.001	0.001
1500	0	3	0	0.001	0.001
1500	0	3	0	0.001	0.001
1500	0	3	0	0.001	0.001
1500	0	3	0	0.001	0.001
1500	0	3	0	0.001	0.001
1500	0	3	0.008342	12.3883	382.2391
1500	0	3	0.008342	12.3883	382.2391
1500	0	3	0.004895	11.8495	665.1094

N = number of cost coefficients for polynomial cost function or number of data points for piecewise linear

Appendix D List of Author's Thesis Based Publications

[D1] **X. Hu**, I. Cotton, "Impact of climate change on overhead lines operated using dynamic rating in a smart gird," *4th IEEE ISGT Europe*, Copenhagen, Denmark, 6-9 October, 2013.

[D2] **X. Hu**, I. Cotton, "Impact of climate change on static ratings of overhead line in Edinburgh," *48th International Universities' Power Engineering Conference (UPEC)*, Dublin, Ireland, 2-5 September, 2013.

[D3] M Panteli, P Mancarella, **X Hu**, I Cotton, D Calverley, R Wood, K Anderson,, S Wilkinson, R Dawson , "", *The IET International Impact of Climate Change on the Resilience of UK Power System Conference on Resilience of Transmission and Distribution Networks (RTDN)*, Birmingham, UK, 22-24 September, 2015

[D4] Science and Technology Select Committee, "The Resilience of the Electricity System," House of Lords, UK (2014).